

AD-A044 032

DENVER RESEARCH INST COLO
DIPOLE WEST TECHNICAL PHOTOGRAPHY. (U)
FEB 77 J WISOTSKI

F/G 15/6

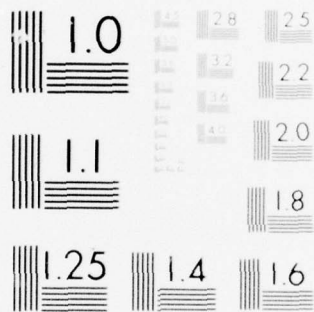
UNCLASSIFIED

DNA-4325F

DNA001-73-C-0256
NL

1 OF 2
40
A044032





MICROCOPY RESOLUTION TEST CHART
NATIONAL BUREAU OF STANDARDS-1963-A

AD A 044032

DNA 4325F

DIPOLE WEST TECHNICAL PHOTOGRAPHY

University of Denver
Denver Research Institute
Denver, Colorado 80208

12

15 February 1977

Final Report for Period 1973-1975

CONTRACT No. DNA 001-73-C-0256

APPROVED FOR PUBLIC RELEASE;
DISTRIBUTION UNLIMITED.

THIS WORK SPONSORED BY THE DEFENSE NUCLEAR AGENCY
UNDER RDT&E RMSS CODE B342076464 N99QAXAA11103 H2590D.

AD NU.
DDC FILE COPY

Prepared for
Director
DEFENSE NUCLEAR AGENCY
Washington, D. C. 20305

DDC
RECEIVED
SEP 12 1977
B

Destroy this report when it is no longer
needed. Do not return to sender.



UNCLASSIFIED

SECURITY CLASSIFICATION OF THIS PAGE (When Data Entered)

REPORT DOCUMENTATION PAGE		READ INSTRUCTIONS BEFORE COMPLETING FORM															
1. REPORT NUMBER DNA 4325F	2. GOVT ACCESSION NO.	3. RECIPIENT'S CATALOG NUMBER															
4. TITLE (and Subtitle) DIPOLE WEST TECHNICAL PHOTOGRAPHY		5. TYPE OF REPORT & PERIOD COVERED Final Report for Period 1973-1975															
		6. PERFORMING ORG. REPORT NUMBER															
7. AUTHOR(s) John Wisotski	8. CONTRACT OR GRANT NUMBER(s) DNA 001-73-C-0256																
9. PERFORMING ORGANIZATION NAME AND ADDRESS University of Denver Denver Research Institute Denver, Colorado 80208		10. PROGRAM ELEMENT PROJECT, TASK AREA & WORK UNIT NUMBERS Subtask N99QAXAA111-03															
11. CONTROLLING OFFICE NAME AND ADDRESS Director Defense Nuclear Agency Washington, D.C. 20305		12. REPORT DATE 15 February 1977															
		13. NUMBER OF PAGES 156															
14. MONITORING AGENCY NAME & ADDRESS (if different from Controlling Office)		15. SECURITY CLASS (of this report) UNCLASSIFIED															
		15a. DECLASSIFICATION/DOWNGRADING SCHEDULE															
16. DISTRIBUTION STATEMENT (of this Report) Approved for public release; distribution unlimited.																	
17. DISTRIBUTION STATEMENT (of the abstract entered in Block 20, if different from Report)																	
18. SUPPLEMENTARY NOTES This work sponsored by the Defense Nuclear Agency under RDT&E RMSS Code B342076464 N99QAXAA11103 H2590D.																	
19. KEY WORDS (Continue on reverse side if necessary and identify by block number) <table border="0"> <tr> <td>DIPOLE WEST Series</td> <td>Mach-region</td> <td>Multiple-detonations</td> </tr> <tr> <td>Phases 1 through 4</td> <td>Triple-point</td> <td>Simultaneous</td> </tr> <tr> <td>Technical Photography</td> <td>Intersection-point</td> <td>Nonsimultaneous</td> </tr> <tr> <td>Detonation Phenomena</td> <td>Height-of-burst</td> <td>Reflection Coefficients</td> </tr> <tr> <td>Shockwaves</td> <td>Singular-detonations</td> <td></td> </tr> </table>			DIPOLE WEST Series	Mach-region	Multiple-detonations	Phases 1 through 4	Triple-point	Simultaneous	Technical Photography	Intersection-point	Nonsimultaneous	Detonation Phenomena	Height-of-burst	Reflection Coefficients	Shockwaves	Singular-detonations	
DIPOLE WEST Series	Mach-region	Multiple-detonations															
Phases 1 through 4	Triple-point	Simultaneous															
Technical Photography	Intersection-point	Nonsimultaneous															
Detonation Phenomena	Height-of-burst	Reflection Coefficients															
Shockwaves	Singular-detonations																
20. ABSTRACT (Continue on reverse side if necessary and identify by block number) <p>Technical information pertaining to singular and multiple detonations above a real ground surface were obtained photographically from the DIPOLE WEST Series. The photographic records gave information on time-of-arrival, triple-point paths and intersection points along the real and ideal reflective surfaces. Time-of-arrival data were used in the calculation of peak pressure values.</p>																	

DD FORM 1473

1 JAN 73

EDITION OF 1 NOV 65 IS OBSOLETE

UNCLASSIFIED

SECURITY CLASSIFICATION OF THIS PAGE (When Data Entered)

TABLE OF CONTENTS

SECTION	PAGE
I. INTRODUCTION	11
1.1 OBJECTIVES	11
1.2 BACKGROUND	11
1.3 THEORY	14
II PROCEDURE	17
2.1 EXPERIMENTAL SETUP	17
2.2 INSTRUMENTATION AND FIELD OPERATION	32
III RESULTS AND DISCUSSION	37
3.1 POSITION-TIME DATA FROM EVENTS 8 THROUGH 16	51
3.2 PEAK PRESSURE DATA FROM EVENTS 8 THROUGH 16	85
3.3 REFLECTION COEFFICIENT FROM EVENTS 8 THROUGH 11	87
3.4 TRIPLE-POINT PATHS EVENTS 8 THROUGH 16	90
3.5 INTERSECTION-POINT PATHS EVENTS 13, 15 and 16	103
3.6 POSITION-TIME DATA FROM EVENTS 17 THROUGH 24	104
3.7 PEAK PRESSURE DATA FROM EVENTS 17 THROUGH 24	123
3.8 TRIPLE-POINT PATHS EVENTS 17 THROUGH 24	140
IV CONCLUSIONS AND RECOMMENDATIONS	147
REFERENCES	148

ACCESSION for	
NTIS	White Section <input checked="" type="checkbox"/>
DDC	Buff Section <input type="checkbox"/>
UNANNOUNCED	<input type="checkbox"/>
JUSTIFICATION	
BY	
DISTRIBUTION/AVAILABILITY CODES	
Dist.	or SPECIAL
A	

LIST OF ILLUSTRATIONS

<u>Figure</u>		<u>Page</u>
1.1	Fireball Anomaly from Event 7, Frame 1, Photographed with a Hulcher Camera	12
1.2	Fireball Anomalies from Event 19, Frame 1, Photographed with a Hulcher Camera	13
1.3	Pictorial Representation of Shockwave Interactions from Simultaneous Detonations	15
2.1	Horizontal Charge Configuration for Event 4, 165.5 Foot Spacing, HOB \approx 131.8 Feet, Photographed with a Hulcher Camera	18
2.2	Vertical Charge Configuration for Event 8, 49.86 Foot Spacing, HOB = 24.95 Feet, Photographed with a Hulcher Camera	19
2.3	Incident, Reflected and Mach-Region Shockwaves at a Little Less Than 80 Feet from GZ Above the Hard Reflective Surface Obtained from Event 8 at a Time \approx 28.4 Milliseconds Using a Fastax Camera.	21
2.4	Incident, Reflected and Mach-Region Shockwaves at a Little Less Than 80 Feet from GZ Below the Ideal Reflective Surface Obtained from Event 8 at a Time \approx 28.4 Milliseconds Using a Fastax Camera	22
2.5	Fireball Anomaly from Event 7 at a Time \approx 8.3 Milliseconds, Photographed Using a Fastax Camera	23
2.6	Fireball Anomaly and Distorted Shock Front from Event 7 at a Time \approx 21.4 Milliseconds	24
2.7	Incident, Reflected and Mach-Region Shockwaves at a Little More Than 60 Feet from GZ Above the Soft Reflective Surface Obtained from Event 11 at a Time \approx 23.3 Milliseconds with a Fastax Camera	26
2.8	Incident, Reflected and Mach-Region Shockwaves at a Little Less Than 80 Feet from GZ Above the Soft Reflective Surface Obtained from Event 11 at a Time \approx 28.4 Milliseconds with a Fastax Camera	27
2.9	Incident, Reflected and Mach-Region Shockwaves at a Little More Than 60 Feet from GZ Below the Ideal Reflective Surface Obtained from Event 11 at a Time \approx 23.3 Milliseconds with a Fastax Camera	28

LIST OF ILLUSTRATIONS (Continued)

<u>Figure</u>		<u>Page</u>
2.10	Incident, Reflected and Mach-Region Shockwaves at a Little Less Than 80 Feet from GZ Below the Ideal Reflective Surface Obtained From Event 11 at a Time \approx 28.4 Milliseconds with a Fastax Camera	29
3.1	Fireballs from Simultaneous Detonations of Event 8, 1000-Pound Pentolite Spheres, HOB \approx 24.45 Feet, Frame 2, Photographed with a Hulcher Camera	38
3.2	Event 8, Frame 5, Time \approx 0.25 Second	39
3.3	Event 8, Frame 8, Time \approx 0.40 Second	40
3.4	Event 8, Frame 15, Time \approx 0.75 Second	41
3.5	Event 8, Frame 20, Time \approx 1.00 Second	42
3.6	Event 8, Frame 25, Time \approx 1.25 Seconds	43
3.7	Sequences from 216-Pound Pentolite Spheres, HOB \approx 15 Feet, Obtained with a Hycam Camera	44
3.8	Shockwaves Intersections from Event 12, Delay Time of Zero, Frame 58, Time \approx 13.2 Milliseconds, Photographed with a Fastax Camera	46
3.9	Shockwaves Intersection from Event 13, Delay Time of 10.09 Milliseconds, Frame 59, Time \approx 13.2 Milliseconds, Photographed with a Fastax Camera	47
3.10	Shockwaves Intersection from Event 15, Delay Time of 5.09 Milliseconds, Frame 69, Time \approx 14.4 Milliseconds, Photographed with a Fastax Camera	48
3.11	Shockwaves Intersections from Event 16, Delay Time 2.90 Milliseconds, Frame 62, Time \approx 14.4 Milliseconds, Photographed with a Fastax Camera	49
3.12	Shockwave Position-Time from DRI Photographic Data Points Along Real Reflective Surface from Event 8	52
3.13	Shockwave Position-Time from DRI Photographic Data Points Along Ideal Reflective Surface from Event 8	53
3.14	DRI Shockwave Position-Time Curve and BRL Gage Data Along Real Surface from Event 8, HOB \approx 25 Feet	54

LIST OF ILLUSTRATIONS (Continued)

<u>Figure</u>		<u>Page</u>
3.15	DRI Shockwave Position-Time Curve and BRL Gage Data Along Ideal Surface from Event 8, HOB \approx 25 Feet	55
3.16	DRI Shockwave Position-Time Curve Along Real Surface from Event 9, HOB \approx 15 Feet	56
3.17	DRI Shockwave Position-Time Curve Along Ideal Surface from Event 9, HOB \approx 15 Feet	57
3.18	DRI Shockwave Position-Time Curve and BRL Gage Data Along Real Surface from Event 10, HOB \approx 15 Feet	58
3.19	DRI Shockwave Position-Time Curve and BRL Gage Data Along Ideal Surface from Event 10, HOB \approx 15 Feet	59
3.20	DRI Shockwave Position-Time Curve and BRL Gage Data Along Real Surface from Event 11, HOB \approx 25 Feet	60
3.21	DRI Shockwave Position-Time Curve and BRL Gage Data Along Ideal Surface from Event 11, HOB \approx 25 Feet	61
3.22	DRI Shockwave Position-Time Curves from Events 8, 9, 10 and 11 Along Real Surfaces	62
3.23	DRI Shockwave Position-Time Curves from Events 8, 9, 10 and 11 Along Ideal Surfaces	63
3.24	DRI Shockwave Position-Time Curve and BRL Gage Data Along Real Surface from Event 12, HOB \approx 15 Feet	64
3.25	DRI Shockwave Position-Time Curve and BRL Gage Data Along Ideal Surface from Event 12, HOB \approx 15 Feet	65
3.26	DRI Shockwave Position-Time Curve and BRL Gage Data Along Real Surface from Event 12 Scaled to 1000-Pounds.	66
3.27	DRI Shockwave Position-Time Curve and BRL Gage Data Along Ideal Surface from Event 12 Scaled to 1000-Pounds	67
3.28	Comparison of DRI Shockwave Position-Time Curves Along Real Surface from Event 8 and Event 12 Scaled to 1000-Pounds	68
3.29	Comparison of DRI Shockwave Position-Time Curves Along Ideal Surface from Event 8 and Event 12 Scaled to 1000-Pounds	69

LIST OF ILLUSTRATIONS (Continued)

<u>Figure</u>		<u>Page</u>
3.30	DRI Shockwave Position-Time Curve and BRL Gage Data Along Real Surface from Event 13, HOB \approx 15 Feet	70
3.31	DRI Shockwave Position-Time Curve and BRL Gage Data Along Real Surface from Event 16, HOB \approx 15 Feet	71
3.32	DRI Free-Air Shockwave Position-Time Curve and BRL Gage Data from Event 13	72
3.33	DRI Free-Air Shockwave Position-Time Curve and BRL Gage Data from Event 15	73
3.34	Triple-Point Paths from Real and Ideal Surfaces from Event 8, HOB \approx 25 Feet	91
3.35	Triple-Point Paths from Real and Ideal Surfaces from Event 9, HOB \approx 15 Feet	92
3.36	Comparison of Triple-Point Paths from Real Surface of Events 8 and 9	93
3.37	Comparison of Triple-Point Paths from Ideal Surface of Events 8 and 9	94
3.38	Triple-Point Paths from Real and Ideal Surfaces of Event 10, HOB \approx 15 Feet	95
3.39	Triple-Point Paths from Real and Ideal Surfaces of Event 11, HOB \approx 25 Feet	96
3.40	Comparison of Triple-Point Paths from Real Surface of Events 10 and 11	97
3.41	Comparison of Triple-Point Paths from Ideal Surface of Events 10 and 11	98
3.42	Comparison of Upward and Downward Triple-Point Paths from Ideal Surface of Event 12, HOB \approx 15 Feet	99
3.43	Comparison of Triple-Point Paths from Real and Ideal Surfaces of Event 12, HOB \approx 15 Feet	100
3.44	Comparison of Triple-Point Paths from Real Surface of Events 12 and 13	101
3.45	Triple-Point Path from Real Surface of Event 16, HOB \approx 15 Feet	102

LIST OF ILLUSTRATIONS (Continued)

<u>Figure</u>	<u>Page</u>
3.46 DRI Intersection-Point Path Curve and Data Points for a 10 Millisecond Time-Delay from Event 13	105
3.47 AFWL Intersection-Point Path Curve and Data Points for a 10 Millisecond Time-Delay from Event 13	106
3.48 DRI and AFWL Intersection-Point Path Curves for a 10 Millisecond Time-Delay from Event 13	107
3.49 DRI Intersection-Point Path Curve and Data Points for a 5 Millisecond Time-Delay from Event 15	108
3.50 AFWL Intersection-Point Path Curve and Data Points for a 5 Millisecond Time-Delay from Event 15	109
3.51 DRI and AFWL Intersection-Point Path Curves for a 5 Millisecond Time-Delay from Event 15	110
3.52 DRI Intersection-Point Paths Curve and Data Points of Upper Path for a 3 Millisecond Time-Delay from Event 16	111
3.53 DRI Intersection-Point Paths Curve and Data Points of Lower Path for a 3 Millisecond Time-Delay from Event 16	112
3.54 AFWL Intersection-Point Paths Curve and Data Points of Upper Path for a 3 Millisecond Time-Delay from Event 16	113
3.55 AFWL Intersection-Point Paths Curve and Data Points of Lower Path for a 3 Millisecond Time-Delay from Event 16	114
3.56 Comparison of DRI and AFWL Intersection-Point Paths Curves of Upper Path for a 3 Millisecond Time-Delay from Event 16	115
3.57 Comparison of DRI and AFWL Intersection-Point Path Curves of Lower Path for a 3 Millisecond Time-Delay from Event 16	116
3.58 Comparison of DRI and AFWL Intersection-Point Path Curves of Both Lower and Upper Paths for a 3 Milli- second Time-Delay from Event 16	117

LIST OF ILLUSTRATIONS (Continued)

<u>Figure</u>	<u>Page</u>
3.59 DRI Shockwave Position-Time Curve and BRL Gage Data Along Real Surface from Event 17, HOB \approx 47 Feet	118
3.60 DRI Shockwave Position-Time Curve and BRL Gage Data Along Real Surface from Event 18, HOB \approx 60 Feet	119
3.61 DRI Shockwave Position-Time Curve and BRL Gage Data Along Real Surface from Event 19, HOB \approx 90 Feet	120
3.62 DRI Shockwave Position-Time Curve and BRL Gage Data Along Real Surface from Event 23, HOB \approx 120 Feet	121
3.63 DRI Shockwave Position-Time Curve and BRL Gage Data Along Real Surface from Event 24, HOB \approx 90 Feet	122
3.64 DRI Free-Air Shockwave Position-Time Curve and BRL Gage Data from Event 17, HOB \approx 47 Feet	124
3.65 DRI Free-Air Shockwave Position-Time Curve and BRL Gage Data from Event 18, HOB \approx 60 Feet	125
3.66 DRI Free-Air Shockwave Position-Time Curve and BRL Gage Data from Event 19, HOB \approx 90 Feet	126
3.67 DRI Free-Air Shockwave Position-Time Curve and BRL Gage Data from Event 20, HOB \approx 120 Feet	127
3.68 DRI Free-Air Shockwave Position-Time Curve and BRL Gage Data from Event 21, HOB \approx 144 Feet	128
3.69 DRI Free-Air Shockwave Position-Time Curve and BRL Gage Data from Event 22, HOB \approx 144 Feet	129
3.70 DRI Free-Air Shockwave Position-Time Curve and BRL Gage Data from Event 23, HOB \approx 120 Feet	130
3.71 DRI Free-Air Shockwave Position-Time Curve and BRL Gage Data from Event 24, HOB \approx 90 Feet	131
3.72 Triple-Point Path from Real Surface of Event 17, HOB \approx 47 Feet	141
3.73 Triple-Point Path from Real Surface of Event 18, HOB \approx 60 Feet	142

LIST OF ILLUSTRATIONS (Continued)

<u>Figure</u>		<u>Page</u>
3.74	Triple-Point Path from Real Surface of Event 19, HOB \approx 90 Feet	143
3.75	Triple-Point Path from Real Surface of Event 23, HOB \approx 120 Feet	144
3.76	Triple-Point Path from Real Surface of Event 24, HOB \approx 90 Feet	145
3.77	Comparison of Triple-Point Paths from Real Surface of Events 8, 9, 17, 18, 19, and 23.	146

LIST OF TABLES

<u>Table</u>		<u>Page</u>
2.1	Charge Composition and Configuration Data for Events 7 Through 24	30
2.2	Environmental Conditions at Shot Time	31
2.3	DRI Camera Listing for Events 7 Through 16	33
2.4	DRI Camera Listing for Events 17 Through 24	34
2.5	DRI Camera Fields-of-View for Shockwave Photography for Events 17 Through 24	35
3.1	Time-of-Arrival and Peak Pressure vs. Distance from DRI Photographic Records and BRL Gage Measurements During Event 8	74
3.2	Time-of-Arrival and Peak Pressure vs. Distance from DRI Photographic Records and BRL Gage Measurements During Event 9	75
3.3	Time-of-Arrival and Peak Pressure vs. Distance from DRI Photographic Records and BRL Gage Measurements During Event 10	76
3.4	Time-of-Arrival and Peak Pressure vs. Distance from DRI Photographic Records and BRL Gage Measurements During Event 11	77
3.5	Time-of-Arrival and Peak Pressure vs. Distance from DRI Photographic Records and BRL Gage Measurements During Event 12	78
3.6	Time-of-Arrival and Peak Pressure vs. Distance from DRI Photographic Records and BRL Gage Measurements During Event 12 Scaled to 1,000-Pounds	79
3.7	Time-of-Arrival and Peak Pressure vs. Distance from DRI Photographic Records and BRL Gage Measurements During Event 13	80
3.8	Time-of-Arrival and Peak Pressure vs. Distance from DRI Photographic Records and BRL Gage Measurements During Event 13 Scaled to 1,000-Pounds	81
3.9	Free-Air Time-of-Arrival and Peak Pressure vs. Distance from DRI Photographic Records and BRL Gage Measurements During Event 15	82

LIST OF TABLES (Continued)

<u>Table</u>	<u>Page</u>
3.10 Time-of-Arrival and Peak Pressure vs. Distance from DRI Photographic Records and BRL Gage Measurements During Event 16	83
3.11 Reflection Coefficients for Various Surface Materials . .	90
3.12 Time-of-Arrival and Peak Pressure vs. Distance from DRI Photographic Records and BRL Gage Measurements During Event 17	132
3.13 Time-of-Arrival and Peak Pressure vs. Distance from DRI Photographic Records and BRL Gage Measurements During Event 18	133
3.14 Time-of-Arrival and Peak Pressure vs. Distance from DRI Photographic Records and BRL Gage Measurements During Event 19	134
3.15 Time-of-Arrival and Peak Pressure vs. Distance from DRI Photographic Records and BRL Gage Measurements During Event 20	135
3.16 Time-of-Arrival and Peak Pressure vs. Distance from DRI Photographic Records and BRL Gage Measurements During Event 21	136
3.17 Time-of-Arrival and Peak Pressure vs. Distance from DRI Photographic Records and BRL Gage Measurements During Event 22	137
3.18 Time-of-Arrival and Peak Pressure vs. Distance from DRI Photographic Records and BRL Gage Measurements During Event 23	138
3.19 Time-of-Arrival and Peak Pressure vs. Distance from DRI Photographic Records and BRL Gage Measurements During Event 24	139

SECTION I

INTRODUCTION

1.1 OBJECTIVES

The objectives of this project were to photograph the detonation phenomena from singular and multiple bursts of high explosive (HE) charges in different orientations, i.e., horizontal, vertical and single, above a real ground surface. The multiple bursts in the vertical arrays were initiated simultaneously or nonsimultaneously. Most of the singular bursts were initiated at various height-of-bursts (HOB's) above a real ground surface. The photographic records contained information on fireball growth, shockwave interaction, incident and reflected shockwaves, Mach stem and triple-point paths, cloud rise and development and on whether or not there were any anomalous behaviors in the detonations as shown in Figures 1.1 and 1.2. Note the anomalies (jets) ahead of the fireball expansions.

1.2 BACKGROUND

The Denver Research Institute (DRI) under contract with the Defense Nuclear Agency (DNA) had participated in Operation SNOWBALL, DISTANT PLAIN, PRAIRIE FLAT and the MINE SHAFT, MIDDLE GUST and MIXED COMPANY Series for the express purpose of studying the detonation phenomena using optical instrumentation. The instrumentation included photographic, photoelectric, and spectrographic devices. Only the photographic devices were used on the DIPOLE WEST Series.

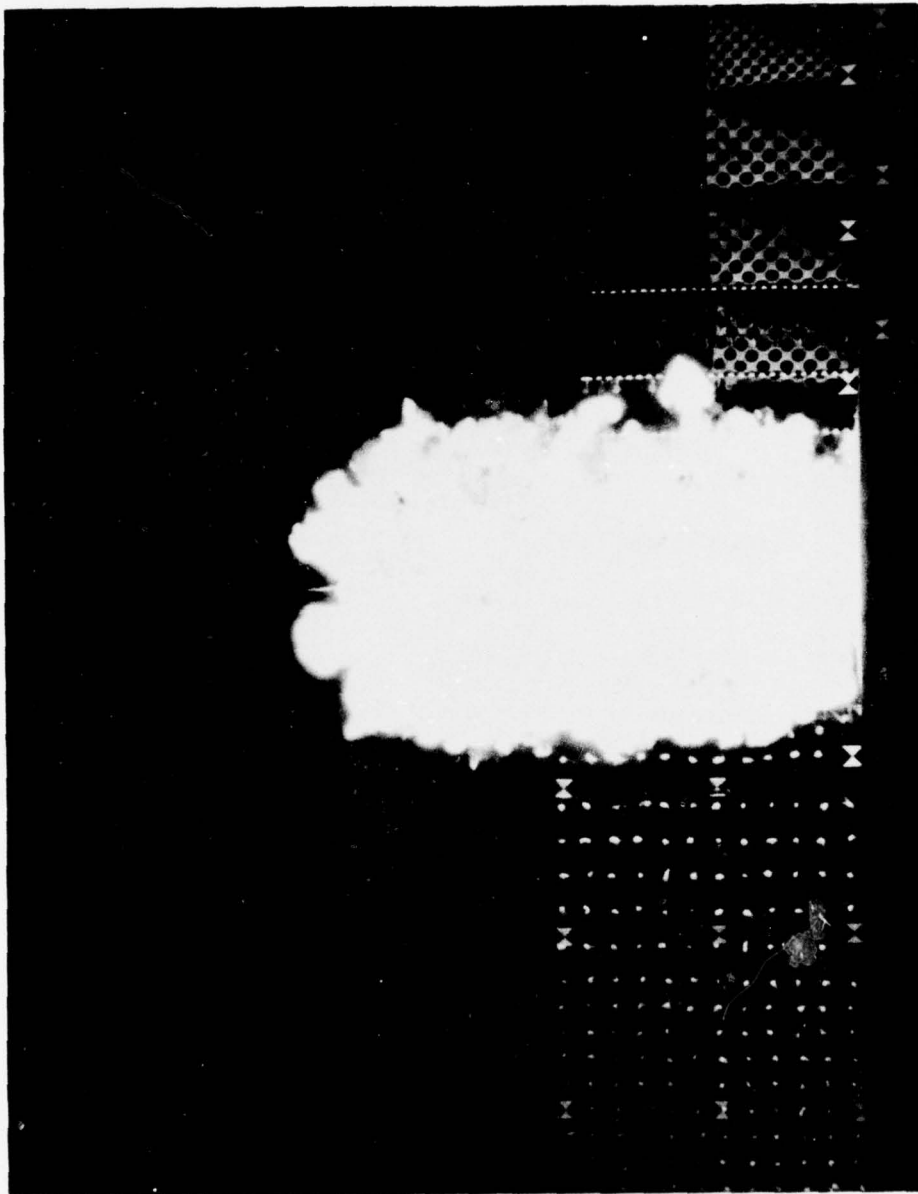


Figure 1.1 Fireball Anomaly from Event 7, Frame 1, Photographed with a Hulcher Camera.

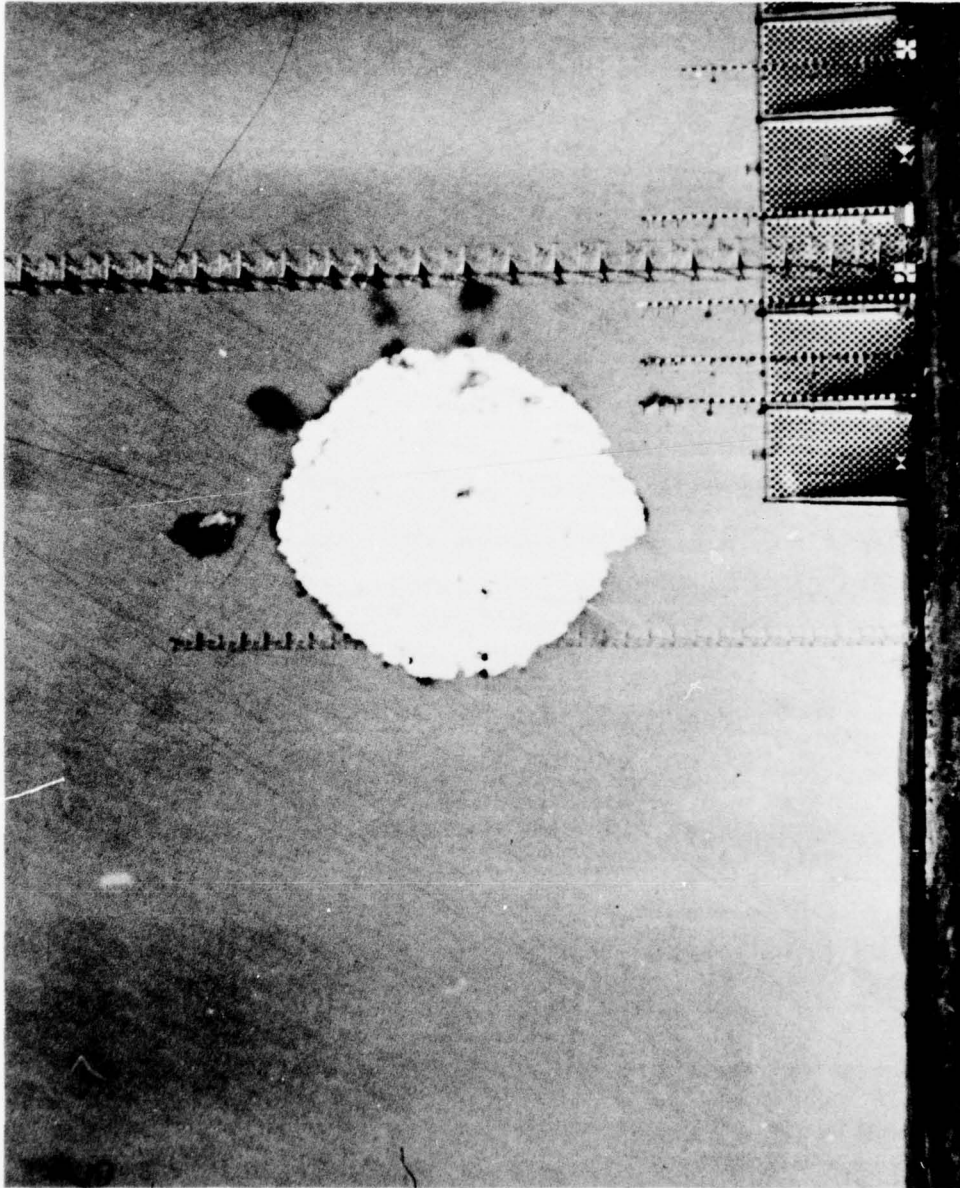


Figure 1.2 Fireball Anomalies from Event 19, Frame 1, Photographed with a Hulcher Camera.

1.3 THEORY

Two dimensional hydrodynamic codes have been developed which are capable of defining the airblast field and its various parameters resulting from nuclear detonations. Some of these codes have been modified to handle large high explosive detonations ranging from 20- to 500-ton of trinitrotoluene (TNT) and other types of HE materials. The results from the codes generally compared favorably with the HE experimental data except for the horizontal dynamic pressure near the ground surface. The discrepancy between the calculated and empirical data has been due to the assumption that the ground is a perfect reflector. In order to modify the code, it was necessary to obtain empirical data on the relationship between shockwave interaction with a real and an ideal reflecting surface. The tests related to this area of interest were detonated in a vertical configuration where the lower charge distance to the real (smooth or rough) surface was one half the distance between the two charges. This placed the ideal reflective surface half way between the two charges when the charges were initiated simultaneously (Phase 2). See Figure 1.3. Similar charge positions were employed for the nonsimultaneous detonations (Phase 3) for which no ideal reflective plane existed.

There was also a need of empirical data on the fireball/cloud interactions, rise and dissipation without the effects of ground reflected shockwaves. As a result, multiple burst tests were performed in a horizontal configuration at a relatively high height-of-burst (HOB); i.e., 125 feet (Phase 1). These multiple bursts gave various parameters

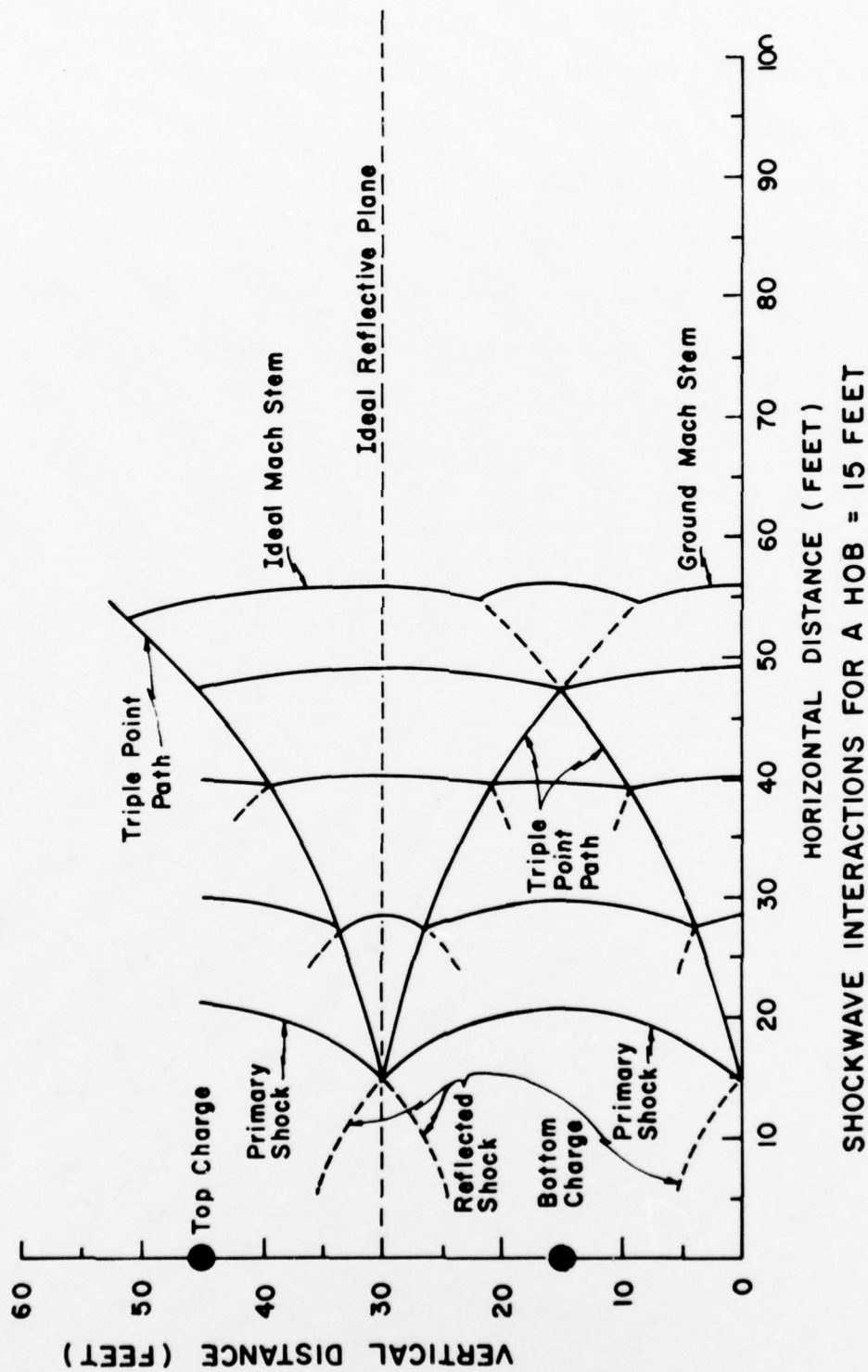


Figure 1.3 Pictorial Representation of Shockwave Interactions From Simultaneous Detonations.

related to the fireball/cloud growth which may be scaled to multiple nuclear detonations. Even though this phase of work was proposed after the formulation of the Phase 2 experimental procedures, it was performed prior to the main project effort which was directed toward the vertical charge configurations.

There were also some data needed to supplement the data obtained from the HOB Series performed at Defence Research Establishment Suffield in CY 1969. Phase 4 was performed to obtain these desired data.

SECTION II

PROCEDURE

2.1 EXPERIMENTAL SETUP

The detonation sources for Phase 1 of the DIPOLE WEST Series were center-initiated 1,000-pound spherical charges composed of either cast TNT or pentolite placed in horizontal orientations. The spheres used in the horizontal charge configurations were never mixed. There were six events in Phase 1. Two out of the six events were single detonations (Events 1 and 6). Event 1 utilized a pentolite charge while Event 6 employed a TNT charge. Of the remaining four events all but Event 5 utilized TNT spheres as the detonation sources. The actual charge spacings for the four multiple detonations were from 50 to 165.5 feet.

All the vertical charge configurations for Events 7 through 16 employed pentolite spheres. Events 7 through 11 (Phase 2) utilized 1000-pound charges while Events 12 through 16 (Phase 3) utilized 216-pound charges. Figures 2.1 and 2.2 show horizontal and vertical charge configurations for Events 4 and 8, respectively. The charges were suspended above the ground between two 200 foot towers which can be partially seen in Figure 2.2. These same towers were used to suspend the 1000-pound TNT spheres in the HOB series of Phase 4. The actual charge positions varied between 45.4 and 144.5 feet above the ground.

Ballistic Research Laboratory (BRL) pressure transducers were used to measure peak pressure, total pressure and time-of-arrival (position-time) from all events. The total number of pressure gages

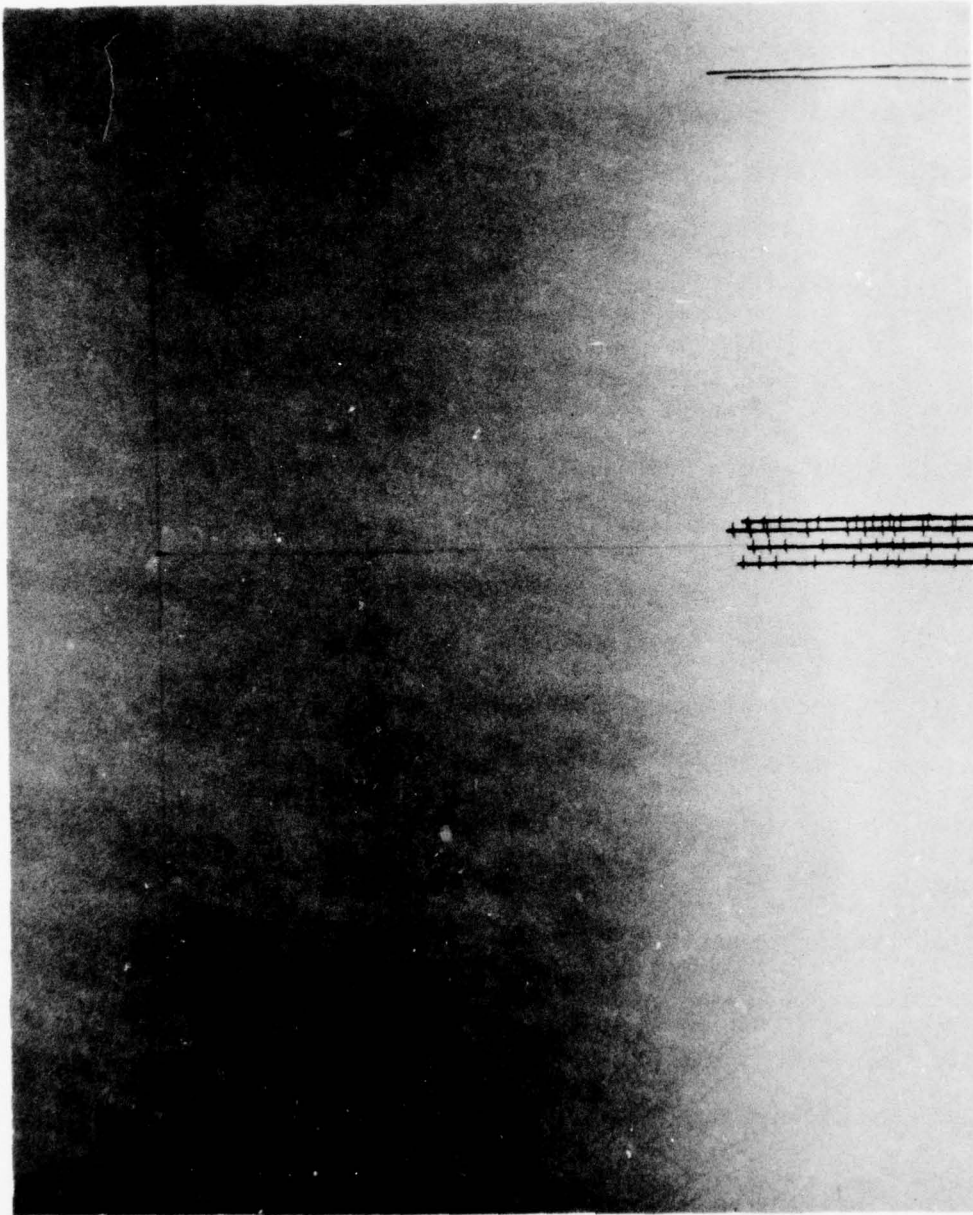


Figure 2.1 Horizontal Charge Configuration for Event 4, 165.5 Foot Spacing, HOB \approx 131.8 Feet, Photographed with a Hulcher Camera.

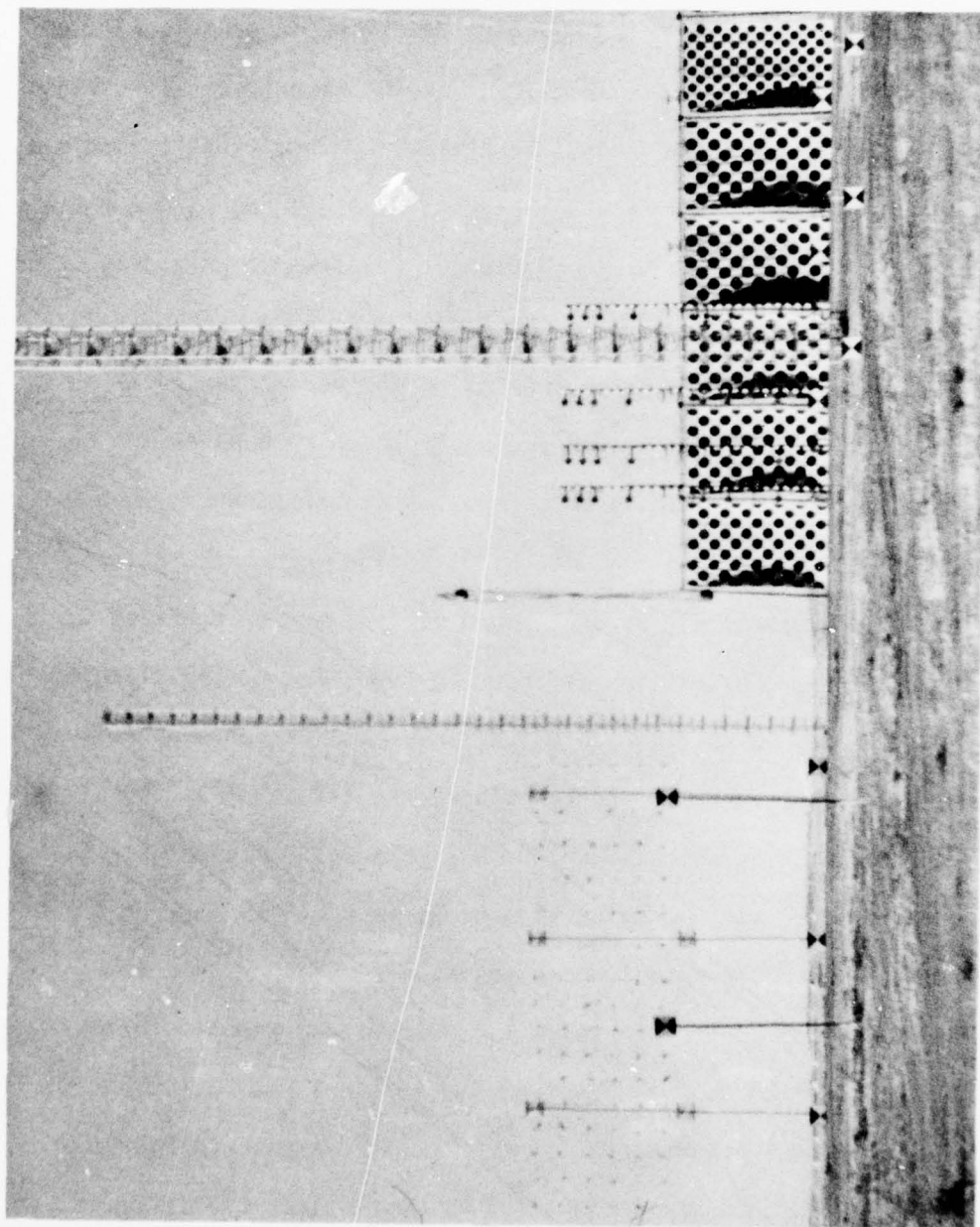


Figure 2.2 Vertical Charge Configuration for Event 8, 49.86 Foot Spacing, HOB = 24.95 Feet, Photographed with a Hulcher Camera.

was less for the horizontal configuration experiments than for either the vertical or the HOB experiments. The gages were mounted near and on the ground in the area around ground zero (GZ) and on four gun barrels as shown in Figures 2.1 and 2.2. The gun barrels were 54 feet high, except the last station was 53 feet high. In addition to pressure gages, smoke puffs and photographic backdrops were used so that the dynamics of shockwaves could be photographed. Figure 2.2 partially shows both the smoke puff array and the ten 50 x 30 foot photographic screens used as aids to photograph the motion of the shockwaves. Examples of the incident, reflected and Mach-region shockwaves and their triple-point as recorded against the photographic screen background are presented in Figures 2.3 and 2.4. The two vertical gun barrels, alternately painted black and white, are 40 and 60 feet to the right of GZ. In Figure 2.3 the shockwaves are at about 80 feet from GZ and along the hard ground surface, while in Figure 2.4, they are further away below the ideal reflective surface. An example of the effect of an anomaly on the shockwaves' interactions are shown in Figures 2.5 and 2.6. Compare the Mach-region shockwaves of Figures 2.4 and 2.6 to see the effect of the jet on the smoothness of the shock front.

The results presented in this report cover shockwave information derived from film records obtained from the vertical configurations and HOB experiments. The planned height-of-bursts for the lower charge of the multiple 1000-pound experiments were 15 and 25 feet and 15 feet for the 216-pound detonations. The positioning of the charges at the required heights was accomplished by placing the lower charge at a

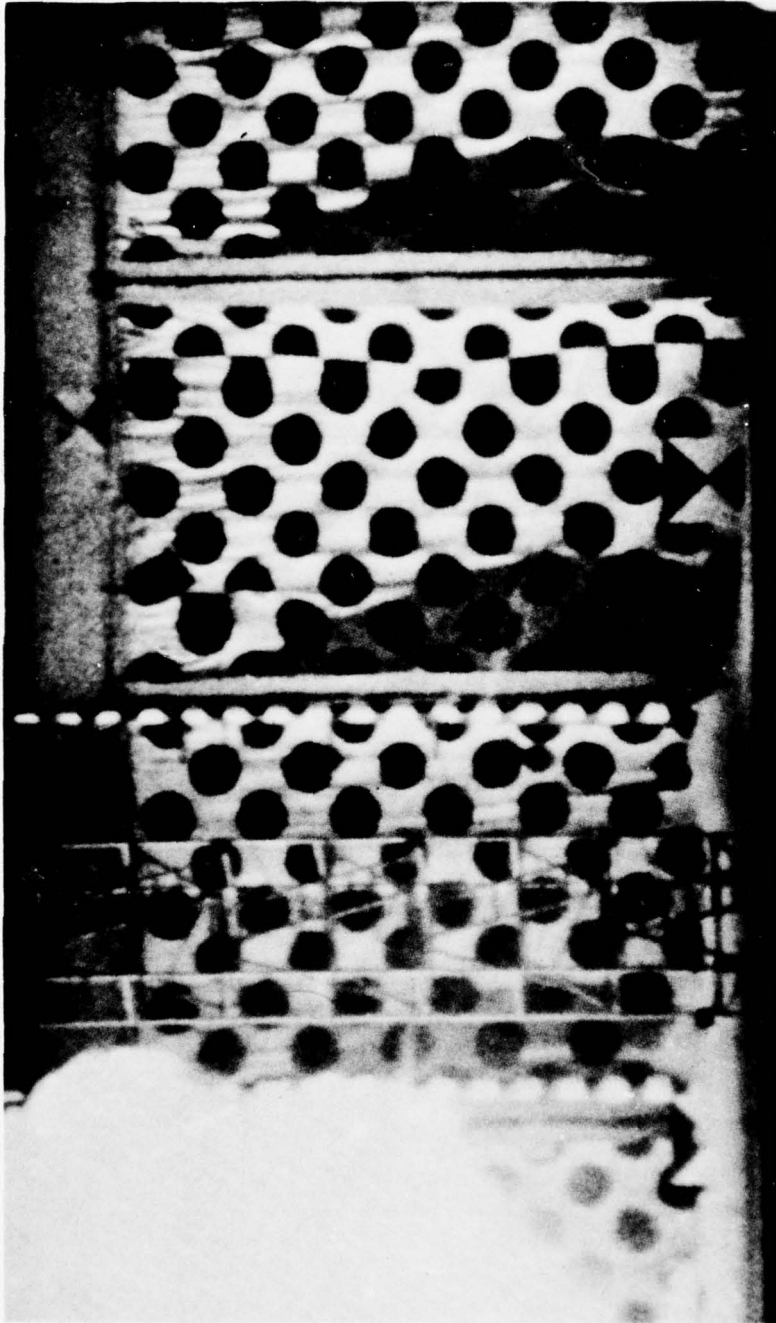


Figure 2.3 Incident, Reflected and Mach-Region Shockwaves at a Little Less Than 80 Feet from GZ Above the Hard Reflective Surface Obtained from Event 8 at a Time \approx 28.4 Milliseconds Using a Fastax Camera.

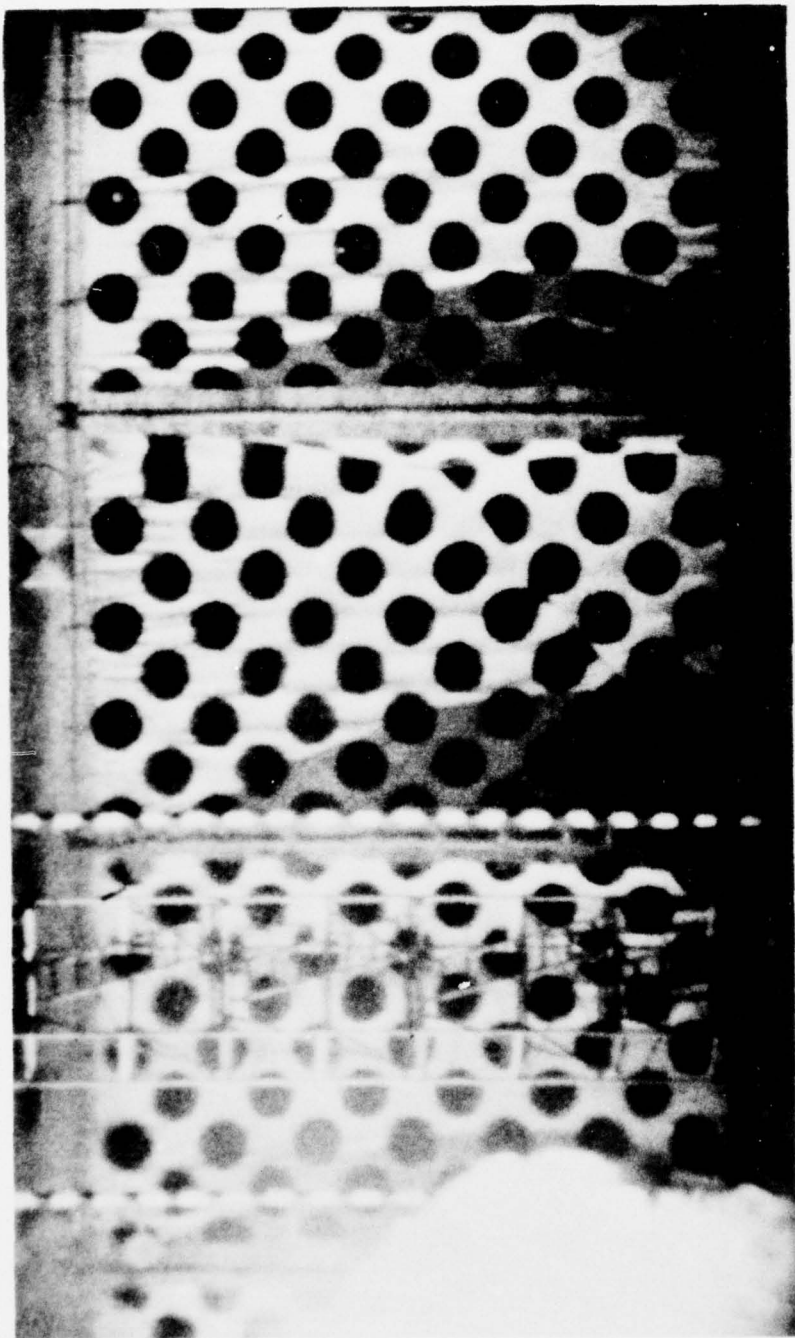


Figure 2.4 Incident, Reflected and Mach-Region Shockwaves at a Little Less Than 80 Feet from GZ Below the Ideal Reflective Surface Obtained from Event 8 at a Time ≈ 28.4 Milliseconds Using a Fastax Camera.

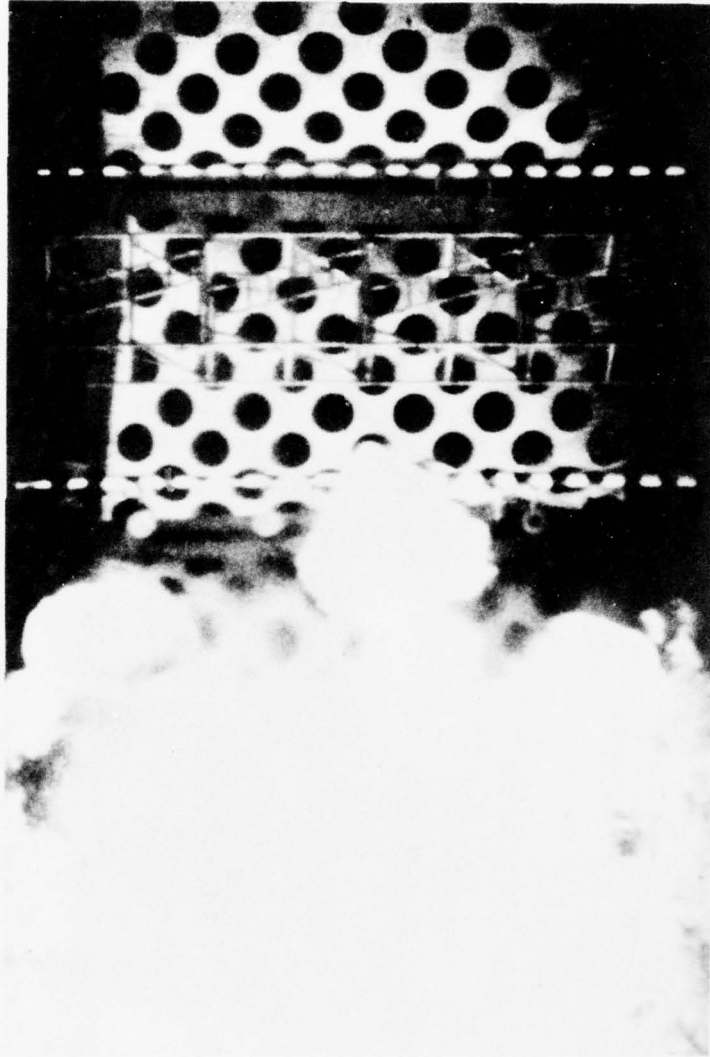


Figure 2.5 Fireball Anomaly from Event 7 at a Time ≈ 8.3 Milliseconds, Photographed Using a Fastax Camera.

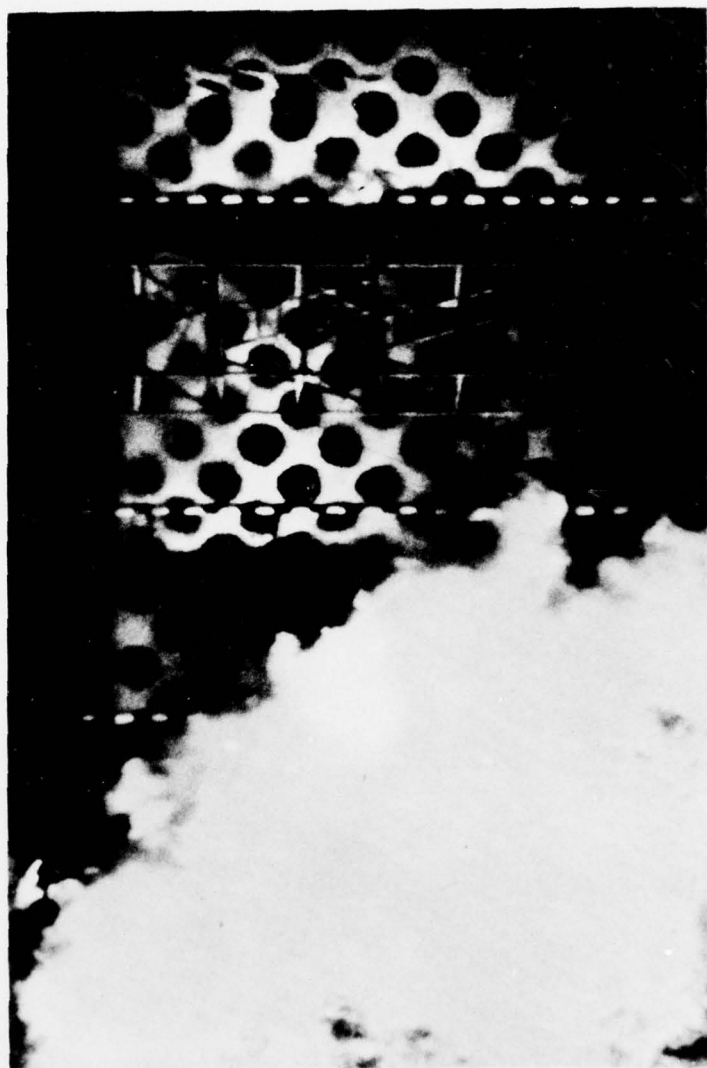


Figure 2.6 Fireball Anomaly and Distorted Shock Front from Event 7 at a Time ≈ 21.4 Milliseconds.

given HOB above the real surface and the upper charge at three times this HOB. When the charges were initiated simultaneously the ideal reflective plane was equidistant to the two charges, i.e., at two times the desired HOB. Ground zero for the ideal reflective plane is a point of intersection of the plane to a line drawn from the surface ground zero point through the center of both charges. The planned charge positions for the HOB Events were 47, 60, 90, 120, and 144 feet above the real reflective surface.

The two, real reflective surfaces for Phase 2 were natural alluvium (smooth) and irregular, soft ground (rough) which was obtained by plowing the natural alluvial surface in concentric furrows around GZ. The furrows were approximately 14 inches deep and contained small scattered amounts of snow which had been deposited over a number of days prior to the detonation of Events 10 and 11. Figures 2.7 through 2.10 present shockwave photographs from the ideal and soft reflective surfaces of Event 11.

The reflective surface for Phase 3 was a specially prepared surface of cemented soil topped with oil. The cement was mixed with the natural earth and water was added after smoothing the mixture. An oil topping was placed soon after the water was added. The surface was changed for the HOB Events to asphalt which extended out to about 70 feet from GZ.

Table 2.1 presents information on the charge HOB, weight and relative time delays for Events 7 through 24, and Table 2.2 presents environmental conditions which existed during shot time for the same events. (Refs. 1, 2, 3 and 4)



Figure 2.7 Incident, Reflected and Mach-Region Shockwaves at a Little More Than 60 Feet from GZ Above the Soft Reflective Surface Obtained from Event 11 at a Time = 23.3 Milliseconds with a Fastax Camera.

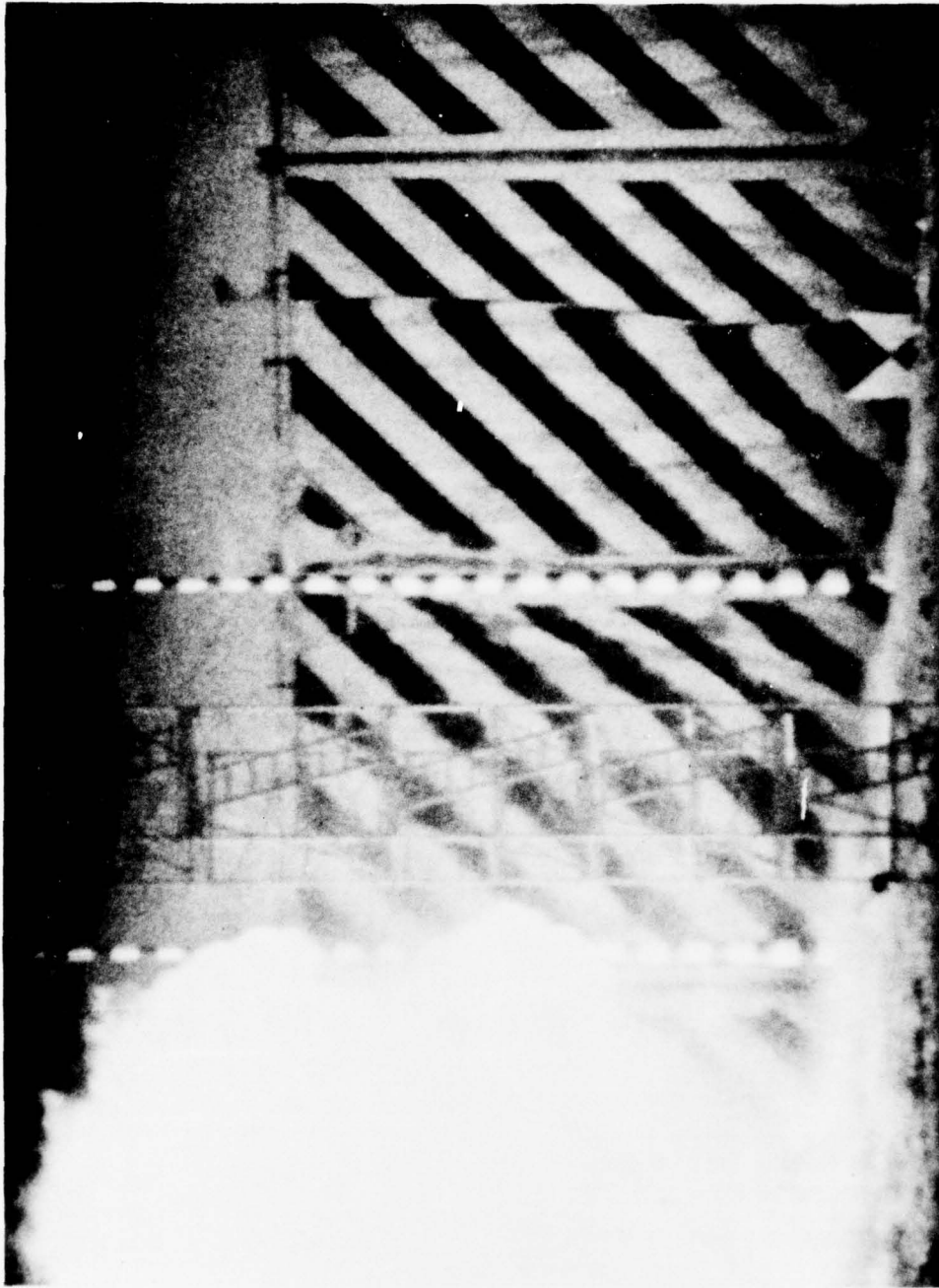


Figure 2.8 Incident, Reflected and Mach-REgion Shockwaves at a Little Less Than 80 Feet from GZ Above the Soft Reflective Surface Obtained from Event 11 at a Time = 28.4 Milliseconds with a Fastax Camera.

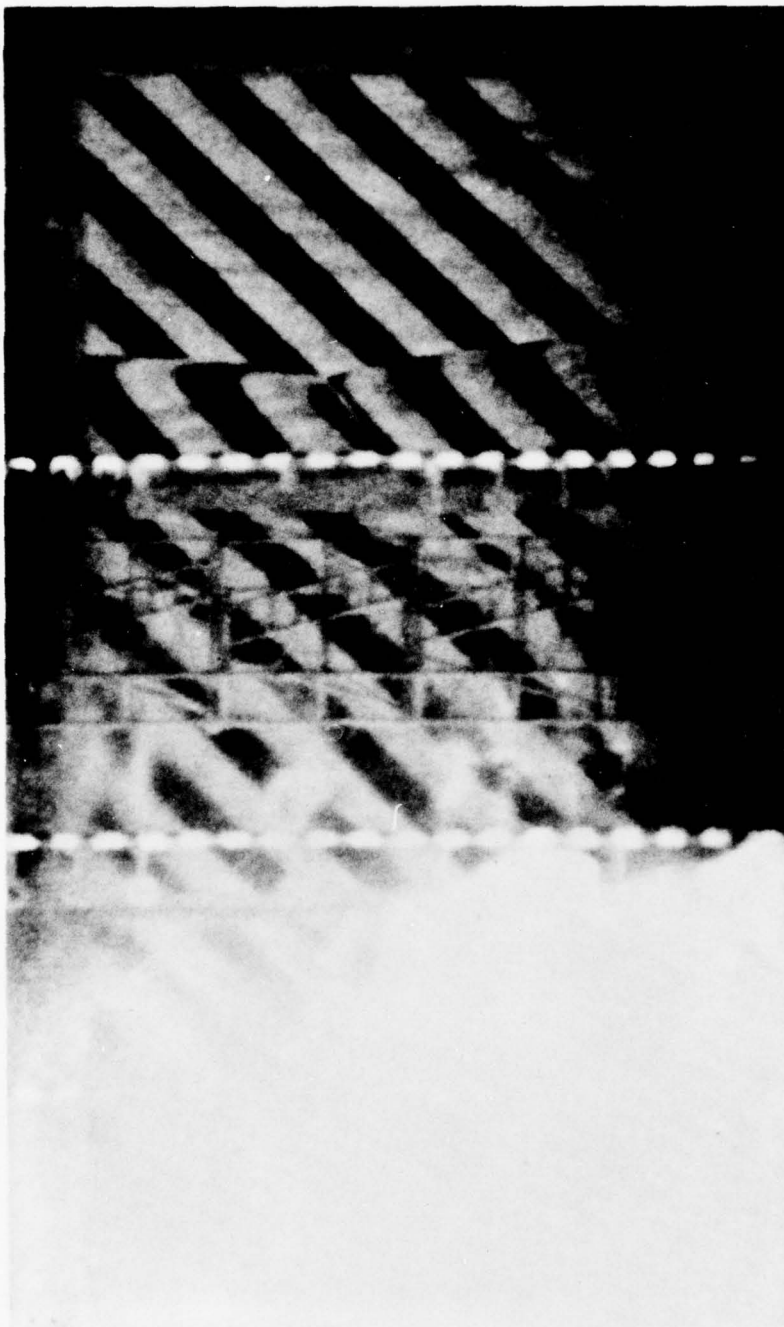


Figure 2.9 Incident, Reflected and Mach-Region Shockwaves at a Little More Than 60 Feet from GZ Below the Ideal Reflective Surface Obtained from Event 11 at a Time ≈ 23.3 Milliseconds with a Fastax Camera.

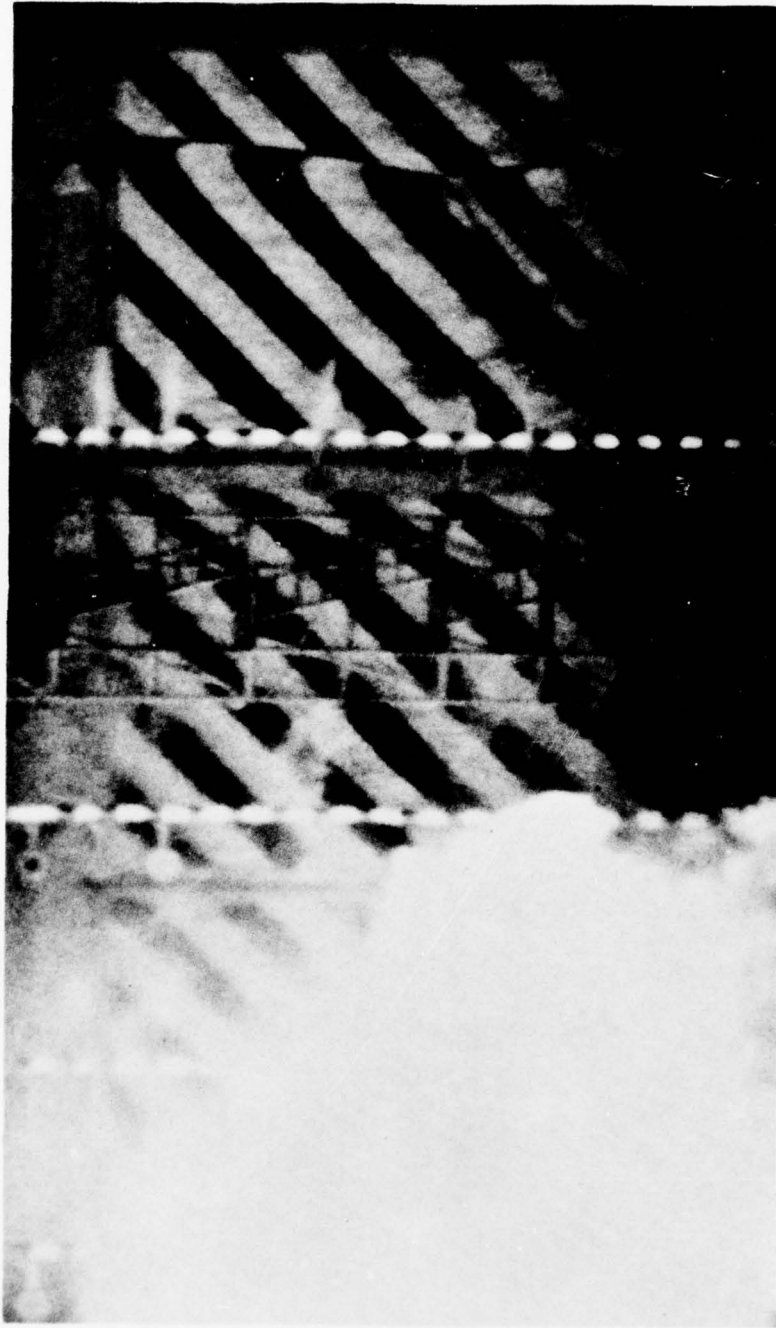


Figure 2.10 Incident, Reflected and Mach-Region Shockwaves at a Little Less Than 80 Feet from GZ Below the Ideal Reflective Surface Obtained From Event 11 at a Time ≈ 28.4 Milliseconds with a Fastax Camera.

TABLE 2.1

Charge Composition and Configuration Data for Events 7 Through 24

Event	No. of Charges	Charge Weight (pounds)	Charge Composition	Charge Separation (ft)		Charge HOB (ft)		Separation Time (msec)		Comments
				Planned	Actual	Planned	Actual	Planned	Actual	
7	2	1080	Pentolite	50	46.73	25	25.46	0	0	Smooth-Hard
8	2	1080	Pentolite	50	49.86	25	24.45	0	0	Smooth-Hard
9	2	1080	Pentolite	30	30.30	15	15.15	0	0	Smooth-Hard
10	2	1080	Pentolite	30	30.54	15	14.92	0	0	Soft-Rough
11	2	1080	Pentolite	50	50.13	25	23.99	0	0	Soft-Rough
12	2	216	Pentolite	30	30.11	15	14.74	0	0	Cemented*
13	2	216	Pentolite	30	30.01	15	14.86	10	10.09	Cemented*
14	1	216	Pentolite	30	-	15	14.86	-	-	Cemented*
15	2	216	Pentolite	30	30.09	15	14.87	5	5.09	Cemented*
16	2	216	Pentolite	30	30.29	15	15.05	3	2.90	Cemented*
17	1	1040	TNT	-	-	47	45.44	-	-	Asphalt
18	1	1040	TNT	-	-	60	60.18	-	-	Asphalt
19	1	1040	TNT	-	-	90	89.88	-	-	Asphalt
20	1	1040	TNT	-	-	120	120.65	-	-	Asphalt
21	1	1040	TNT	-	-	144	144.29	-	-	Asphalt
22	1	1040	TNT	-	-	144	144.47	-	-	Asphalt
23	1	1040	TNT	-	-	120	120.42	-	-	Asphalt
24	1	1040	TNT	-	-	90	89.82	-	-	Asphalt

*Cemented-soil-oil

TABLE 2.2

Environmental Conditions at Shot Time

Event	Date	Firing Time	Ambient Pressure (psi)	Temp. (F°)	Relative Humidity (%)	Wind Velocity (mph) @ 2 Meters @ 14 Meters	Wind Direction @ 2 Meters (°)	Sky Conditions**
7	9/4/73	1650 MDT	13.59	72.1	37	7.9 10.0*	330	Clear
8	9/17/73	1730 MDT	13.52	67.5	31	2.5 6.5*	150	Bright, 4/10 CI
9	10/22/73	1156 MDST	13.49	57.5	55	3.8 4.5*	245	Sun Moderate, 6/10 CI
10	11/2/73	1400 MDST	13.69	21.3	81	7.2 7.5*	030	Sun Slightly Visible, 4/10 CI
11	11/8/73	1535 MDST	13.68	-2.4	60	calm calm*	-	Sun Fairly Bright, 4/10 AC, 3/10 CI
12	10/24/74	1100 MDST	13.63	43.3	65	2.1 0.7	297	Bright Sunshine Scattered CI
13	10/28/74	1200 MST	13.26	63.0	67	calm	-	Bright, 3/10 CI
14	10/30/74	1500 MST	13.46	39.8	86	4.8 5.4	110	Overcast, SC
15	11/1/74	1200 MST	13.47	35.7	68	6.7 7.2	071	Overcast, SC
16	6/10/75	1450 MST	13.58	73.2	27	2.7 4.7	295	Bright, Scattered CI
17	6/23/75	1405 MST	13.49	81.4	42	10.8 6.4	155	Sunshine, Scattered CU, Broken CI
18	7/3/75	1115 MST	13.59	81.2	63	3.1 2.7	340	Clear
19	7/9/75	1051 MST	13.82	78.1	46	2.5 4.1	065	Sunny, Scattered CU
20	7/22/75	1058 MST	13.54	73.8	54	6.1 7.0	315	Scattered to Broken CU
21	8/6/75	1302 MST	13.46	74.5	51	0.9 1.5	265	Bright Sunshine Scattered AC
22	8/12/75	1313 MST	13.62	72.0	38	2.1 1.8	335	Bright Sunshine Scattered CU
23	8/14/75	1134 MST	13.64	67.0	45	1.7 2.6	075	Bright Sunshine Scattered CU and AC
24	8/18/75	1127 MST	13.50	65.0	68	0.9 1.1	325	Sunshine, Scattered CU, AC and CI

* @ 75 Feet Events 7 Thru 11

** Cloud Abbreviations: CI (Cirrus), CU (Cumulus), AC (Alto-Cumulus), SC (Strato-Cumulus)

2.2 INSTRUMENTATION AND FIELD OPERATION

The DIPOLE WEST Series were photographed from as many as five camera stations for Events 1 through 6 and four camera stations for Events 7 through 11 and backup to six stations for Events 17 through 24. The cloud development and rise for Event 1 through 6 were photographed at three remote stations located at approximately 0° (north), 120° and 240° at distances of 2,300 to 2,500 feet from GZ. The main camera station (MCS) which housed the very early-time recording cameras, was located 600 feet from GZ at approximately 90° (Events 1 through 6) or 180° (Events 7 through 24). In addition, shockwave/surface interaction was photographed from a camera station located 1,000 feet from GZ at 270° (west) for Events 1 through 6. The smoke puffs and photographic backdrops which were viewed from the main camera station were used for Events 7 through 24.

The high-speed cameras were not only located on the ground surface at the main camera station but also in two tower locations 30 or 57 feet above the ground depending on the separation distance between the charges. During the HOB series the shockwave propagation out to over 360 feet from GZ was photographed from two additional stations (A & B) which were situated to one side of the main camera station at locations which kept the backdrop screens in view. Tables 2.3, 2.4 and 2.5 present camera information for Events 7 through 24.

The Defence Research Establishment Suffield (DRES) was responsible for the timing and firing (T&F) and the smoke-puff technical photography; whereas, the Denver Research Institute was responsible for the technical photography of the shockwaves along the real and ideal

TABLE 2.3

DRI Camera Listing for Events 7 Through 16

<u>Camera Type</u>	<u>Position</u>	<u>Framing Rate</u>	<u>View</u>	<u>Field-of-View</u>
16mm Fastax	MCS GND	4500	Smoke Puffs	20-80
16mm Fastax	MCS GND	4500	Backdrop	20-80
16mm Fastax	MCS 30' or 57' above GND	4500	Smoke Puffs	20-80
16mm Fastax	MCS 30' or 57' above GND	4500	Backdrop	20-80
16mm Milliken	MCS 30' or 57' above GND	400	Fireball/Cloud	120-0-120
16mm Dynafax	MCS GND	25,000	Fireball	60-0-60
16mm Hycam	MCS GND	6000	Fireball	60-0-60
16mm Eastman	MCS GND	3000	Smoke Puffs	0-120
16mm Eastman	MCS GND	3000	Backdrop	0-120
70mm Hulcher	MCS GND	20	Fireball/Cloud	90-0-90
70mm Hulcher	MCS GND	20	Fireball/Cloud	250-0-250
16mm Fastax	60' from GZ Events 12 Through 16	6000	Strobe/Gage	59-61

TABLE 2.4

DRI Camera Listing for Events 17 Through 24

<u>Camera Type</u>	<u>Position</u>	<u>Framing Rate</u>	<u>View</u>	<u>Field-of-View</u>
16mm Nova	MCS	5000	Backdrop	(See Table 2.4)
16mm Fastax	MCS (A)	4500	Backdrop	(See Table 2.4)
16mm Fastax	MCS (A)	4500	Backdrop	(See Table 2.4)
16mm Fastax	MCS (B)	4500	Backdrop	(See Table 2.4)
16mm Fastax	MCS (B)	4500	Backdrop	(See Table 2.4)
16mm Milliken	MCS 30'	400	Fireball/Cloud	120-0-120
16mm Milliken	MCS	400	Fireball/Cloud	180-0-180
16mm Hycam	MCS	6000	Fireball	60-0-60
70mm Hulcher	MCS	20	Fireball/Cloud	120-0-120
70mm Hulcher	MCS	20	Fireball/Cloud	120-0-120
16mm Fastax	75' from GZ	6000	Strobe/Gage	59-61

TABLE 2.5

DRI Camera Fields-of-View for Shockwave
Photography Events 17 Through 24

<u>Event</u>	<u>NOVA (ft)</u>	<u>Fastax 1 (ft)</u>	<u>Fastax 2 (ft)</u>	<u>Fastax 3 (ft)</u>	<u>Fastax 4 (ft)</u>
17	GZ-50	50-100	100-150	150-198	198-250
18	GZ-50	50-100	100-150	150-198	198-250
19	50-100	100-150	150-198	198-250	250-300
20	100-150	150-198	198-250	250-300	300-350
21	100-150	150-198	198-250	250-300	300-350
22	100-150	150-198	198-250	250-300	300-350
23	100-150	150-198	198-250	250-300	300-350
24	50-100	100-150	150-198	198-250	250-300

reflective surfaces with the photographic screens in the background and all other aspects of the detonation phenomena.

The DRES T&F bunker was located approximately 1,500 feet from GZ near the BRL recording van which contained tape decks and conditioning equipment which recorded the dynamics of the shockwave interactions.

SECTION 3

RESULTS AND DISCUSSION

The results and discussion from seven of the nine vertical configuration experiments (Events 7 through 16) and all eight of the HOB experiments (Events 17 through 24) are presented in the following paragraphs. Event 7 produced a fireball anomaly (jet) which degraded the shockwaves that developed along the real and ideal reflective surfaces in the direction of the photographic backdrops; also, Event 14 was detonated under poor ambient light conditions so that no good photographic records were available for data reduction. As a result, Events 7 and 14 data are omitted from this report.

Figures 3.1 through 3.6 show a sequence of photographs of the fireballs from Event 8 which were obtained from two simultaneously detonated 1,000-pound pentolite spheres positioned at a planned HOB of 25 feet. Figure 3.7 presents fireball sequences from simultaneous and nonsimultaneous detonations which were obtained from 216-pound pentolite spheres placed at a planned HOB of 15 feet. Note how different the geometries of the fireballs are at similar times. The upper charge was always detonated before the lower charge during the nonsimultaneous events. The planned separation time of 10 milliseconds was the largest value used. This time increment was still short enough so as not to cause any adverse effect upon the second charge prior to its detonation. Figures 3.8 through 3.11 present shockwaves generated at nearly similar times from the events presented in Figure 3.7.

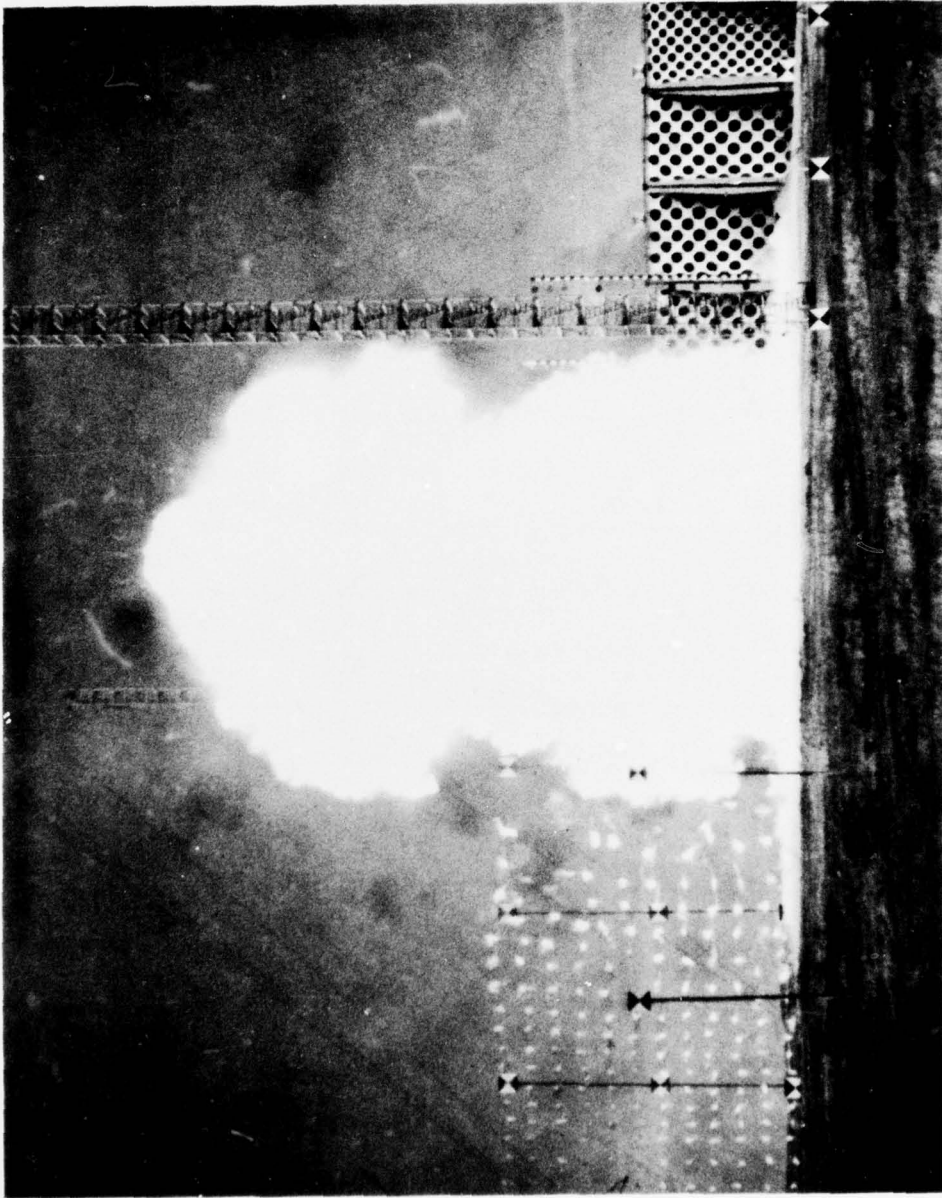


Figure 3.1 Fireballs from Simultaneous Detonations of Event 8, 1000-Pound Pentolite Spheres, HOB = 24.45 Feet, Frame 2, Photographed with a Hulcher Camera.

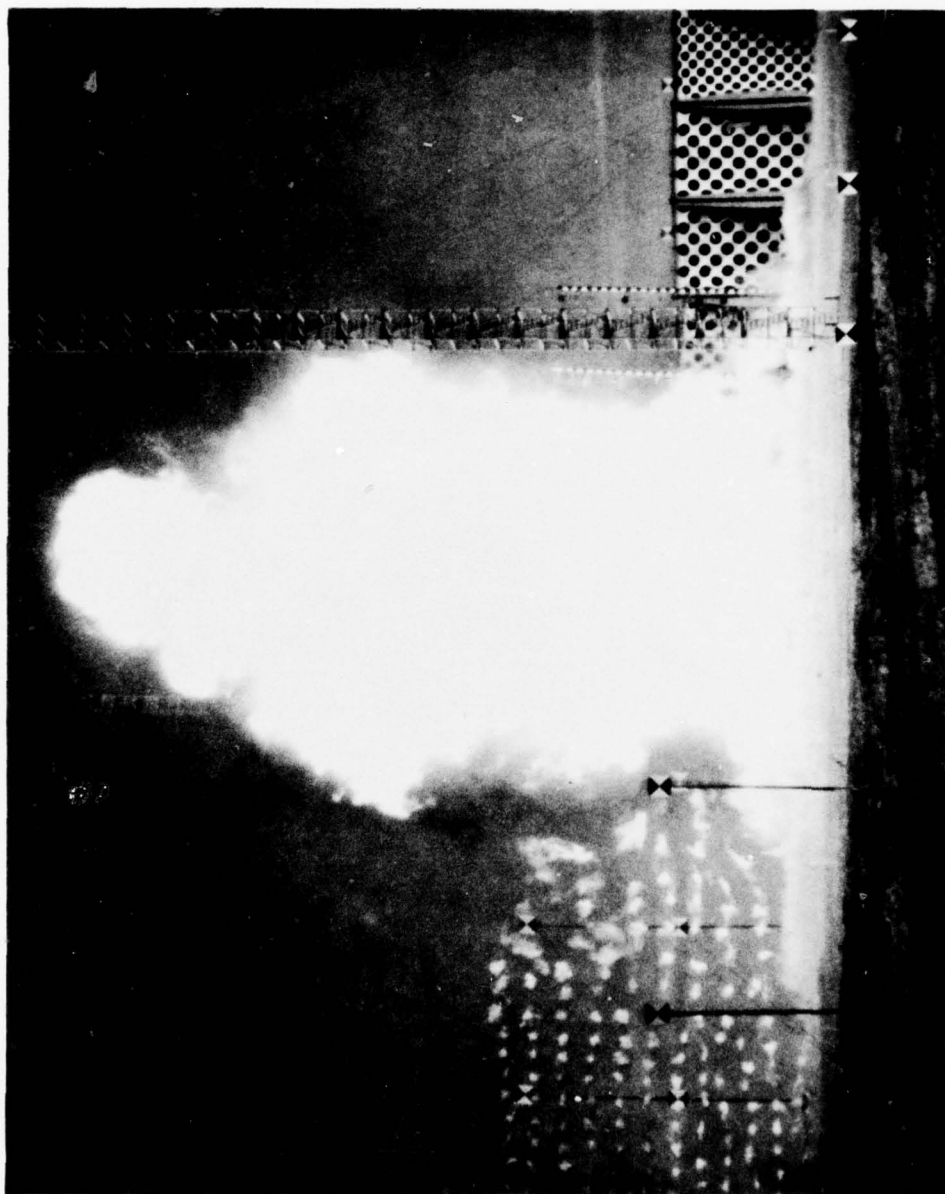


Figure 3.2 Event 8, Frame 5, Time ≈ 0.25 Second.

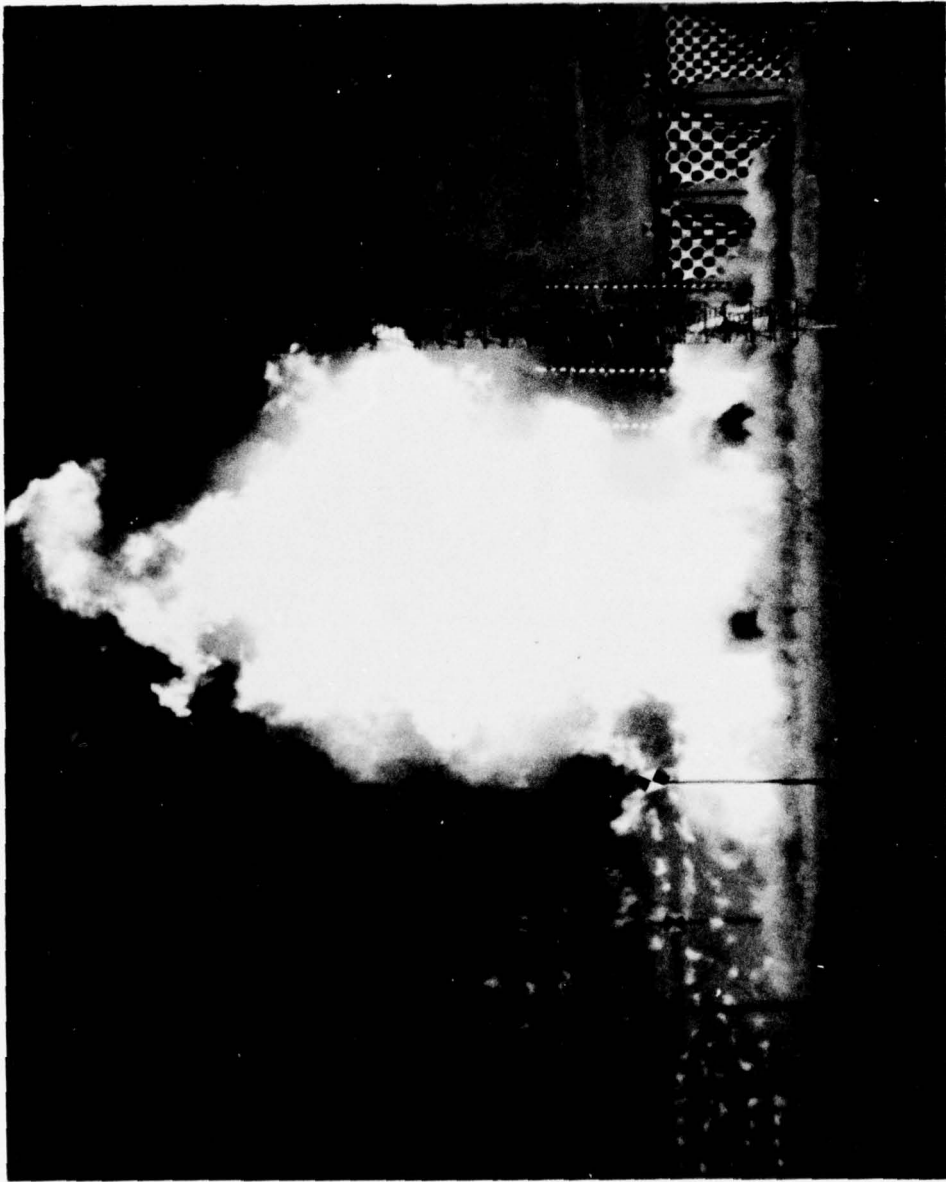


Figure 3.3 Event 8, Frame 8, Time ≈ 0.40 Second.

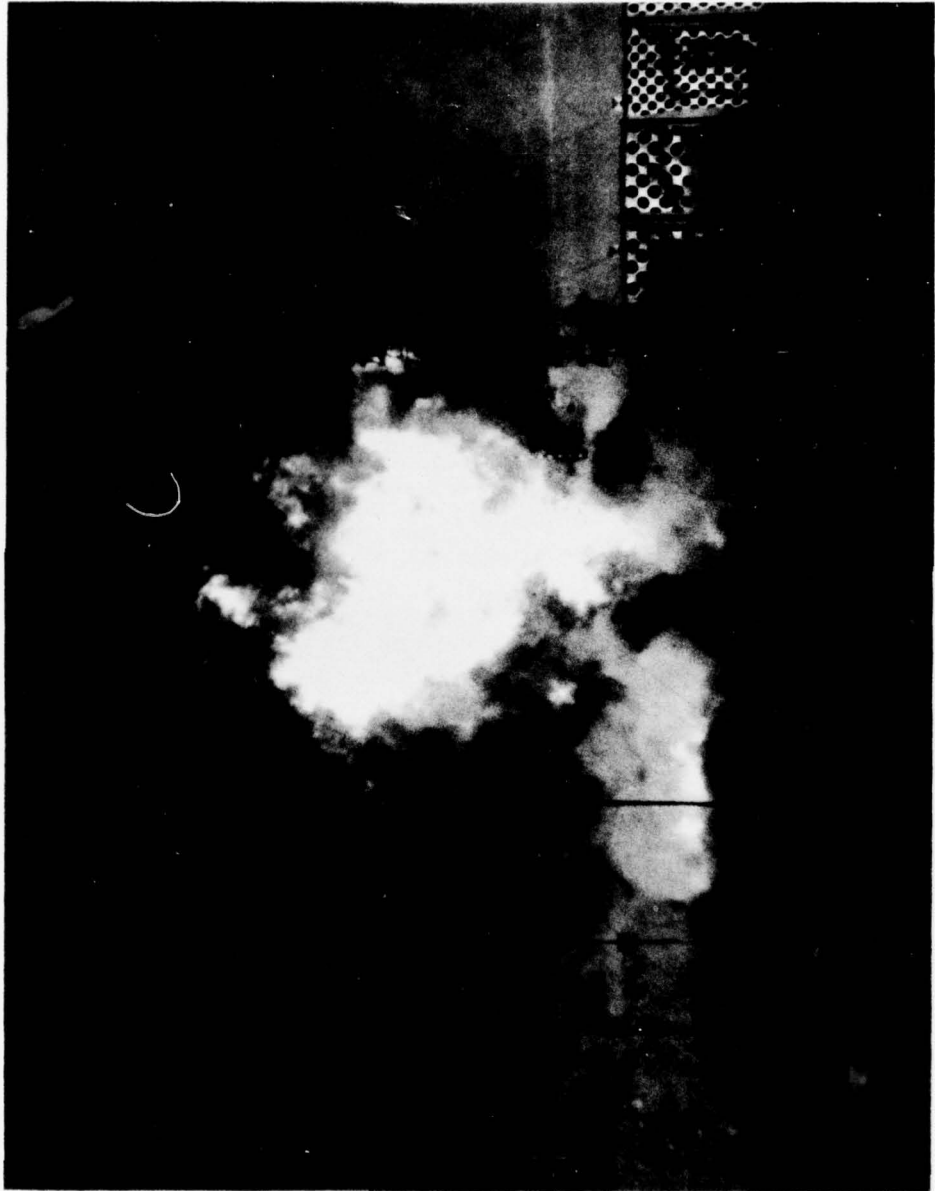


Figure 3.4 Event 8, Frame 15, Time ≈ 0.75 Second.

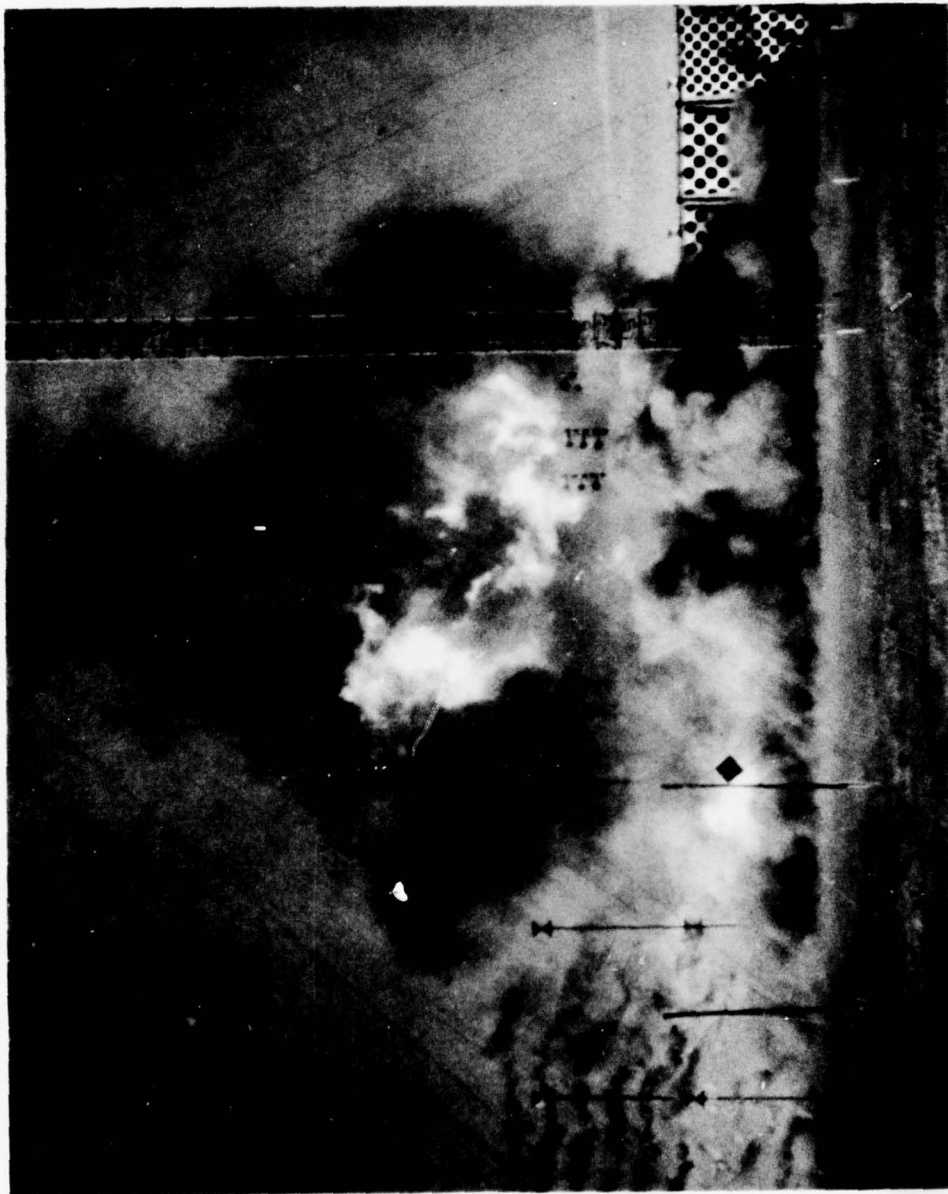


Figure 3.5 Event 8, Frame 20, Time \approx 1.00 Second.

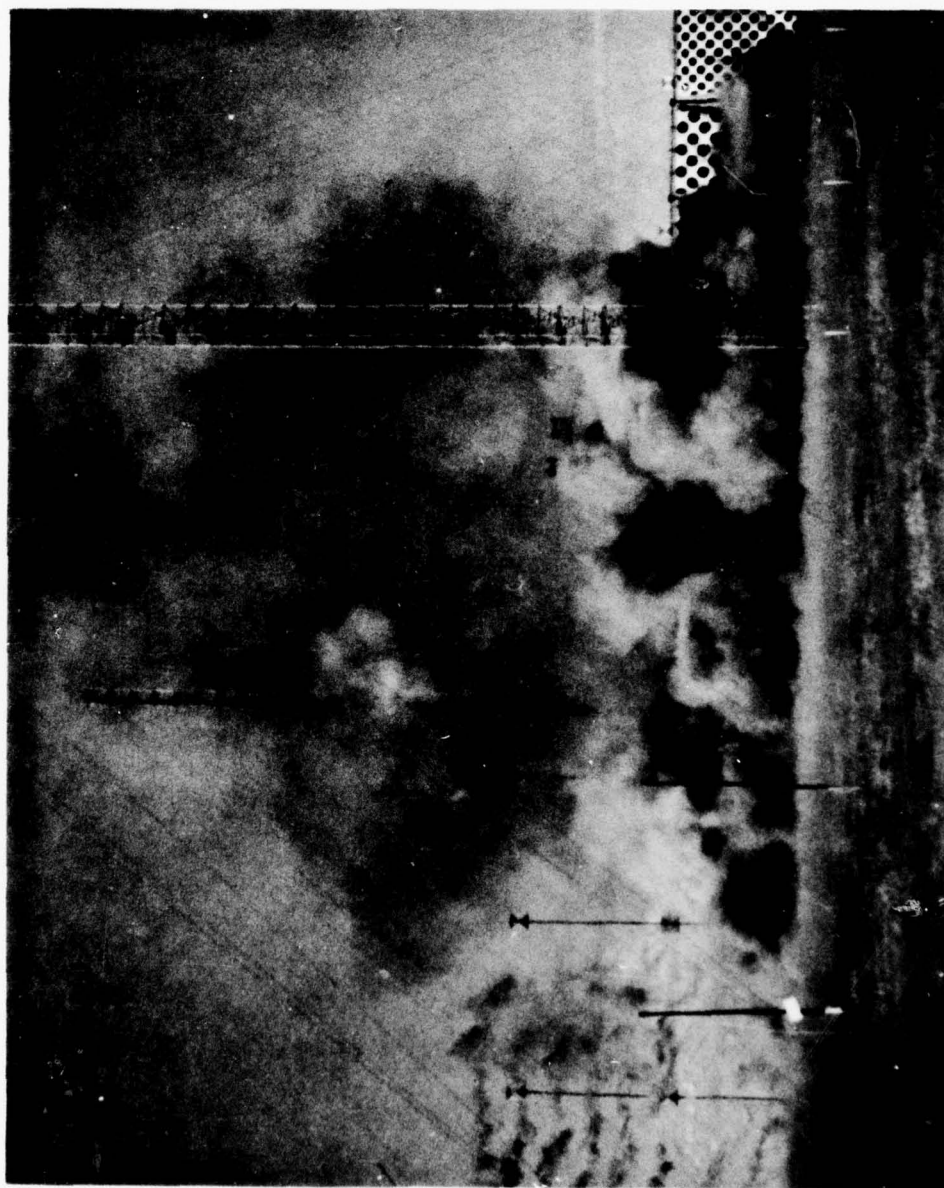
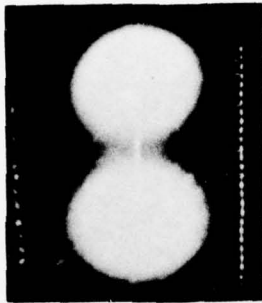


Figure 3.6 Event 8, Frame 25, Time = 1.25 Seconds.

DIPOLE WEST

1.5 mSEC

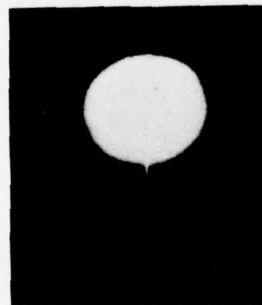


EVENT 12
SIMULTANEOUS
TIME

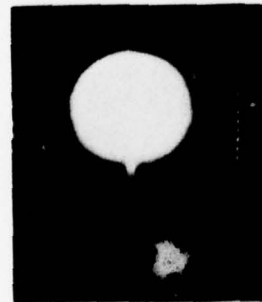
6.2 mSEC



EVENT 16
3 mSEC SEPARATION
TIME



EVENT 15
5 mSEC SEPARATION
TIME



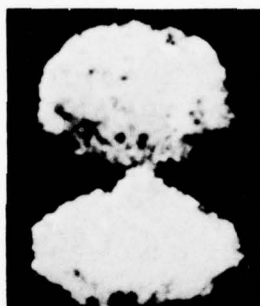
EVENT 13
10 mSEC SEPARATION
TIME



Figure 3.7 Sequences From 216-Pound Pentolite Spheres, HOB = 15 Feet, Obtained with a Hycam Camera.

DIPOLE WEST

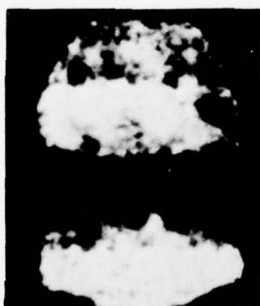
11.2 mSEC



16.3 mSEC



EVENT 12
SIMULTANEOUS
TIME



EVENT 16
3 mSEC SEPARATION
TIME



EVENT 15
5 mSEC SEPARATION
TIME



EVENT 13
10 mSEC SEPARATION
TIME

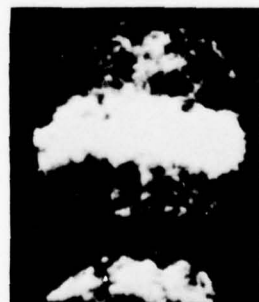


Figure 3.7 Continued

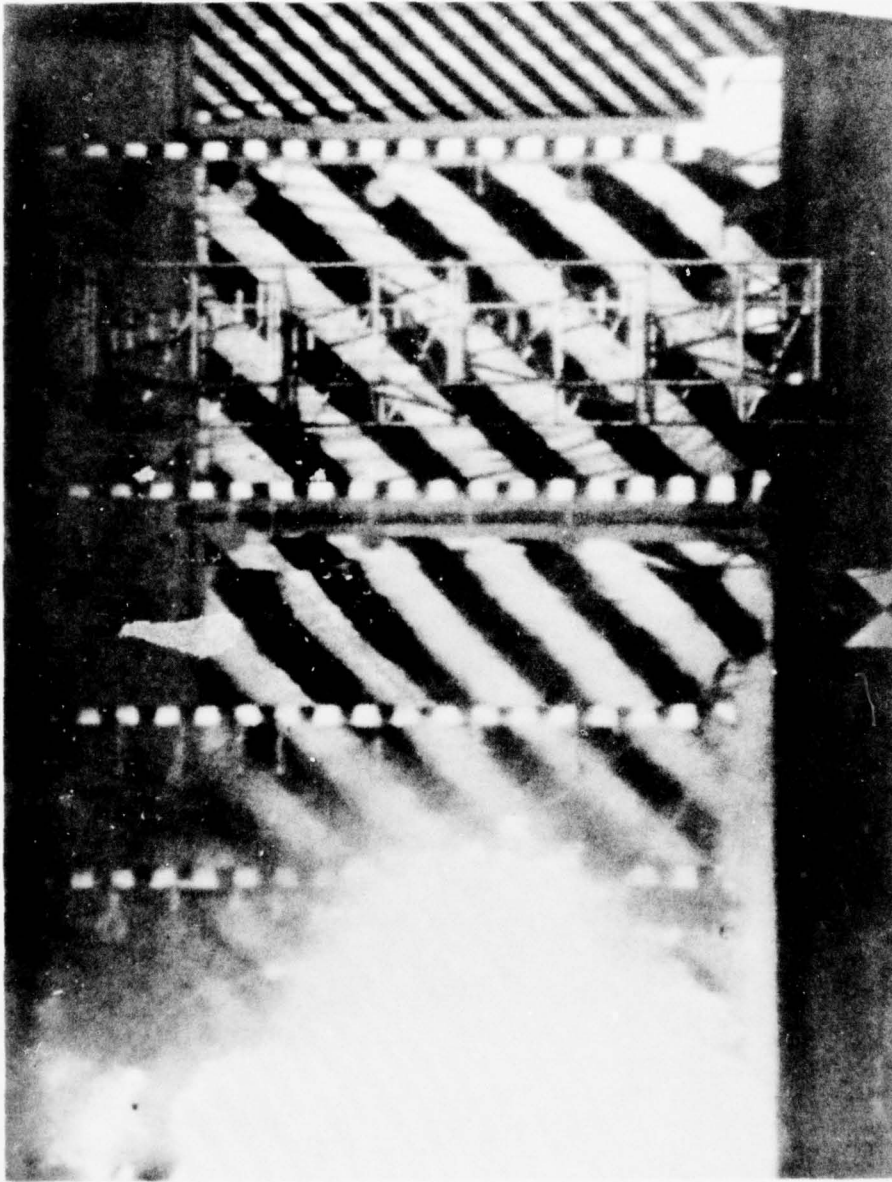


Figure 3.8 Shockwaves Intersections from Event 12, Delay Time of Zero, Frame 58, Time ≈ 13.2 Milliseconds, Photographed with a Fastax Camera.

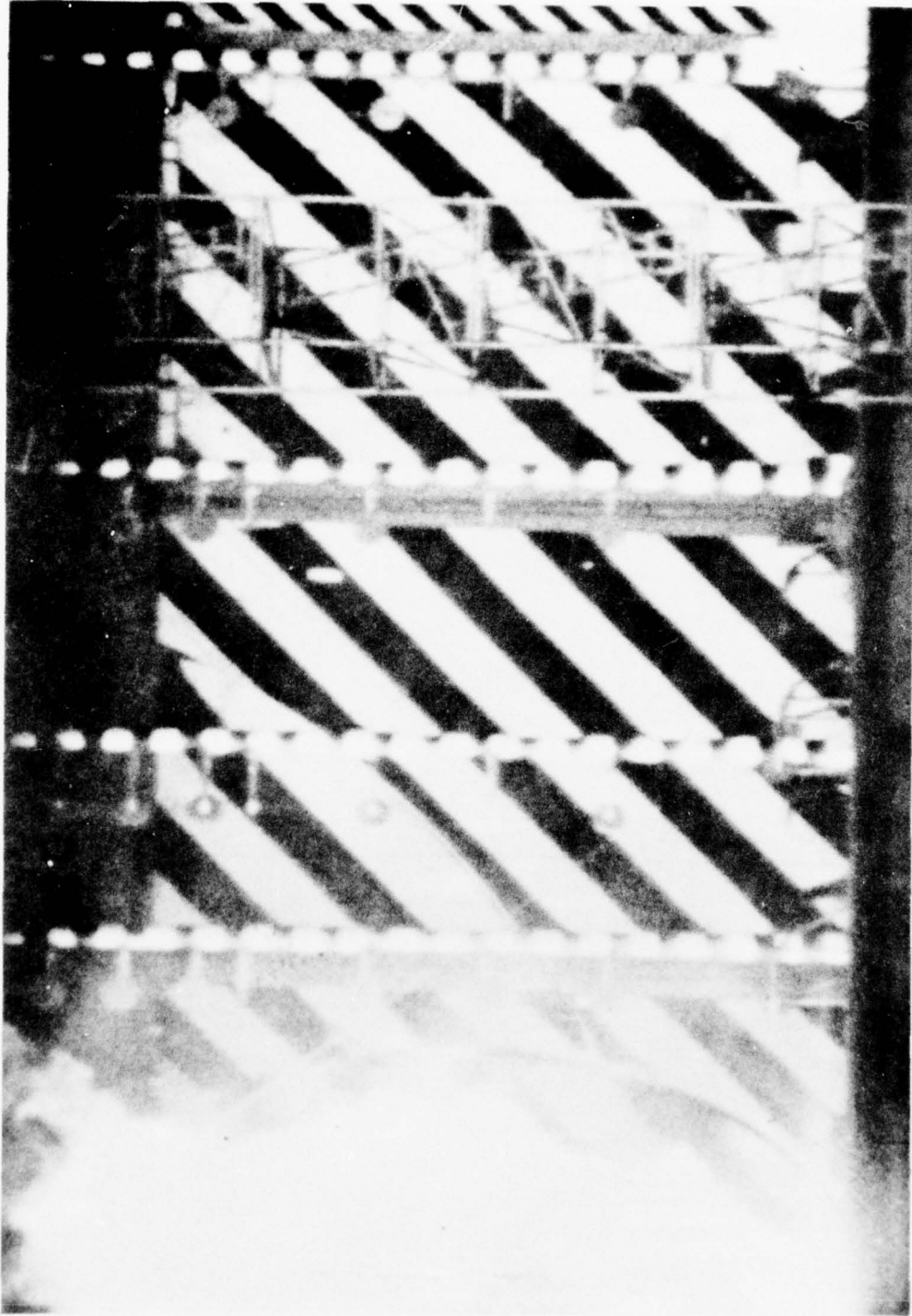


Figure 3.9 Shockwaves Intersection from Event 13, Delay Time of 10.09 Milliseconds, Frame 59, Time = 13.2 Milliseconds, Photographed with a Fastax Camera.

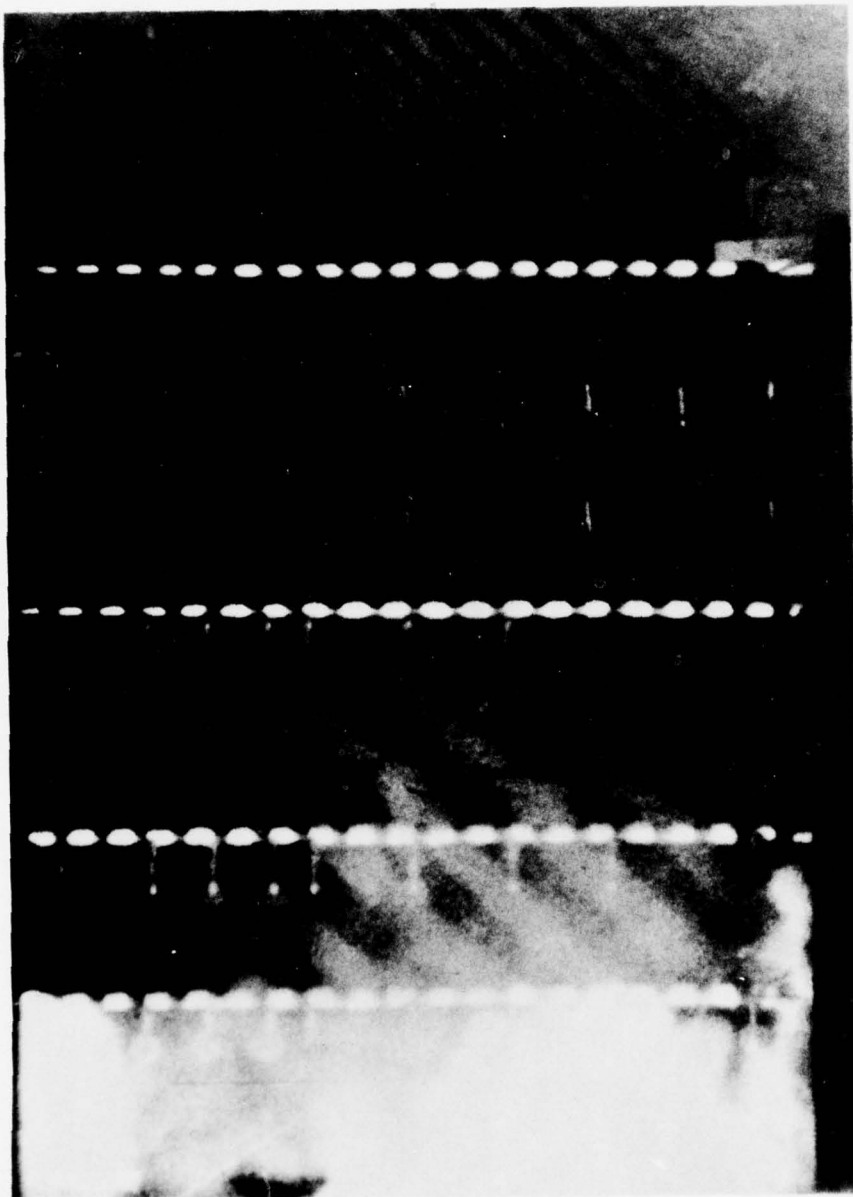


Figure 3.10 Shockwaves Intersection from Event 15, Delay Time of 5.09 Milliseconds,
Frame 69, Time \approx 14.4 Milliseconds, Photographed with a Fastax Camera.

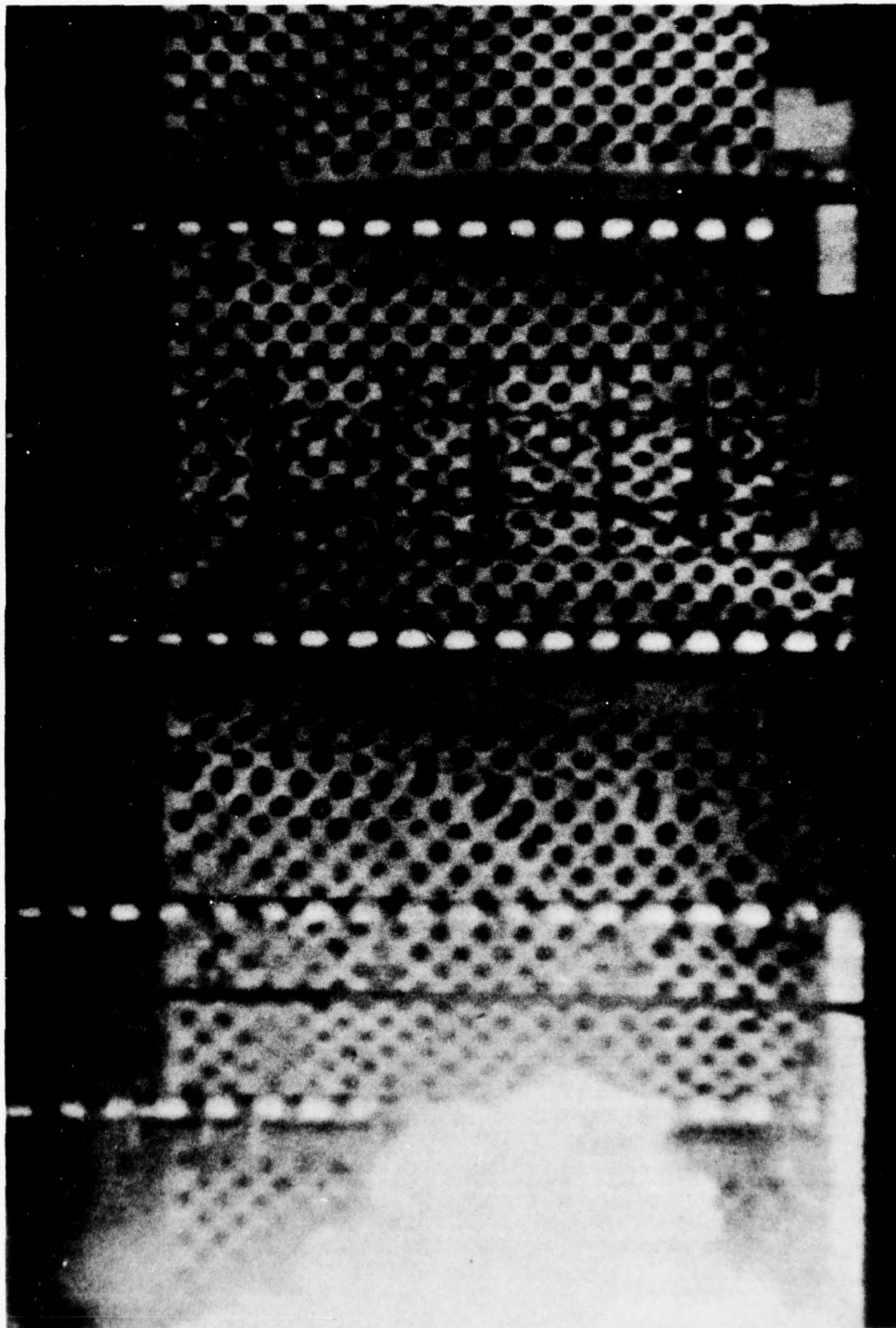


Figure 3.11 Shockwaves Intersections from Event 16, Delay Time 2.90 Milliseconds, Frame 62, Time \approx 14.4 Milliseconds, Photographed with a Fastax Camera.

The data which follow were derived from high-speed photographic sequences of shockwaves obtained with the aid of the photographic backdrops. Shockwave data derived from the smoke puff array will be presented in another document which will be forthcoming from the University of Victoria, B.C., Canada.

The position-time data of shockwaves from Events 7 through 16 were obtained over distances of approximately 35 to 85 feet from GZ along both the real and ideal reflective surfaces; whereas, free-air and Mach-region shockwaves' position-time data were obtained at distances ranging anywhere from 30 to 360 feet from GZ for the HOB Events 17 through 24. Least-squares 2nd degree curve fits were made to these data. Time-of-arrival data were derived from these curve fits at five foot increments over the range of measurements made. Slopes (incremental velocities) were determined at these same distances. These velocities were then used in the Rankin-Hugoniot equation to determine peak overpressures.

The simultaneity or the time differential of the multiple detonations were determined photographically from Dynafax camera records obtained at over 25,000 frames per second at an exposure time of under one microsecond and electronically with tape recording equipment. The photographic results indicated that the charges detonated on the average within 5 microseconds of each other for the simultaneous detonations and within 40 microseconds of the prescribed time differential for the nonsimultaneous detonations.

3.1 POSITION-TIME DATA FROM EVENTS 8 THROUGH 16

The DRI position-time curves from shockwaves photographed during Events 8 through 16 are plotted with BRL gage data in Figures 3.12 through 3.33 along both the real and ideal surfaces and in free-air (FA) with the exception of Figures 3.12 and 3.13 which present raw position-time data points obtained from DRI photographic records. These two figures are presented to show the degree of variations in the raw position-time data obtained photographically. Due to a loss of the detonation zero signal, BRL time-of-arrival gage data are missing from Event 9. Mach position-time data derived from the least-squares parabolic curve fits to the raw data are presented in Tables 3.1 through 3.10. Free-air shockwave positions were measured from the center of the upper charge (CC) during the nonsimultaneous detonations of Event 13 and 15. Due to poor ambient light, Event 15 position-time data are limited to FA only. Event 16 photographic records did not allow FA time-of-arrival to be obtained due to the small time differential of 3 milliseconds. The BRL FA gage data furnished with the DRI position-time data were obtained at gage distances from GZ of 20, 30, 40 and 60 feet at a height of 30 feet above the ground surface. The distances from CC to these gages give slant ranges of 22.4, 33.5, 44.7 and 67.0 feet. (Refs. 1 and 2)

There is generally good correlation between the photographic shockwave time-of-arrival data and the gage data for these events. There are some differences between the photographic data and the gage data for a few of the events. Since the photographed positions of the

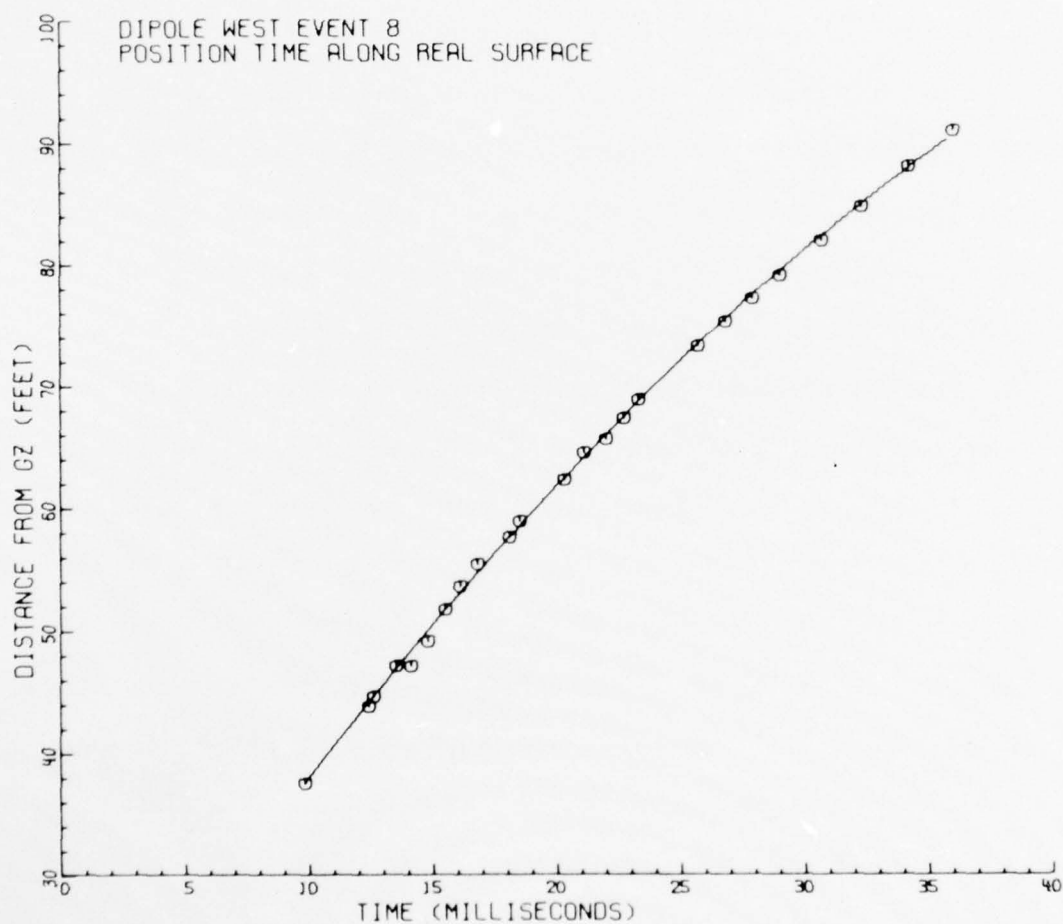


Figure 3.12. Shockwave Position-Time from DRI Photographic Data
Points Along Real Reflective Surface From Event 8.

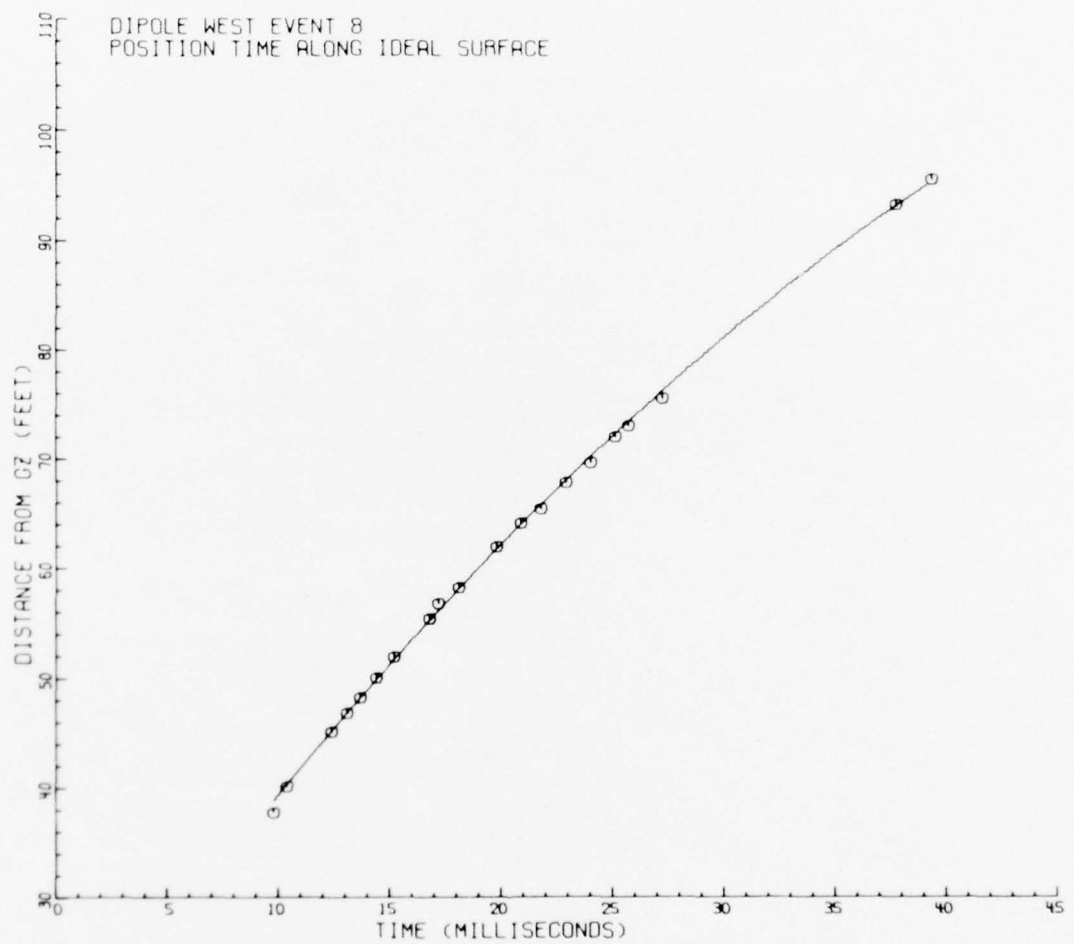


Figure 3.13. Shockwave Position-Time From DRI Photographic Data
Points Along Ideal Reflective Surface From Event 8.

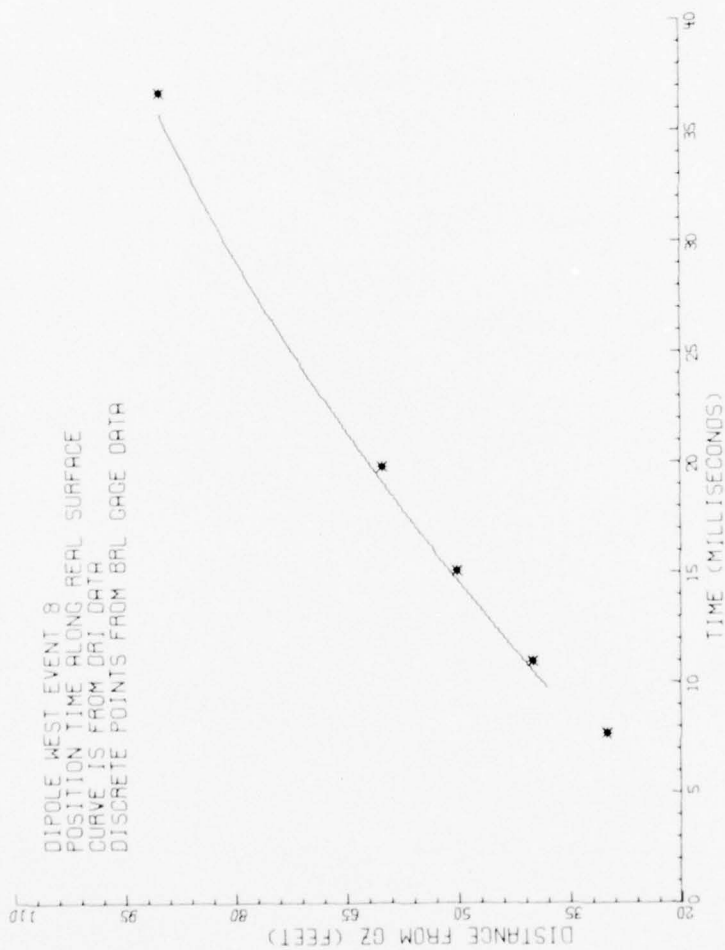


Figure 3.14. DRI Shockwave Position-Time Curve and BRL Gage Data Along Real Surface from Event 8, HOB \approx 25 Feet.

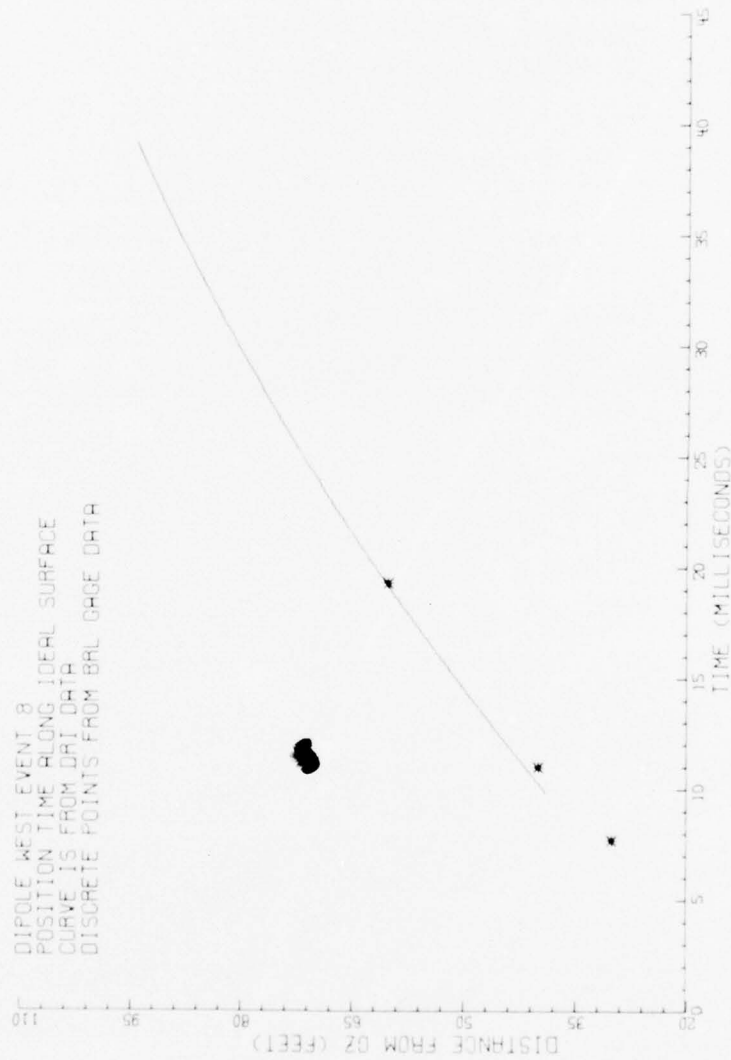


Figure 3.15. DRI Shockwave Position-Time Curve and BRL Gage Data
 Along Ideal Surface From Event 8, HOB \approx 25 Feet.



Figure 3.16. DRI Shockwave Position-Time Curve Along Real Surface From Event 9, HOB \approx 15 Feet.

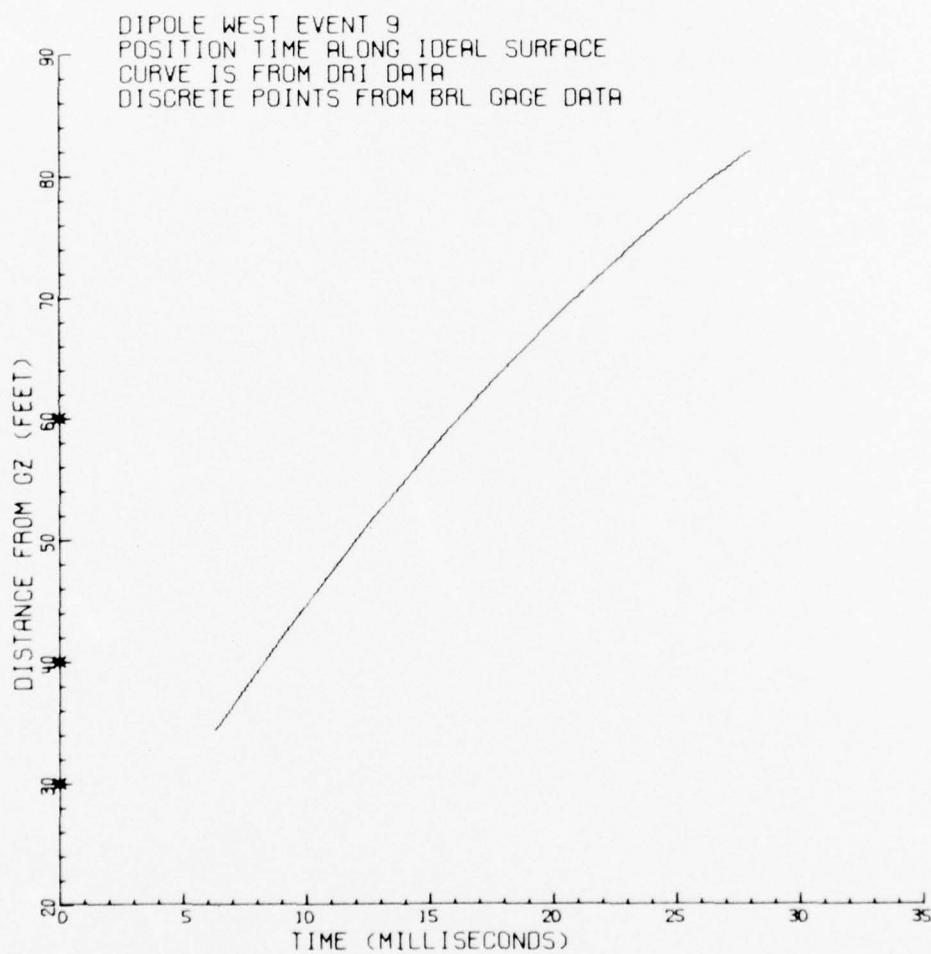


Figure 3.17. DRI Shockwave Position-Time Curve Along
Ideal Surface From Event 9, HOB \approx 15 Feet.

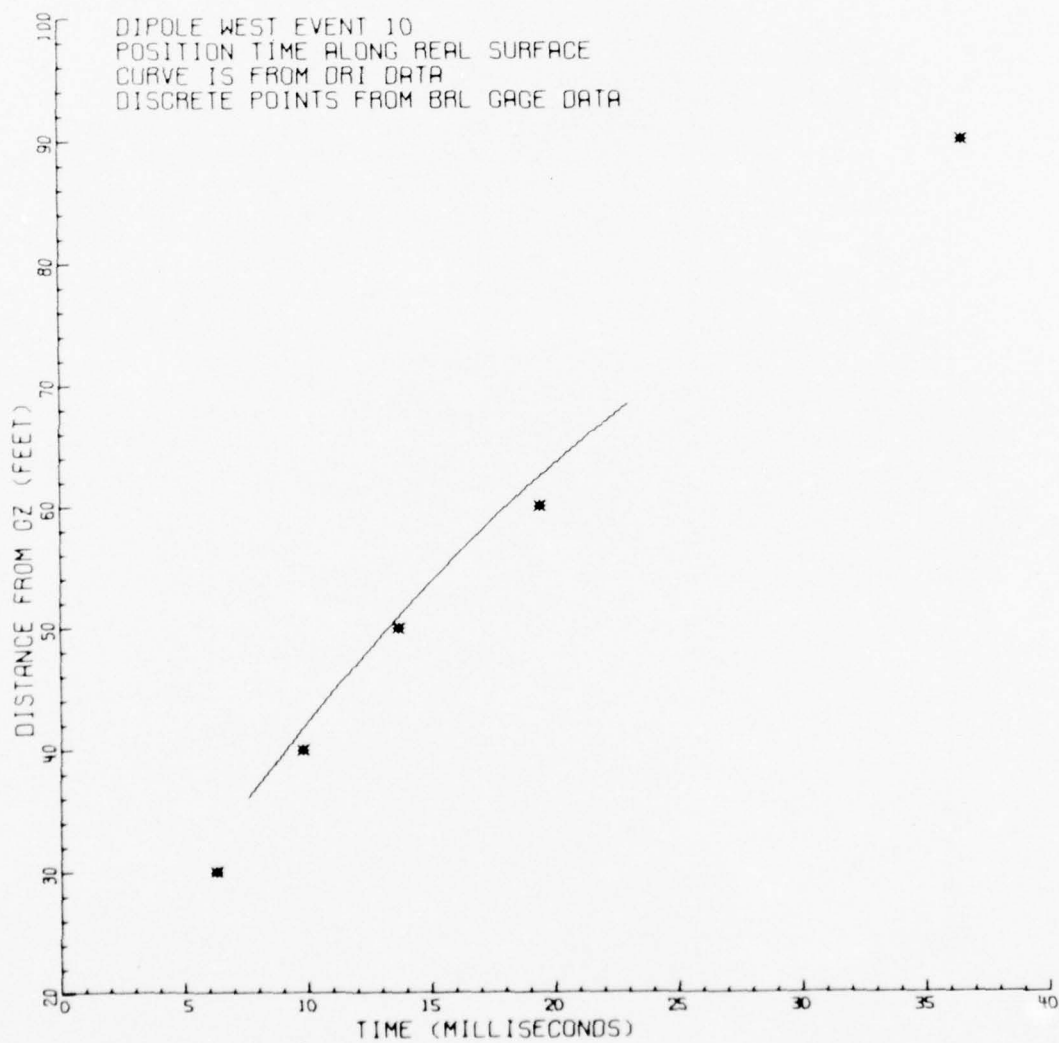


Figure 3.18. DRI Shockwave Position-Time Curve and BRL Gage Data Along Real Surface From Event 10, HOB \approx 15 Feet.

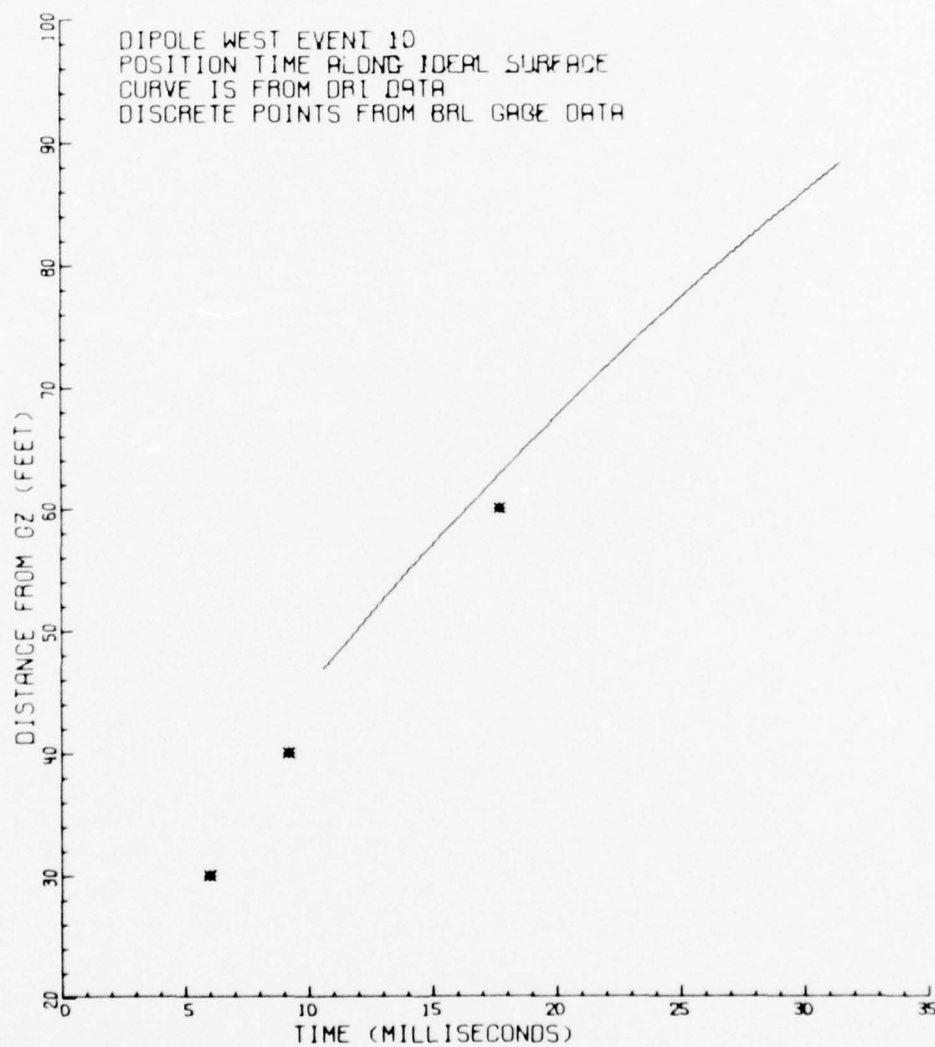


Figure 3.19. DRI Shockwave Position-Time Curve and BRL Gage Data Along Ideal Surface From Event 10, HOB \approx 15 Feet.

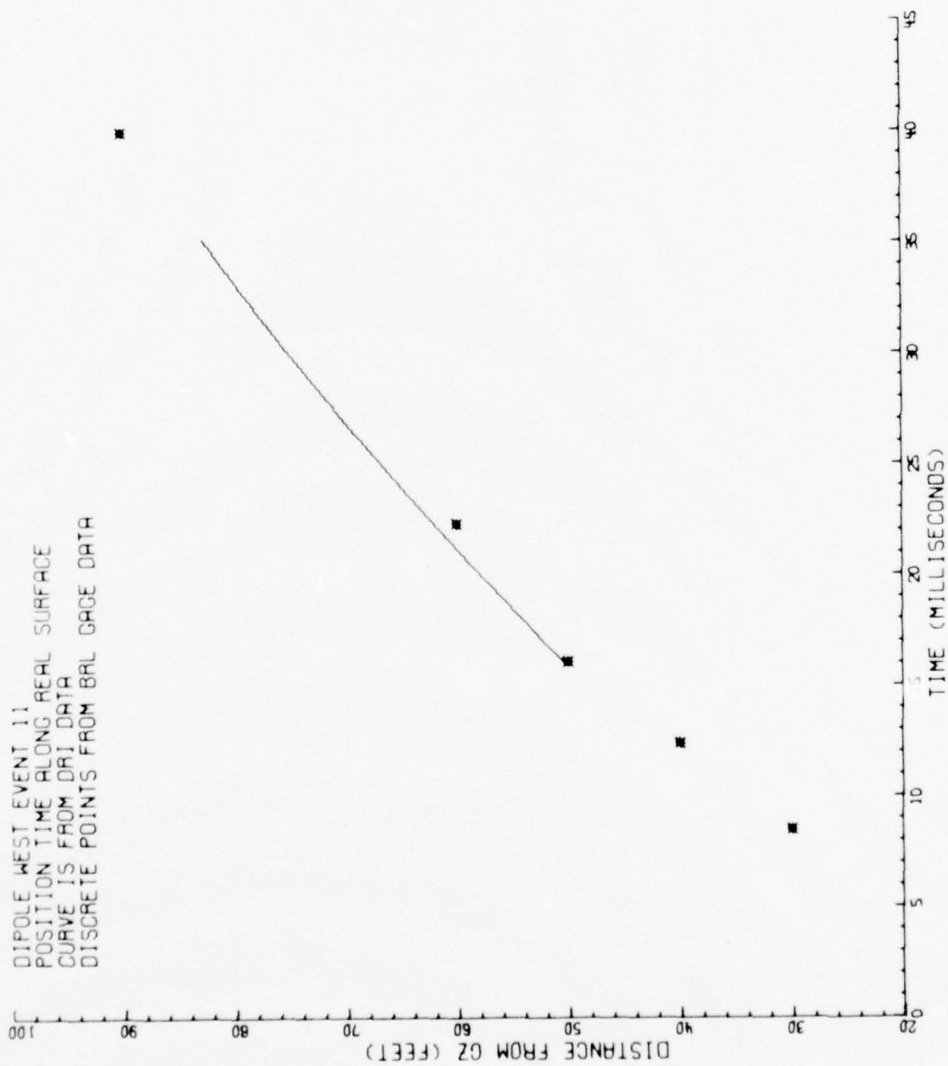


Figure 3.20. DRI Shockwave Position-Time Curve and BRL Gage Data Along Real Surface From Event 11, HOB \approx 25 Feet.

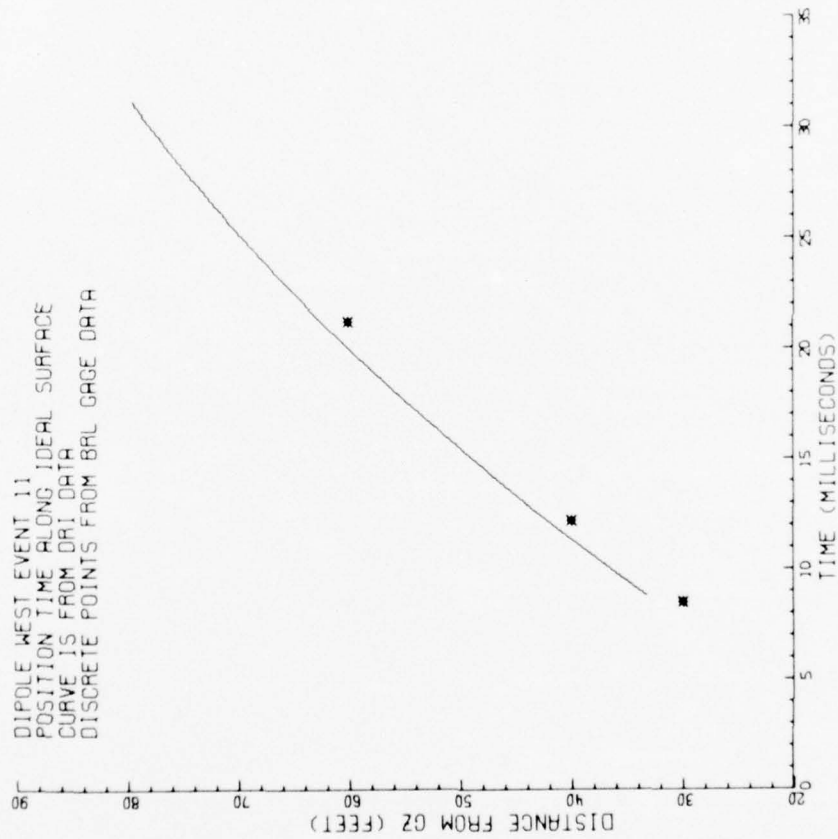


Figure 3.21. DRI Shockwave Position-Time Curve and BRL Gage
 Data Along Ideal Surface From Event 11, HOB =
 25 Feet.

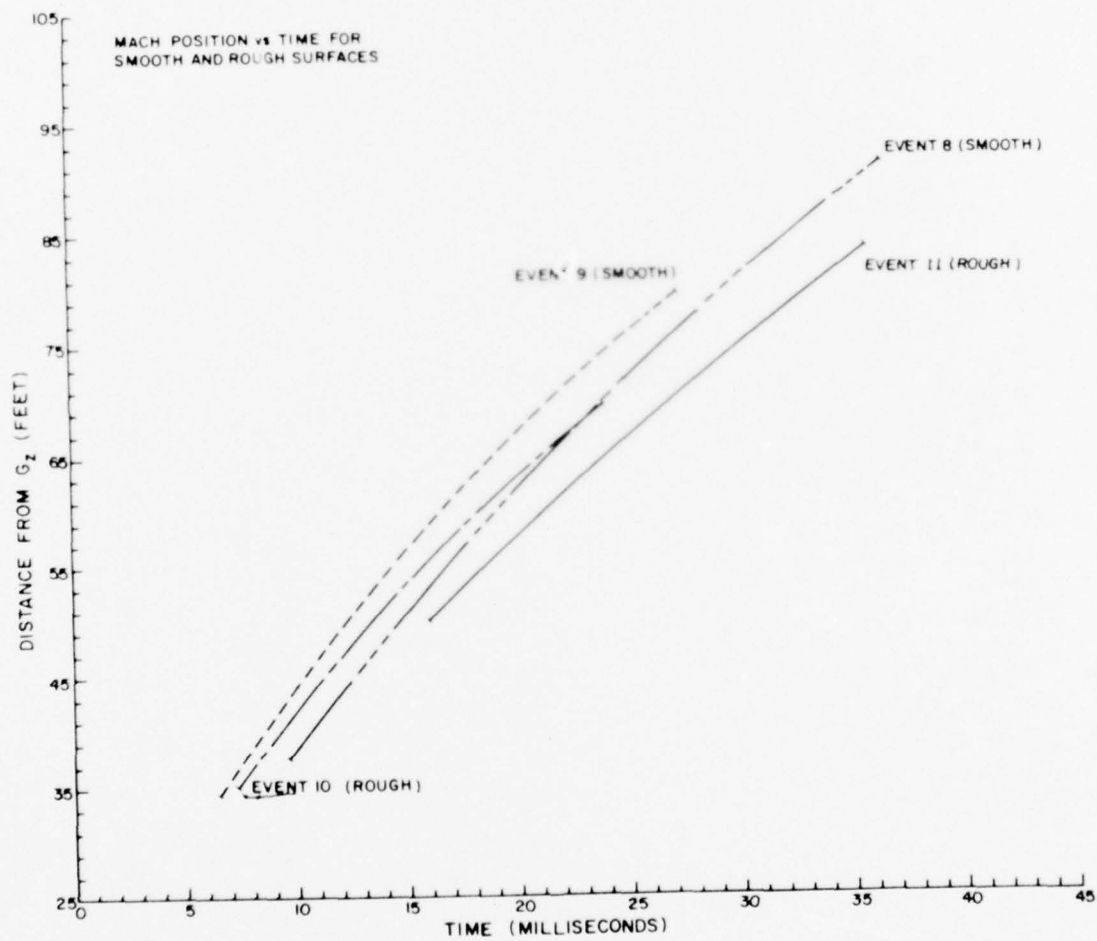


Figure 3.22. DRI Shockwave Position-Time Curves From Events 8, 9, 10 and 11 Along Real Surfaces.

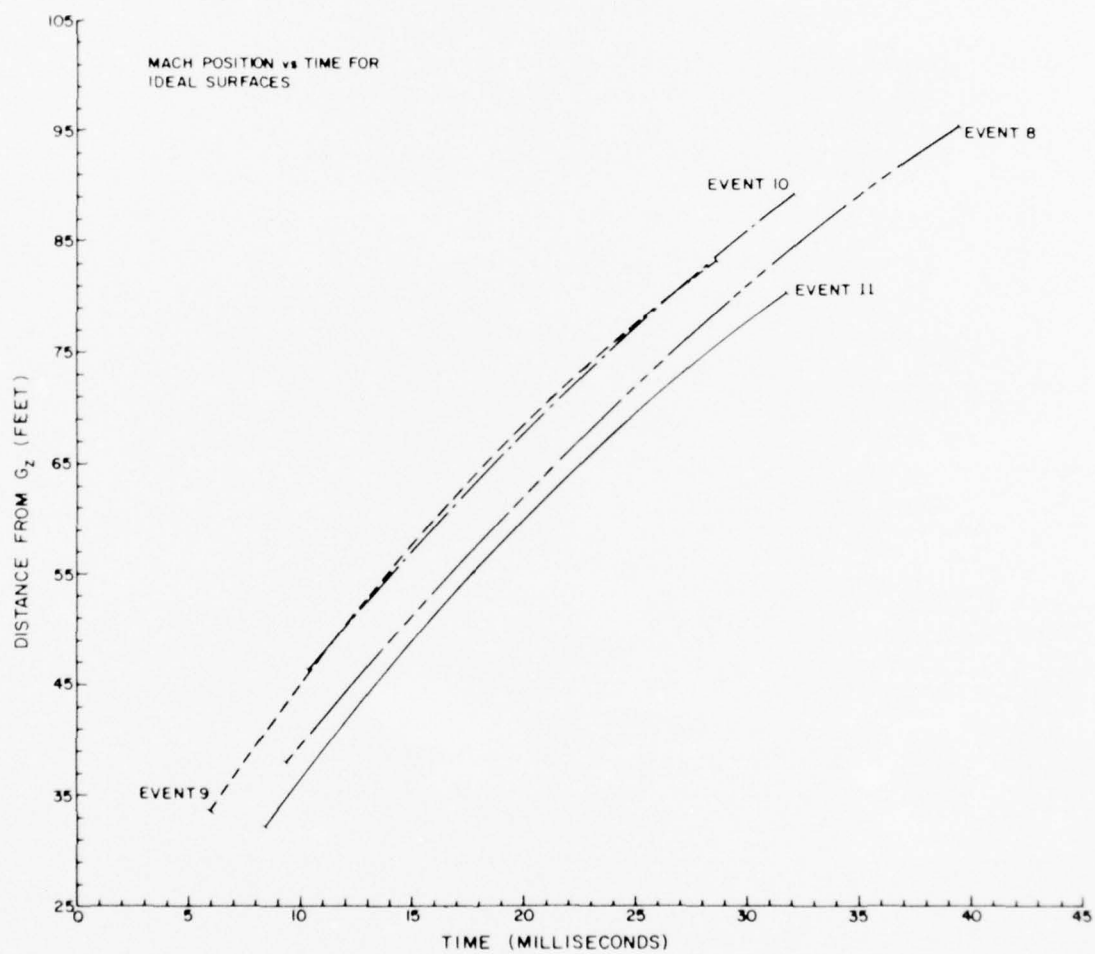


Figure 3.23. DRI Shockwave Position-Time Curves From Events 8, 9, 10 and 11 Along Ideal Surfaces.

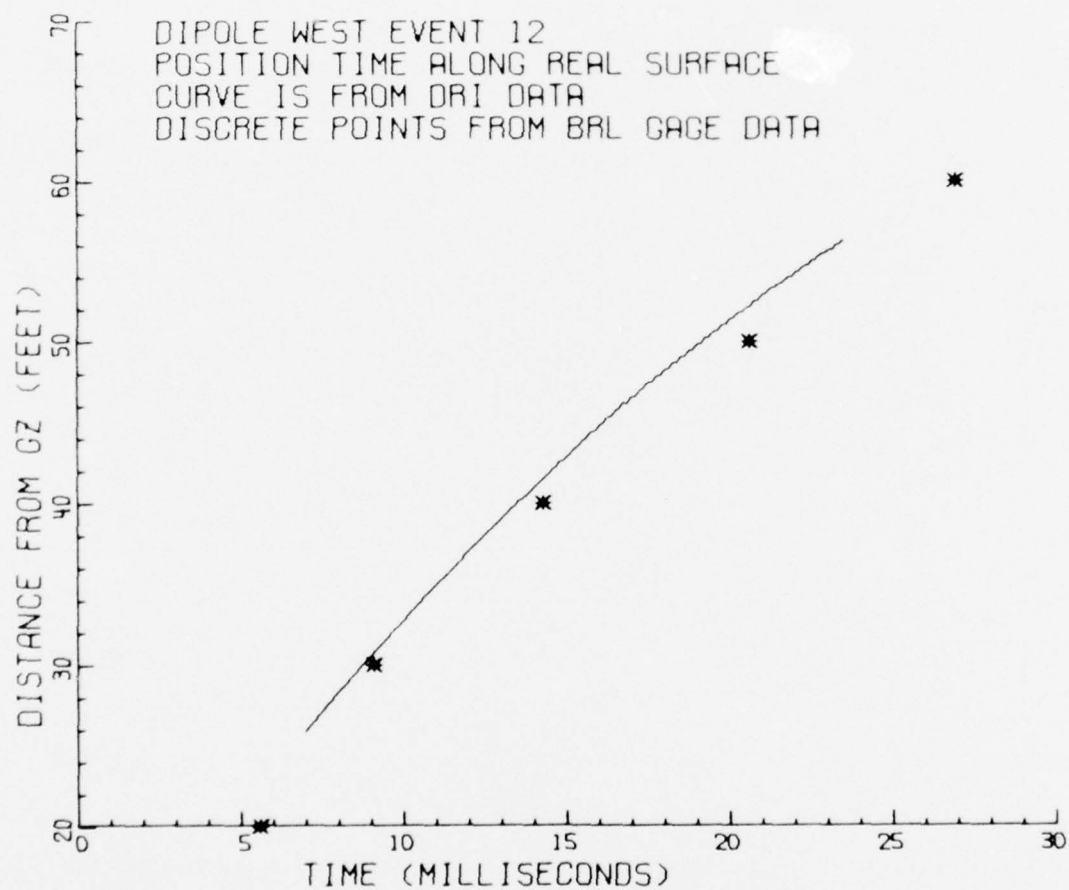


Figure 3.24. DRI Shockwave Position-Time Curve and BRL Gage Data Along Real Surface From Event 12, HOB \approx 15 Feet.

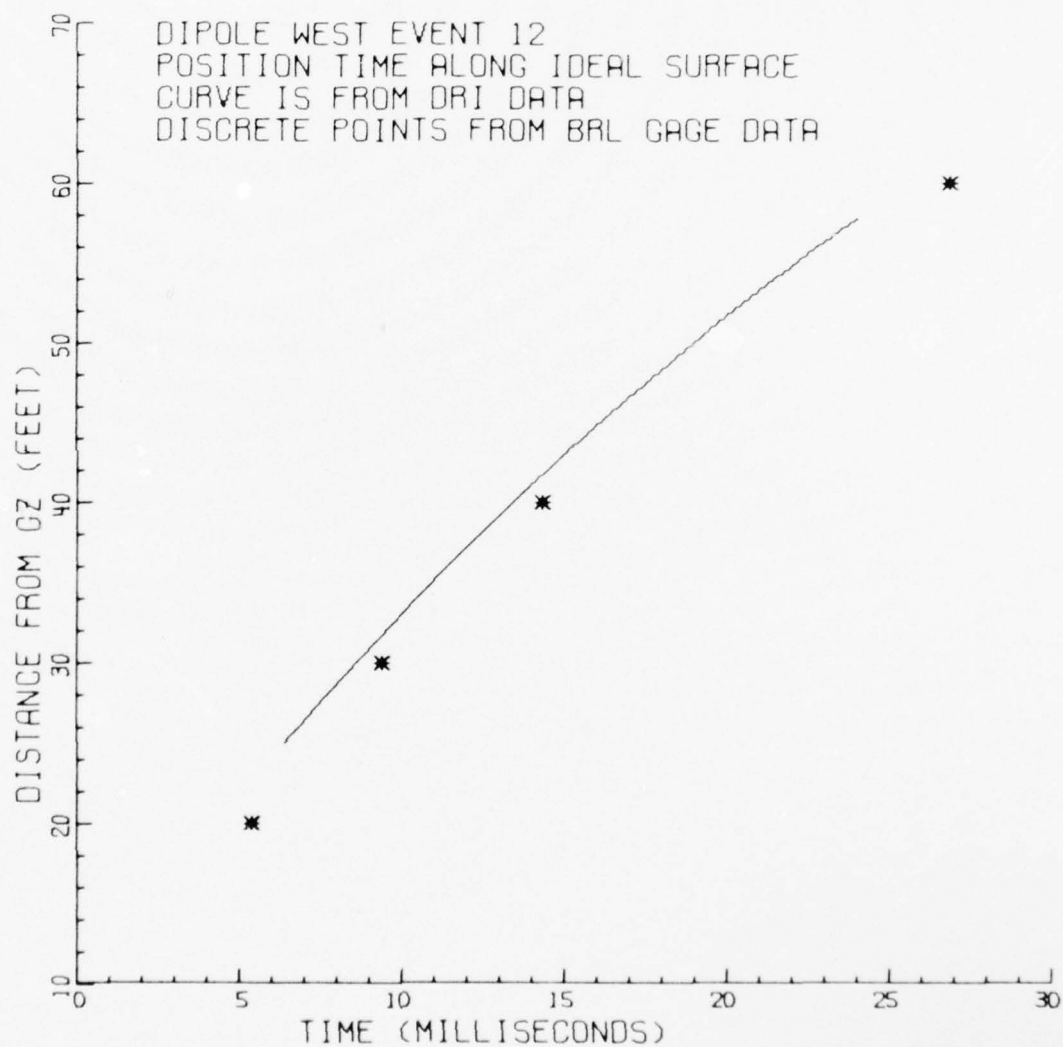


Figure 3.25. DRI Shockwave Position-Time Curve and BRL Gage Data Along Ideal Surface From Event 12, HOB \approx 15 Feet.

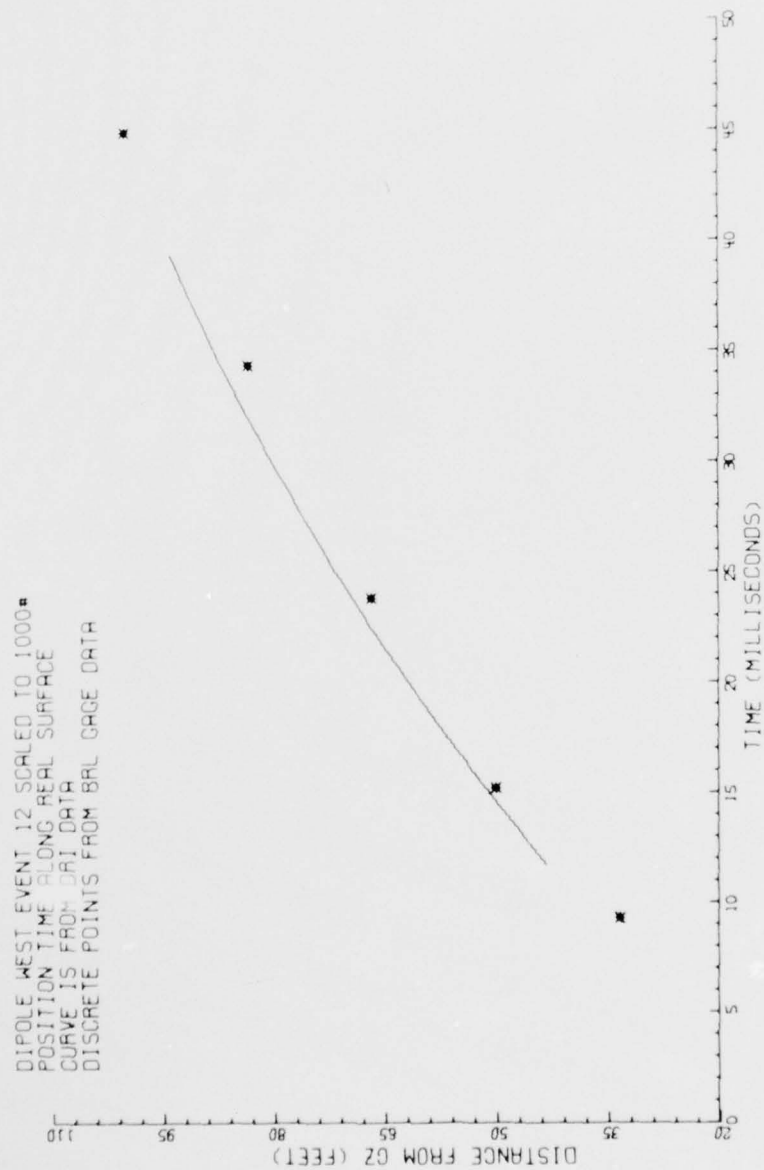


Figure 3.26. DRI Shockwave Position-Time Curve and BRL Gage Data
 Along Real Surface From Event 12 Scaled to 1,000-Pounds.

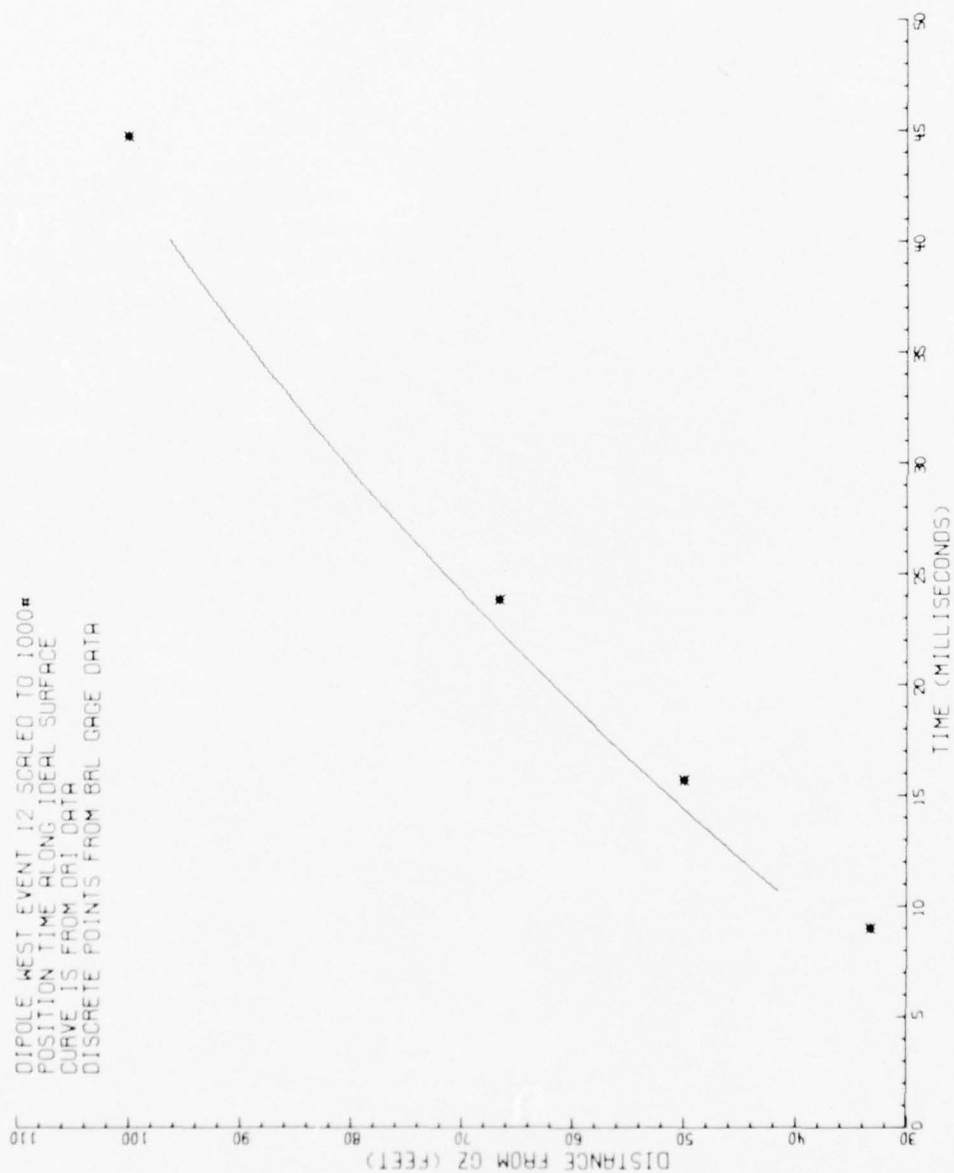


Figure 3.27. DRI Shockwave Position-Time Curve and BRL Gage Data
 Along Ideal Surface From Event 12 Scaled to 1,000-Pounds.

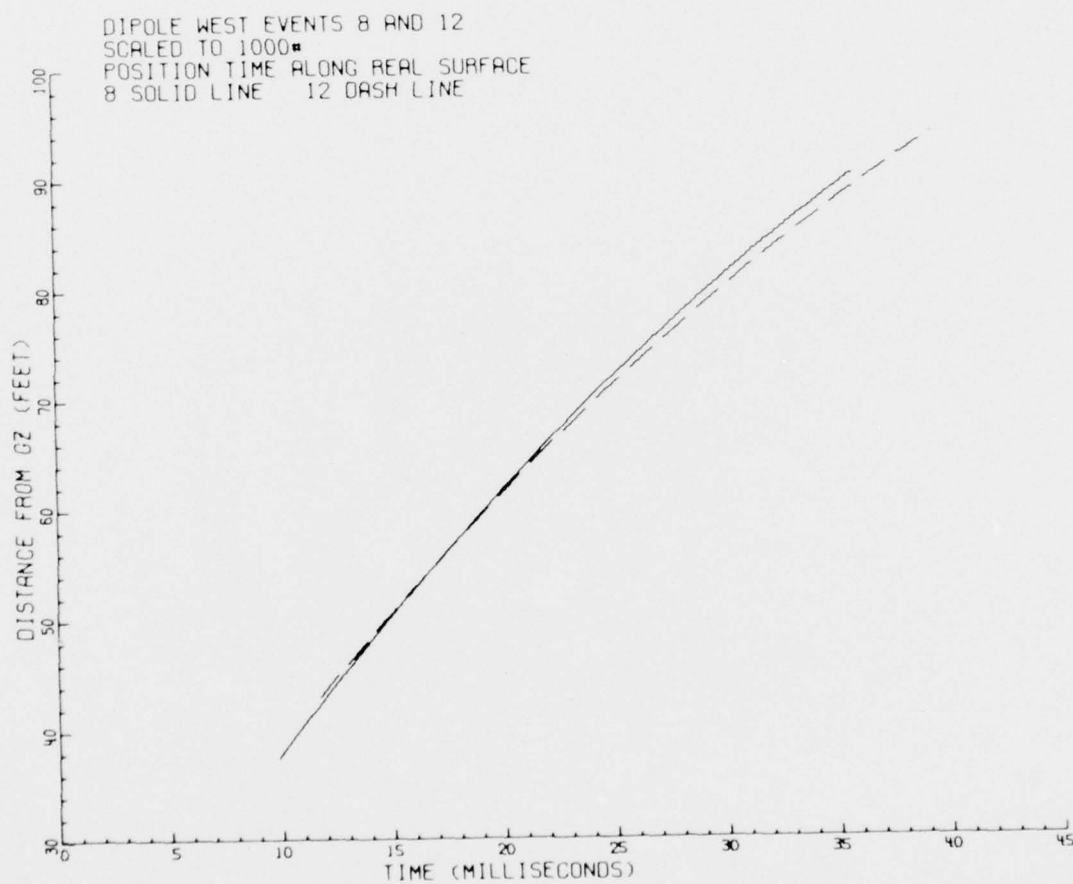


Figure 3.28. Comparison of DRI Shockwave Position-Time Curves
Along Real Surface From Event 8 and Event 12
Scaled to 1,000-Pounds.

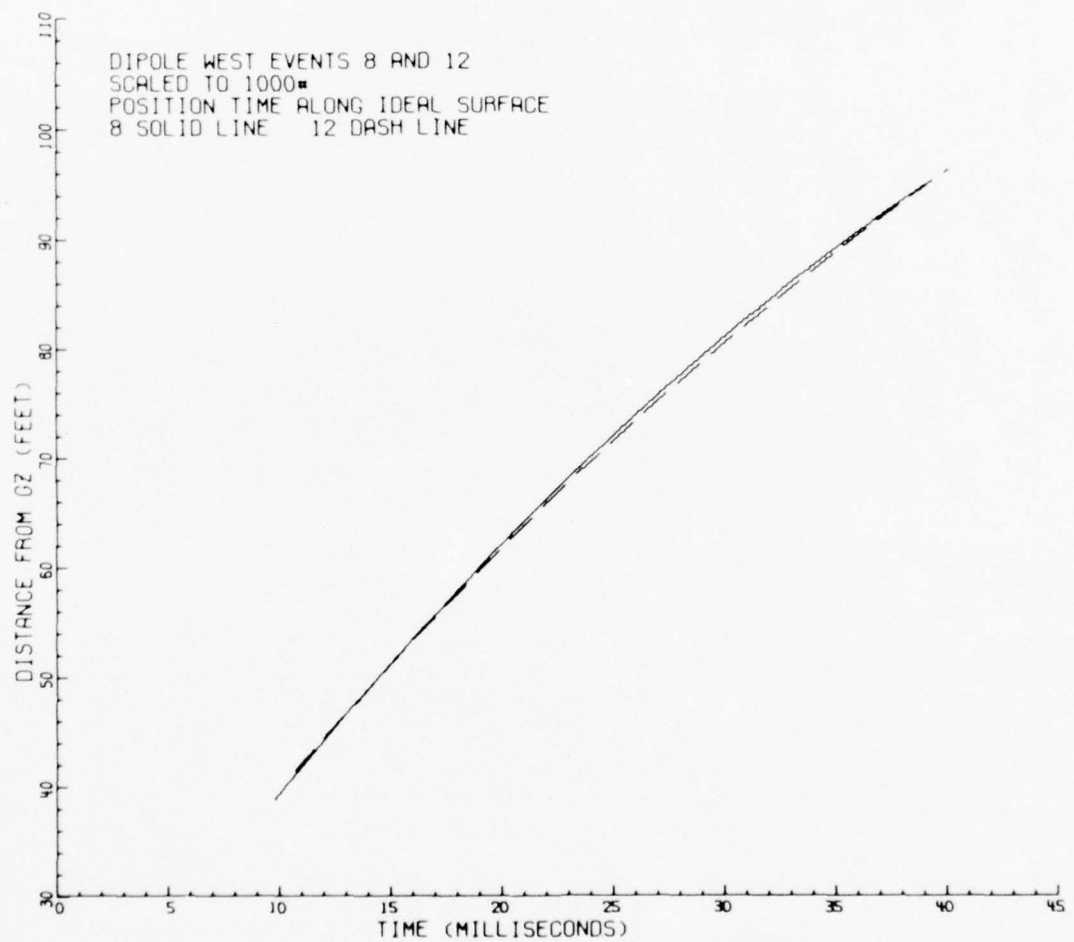


Figure 3.29. Comparison of DRI Shockwave Position-Time Curves Along Ideal Surface From Event 8 and Event 12 Scaled to 1,000-Pounds.

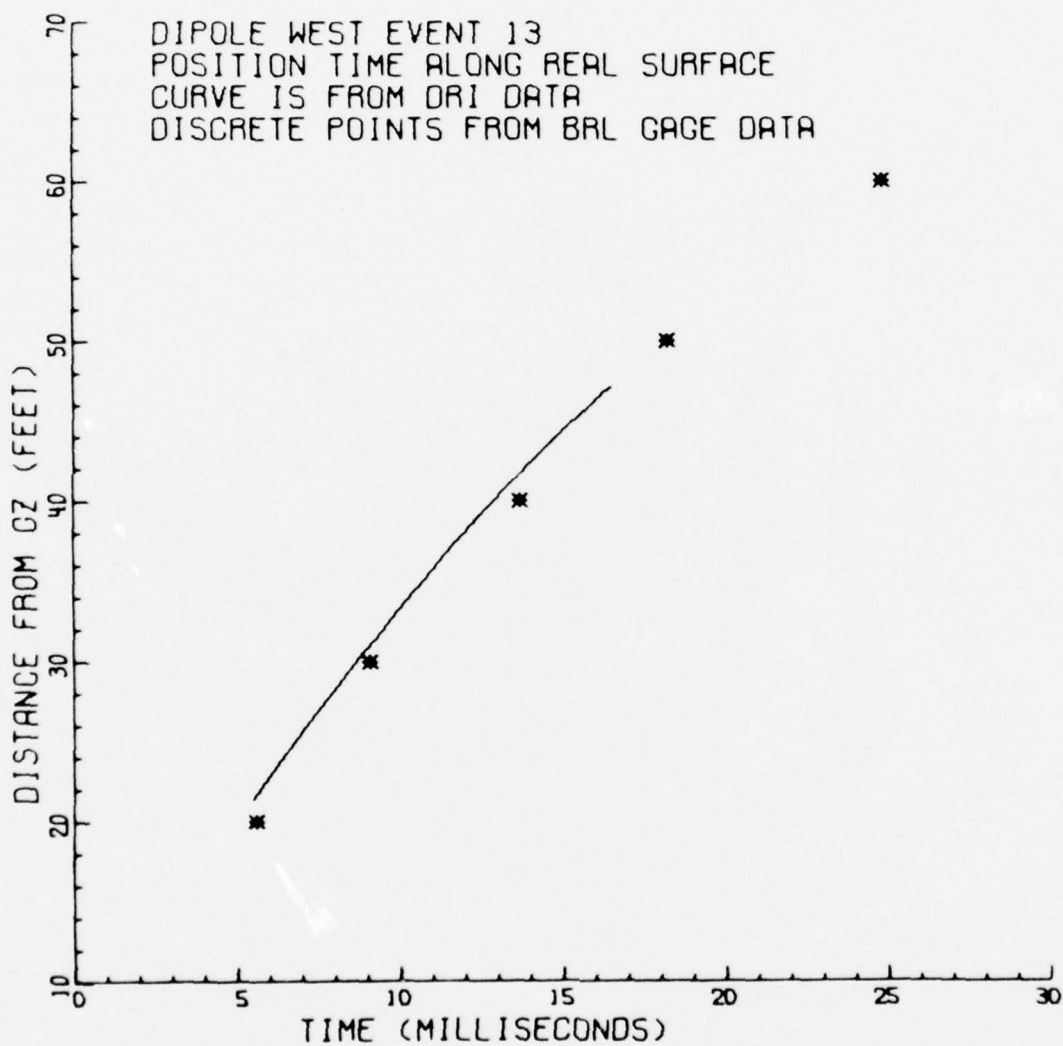


Figure 3.30. DRI Shockwave Position-Time Curve and BRL Gage Data Along Real Surface From Event 13, HOB \approx 15 Feet.

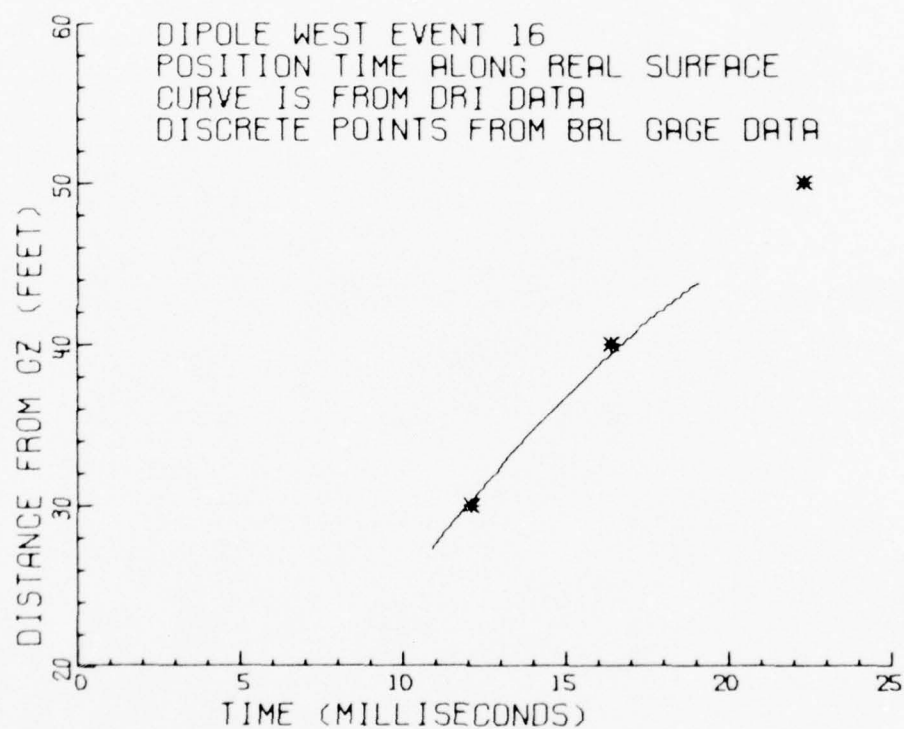


Figure 3.31. DRI Shockwave Position-Time Curve and BRL Gage Data Along Real Surface From Event 16, HOB \approx 15 Feet.

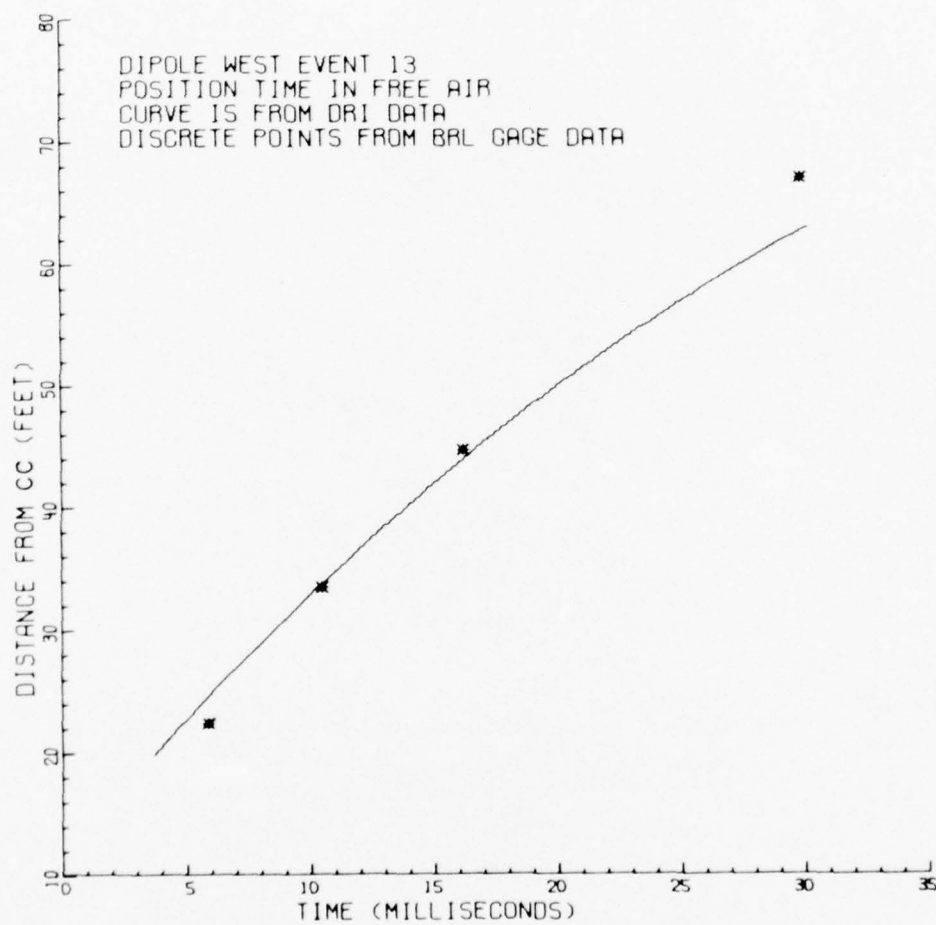


Figure 3.32. DRI Free-Air Shockwave Position-Time Curve and BRL Gage Data From Event 13.

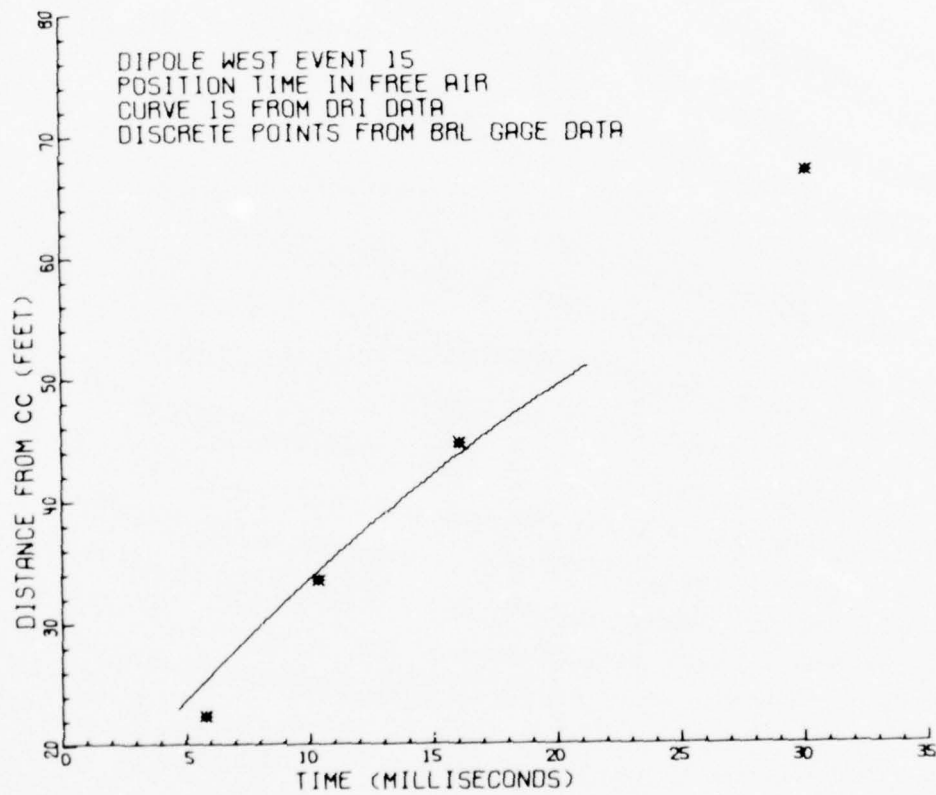


Figure 3.33. DRI Free-Air Shockwave Position-Time Curve and BRL Gage Data From Event 15.

TABLE 3.1

DIPLOE WEST
EVENT 8

TIME-OF-ARRIVAL/PEAK PRESSURE VERSUS DISTANCE
FROM PHOTOGRAPHIC RECORDS

NUMBER OF CHARGES: TWO
CHARGE WEIGHT: 1000g
CHARGE CONFIGURATION: VERTICAL
CHARGE TO SURFACE SEPARATION: 25 FT.
CHARGE TO CHARGE SEPARATION: 50 FT.
INITIATION TIME DIFFERENTIAL: 0.0 MSEC.

DISTANCE (FT)	ORT PHOTOGRAPHIC VALUES				BRL GUAGE VALUES			
	IDEAL SURFACE	SMOOTH SURFACE	PEAK PRESSURE (PSI)	TIME (MSEC)	IDEAL SURFACE	SMOOTH SURFACE	PEAK PRESSURE (PSI)	TIME (MSEC)
30.0	I	I	57.8	10.6	I	I	154.0	7.7
40.0	I	I	53.2	12.6	I	I	75.0	11.0
45.0	I	I	48.6	14.7	I	I		
50.0	I	I	48.0	16.9	I	I		
55.0	I	I	39.3	19.1	I	I	38.0	19.8
60.0	I	I	34.7	21.5	I	I		
65.0	I	I	30.1	24.0	I	I		
70.0	I	I	25.4	26.6	I	I		
75.0	I	I	20.8	29.4	I	I		
80.0	I	I	16.2	32.4	I	I		
85.0	I	I	11.5	35.7	I	I		
90.0	I	I	6.9		I	I		
95.0	I	I			I	I		

DIPLOLE WEST
EVENT 9

TIME-OF-ARRIVAL/PEAK PRESSURE VERSUS DISTANCE
FROM PHOTOGRAPHIC RECORDS

NUMBER OF CHARGES: TWO

CHARGE WEIGHT: 10008

CHARGE CONFIGURATION: VERTICAL

CHARGE TO SURFACE SEPARATION: 15 FT.

CHARGE TO CHARGE SEPARATION: 30 FT.

INITIATION TIME DIFFERENTIAL: 0.0 MSEC.

ORI PHOTOGRAPHIC VALUES				BRL GUAGE VALUES				
DISTANCE (FT)	IDEAL SURFACE	SMOOTH SURFACE	PEAK PRESSURE (PSI)	TIME (MSEC)	IDEAL SURFACE	SMOOTH SURFACE	PEAK PRESSURE (PSI)	TIME (MSEC)
30.0								
35.0								
40.0								
45.0								
50.0								
55.0								
60.0								
65.0								
70.0								
75.0								
80.0								
85.0								
90.0								
95.0								
100.0								
105.0								
110.0								
115.0								
120.0								
125.0								
130.0								
135.0								
140.0								
145.0								
150.0								
155.0								
160.0								
165.0								
170.0								
175.0								
180.0								
185.0								
190.0								
195.0								
200.0								
205.0								
210.0								
215.0								
220.0								
225.0								
230.0								
235.0								
240.0								
245.0								
250.0								
255.0								
260.0								
265.0								
270.0								
275.0								
280.0								
285.0								
290.0								
295.0								
300.0								

TABLE 3.3

DIPOLE WEST
EVENT 10

TIME-OF-ARRIVAL/PEAK PRESSURE VERSUS DISTANCE
FROM PHOTOGRAPHIC RECORDS

NUMBER OF CHARGES: TWO
CHARGE WEIGHT: 1000g
CHARGE CONFIGURATION: VERTICAL
CHARGE TO SURFACE SEPARATION: 15 FT.
CHARGE TO CHARGE SEPARATION: 30 FT.
INITIATION TIME DIFFERENTIAL: 0.0 MSEC.

DISTANCE (FT)	DRT PHOTOGRAPHIC VALUES				PRL GUAGE VALUES			
	IDEAL SURFACE	ROUGH SURFACE	IDEAL SURFACE	ROUGH SURFACE	IDEAL SURFACE	ROUGH SURFACE	IDEAL SURFACE	ROUGH SURFACE
	TIME (MSEC)	PEAK PRESSURE (PSI)	TIME (MSEC)	PEAK PRESSURE (PSI)	TIME (MSEC)	PEAK PRESSURE (PSI)	TIME (MSEC)	PEAK PRESSURE (PSI)
30.0			9.2	73.8	6.0	166.0	6.3	148.0
40.0			11.2	63.8	9.2	96.0	9.8	67.5
45.0			13.3	53.8			13.7	53.4
50.0	11.9	40.2	15.6	43.8			19.4	30.8
55.0	14.1	54.7	18.1	33.8	17.7	36.0		
60.0	16.3	49.2	20.9	23.8				
65.0	18.7	43.7						
70.0	21.2	38.2						
75.0	23.8	32.7						
80.0	26.5	27.2						
85.0	29.4	21.7					36.5	33.0
90.0								

BEST AVAILABLE COPY

TABLE 3.4

LIFELINE TEST
EVENT 11

TIME OF ARRIVAL/PEAK PRESSURE VERSUS DISTANCE
FROM PHOTOGRAPHIC RECORDS

NUMBER OF CHARGES: TWO
CHARGE WEIGHT: 1000
CHARGE CONFIGURATION: VERTICAL
CHARGE TO SURFACE SEPARATION: 25 FT.
CHARGE TO CHARGE SEPARATION: 50 FT.
INITIATION TIME DIFFERENTIAL: 0.0 MSEC.

DISTANCE (FT)	LIFELINE PHOTOGRAPHIC VALUES				PHL GAUGE VALUES			
	TIME (MSEC)	PEAK PRESSURE (PSI)	ROUGH SURFACE	IDEAL SURFACE	TIME (MSEC)	PEAK PRESSURE (PSI)	ROUGH SURFACE	IDEAL SURFACE
30.0	6.5	86.9	I	I	8.5	142.0	I	I
35.0	11.4	76.7	I	I	12.2	73.5	I	I
40.0	13.4	70.5	I	I	12.4	I	I	I
45.0	15.5	62.3	I	I	16.1	I	I	I
50.0	17.7	54.2	I	I	22.5	41.0	I	I
55.0	20.0	46.0	I	I	I	I	I	I
60.0	22.5	37.8	I	I	I	I	I	I
65.0	25.3	29.6	I	I	I	I	I	I
70.0	28.2	21.4	I	I	I	I	I	I
75.0	31.5	13.2	I	I	I	I	I	I
80.0	I	I	I	I	40.0	I	I	I
85.0	I	I	I	I	I	I	I	I
90.0	I	I	I	I	I	I	I	I
95.0	I	I	I	I	I	I	I	I
100.0	I	I	I	I	I	I	I	I
105.0	I	I	I	I	I	I	I	I
110.0	I	I	I	I	I	I	I	I
115.0	I	I	I	I	I	I	I	I
120.0	I	I	I	I	I	I	I	I
125.0	I	I	I	I	I	I	I	I
130.0	I	I	I	I	I	I	I	I
135.0	I	I	I	I	I	I	I	I
140.0	I	I	I	I	I	I	I	I
145.0	I	I	I	I	I	I	I	I
150.0	I	I	I	I	I	I	I	I
155.0	I	I	I	I	I	I	I	I
160.0	I	I	I	I	I	I	I	I
165.0	I	I	I	I	I	I	I	I
170.0	I	I	I	I	I	I	I	I
175.0	I	I	I	I	I	I	I	I
180.0	I	I	I	I	I	I	I	I
185.0	I	I	I	I	I	I	I	I
190.0	I	I	I	I	I	I	I	I
195.0	I	I	I	I	I	I	I	I
200.0	I	I	I	I	I	I	I	I
205.0	I	I	I	I	I	I	I	I
210.0	I	I	I	I	I	I	I	I
215.0	I	I	I	I	I	I	I	I
220.0	I	I	I	I	I	I	I	I
225.0	I	I	I	I	I	I	I	I
230.0	I	I	I	I	I	I	I	I
235.0	I	I	I	I	I	I	I	I
240.0	I	I	I	I	I	I	I	I
245.0	I	I	I	I	I	I	I	I
250.0	I	I	I	I	I	I	I	I
255.0	I	I	I	I	I	I	I	I
260.0	I	I	I	I	I	I	I	I
265.0	I	I	I	I	I	I	I	I
270.0	I	I	I	I	I	I	I	I
275.0	I	I	I	I	I	I	I	I
280.0	I	I	I	I	I	I	I	I
285.0	I	I	I	I	I	I	I	I
290.0	I	I	I	I	I	I	I	I
295.0	I	I	I	I	I	I	I	I
300.0	I	I	I	I	I	I	I	I

BEST AVAILABLE COPY

TABLE 3.5

DIPLOLE WEST
EVENT 12

TIME-OF-ARRIVAL/PEAK PRESSURE VERSUS DISTANCE
FROM PHOTOGRAPHIC RECORDS

NUMBER OF CHARGES: TWO

CHANGE WEIGHT, 2168

CHARGE CONFIGURATION: VERTICAL

CHARGE TO SURFACE SEPARATION: 15 FT.

CHARGE TO CHARGE SEPARATIONS: 30 FT.

INITIATION TIME DIFFERENTIAL: 0.0 MSEC

DISTANCE (FT)	DRI PHOTOGRAPHIC VALUES				BRL GAGE VALUES			
	IDEAL SURFACE	PEAK PRESSURE (PSI)	TIME (MSEC)	HARD SURFACE	IDEAL SURFACE	PEAK PRESSURE (PSI)	TIME (MSEC)	HARD SURFACE
20.0								
25.0								
30.0								
35.0								
40.0								
45.0								
50.0								
55.0								
60.0								

TABLE 3.6

DIPOLE WEST
EVENT 12 SCALED
TIME-OF-ARRIVAL/PEAK PRESSURE VERSUS DISTANCE
FROM PHOTOGRAPHIC RECORDS

NUMBER OF CHARGES: TWO
CHARGE WEIGHT: SCALED TO 1000#
CHARGE CONFIGURATION: VERTICAL
CHARGE TO SURFACE SEPARATION: SCALED TO 1000# I.E. 25 FT.
CHARGE TO CHARGE SEPARATION: SCALED TO 1000# I.E. 50 FT.
INITIATION TIME DIFFERENTIAL: 0.0 MSEC

DISTANCE (FT)	DRI PHOTOGRAPHIC VALUES				BRL GAGE VALUES			
	IDEAL SURFACE	HARD SURFACE	TIME (MSEC)	PEAK PRESSURE (PSI)	IDEAL SURFACE	HARD SURFACE	TIME (MSEC)	PEAK PRESSURE (PSI)
33.3	I	I	I	I	I	I	I	I
45.0	I	I	I	I	I	I	I	I
50.0	I	I	I	I	I	I	I	I
55.0	I	I	I	I	I	I	I	I
60.0	I	I	I	I	I	I	I	I
65.0	I	I	I	I	I	I	I	I
66.6	I	I	I	I	I	I	I	I
70.0	I	I	I	I	I	I	I	I
75.0	I	I	I	I	I	I	I	I
80.0	I	I	I	I	I	I	I	I
83.3	I	I	I	I	I	I	I	I
85.0	I	I	I	I	I	I	I	I
90.0	I	I	I	I	I	I	I	I
95.0	I	I	I	I	I	I	I	I
100.0	I	I	I	I	I	I	I	I

TABLE 3.7

DIPOLE WEST
EVENT 13TIME-OF-ARRIVAL/PEAK PRESSURE VERSUS DISTANCE
FROM PHOTOGRAPHIC RECORDS

NUMBER OF CHARGES: TWO

CHARGE WEIGHT: 216g

CHARGE CONFIGURATION: VERTICAL

CHARGE TO SURFACE SEPARATION: 15 FT.

CHARGE TO CHARGE SEPARATION: 30 FT.

INITIATION TIME DIFFERENTIAL: 10.0 MSEC.

DISTANCE (FT)	ORI PHOTOGRAPHIC VALUES				BRL GAGE VALUES			
	FREE AIR	REAL SURFACE	TIME (MSEC)	PEAK PRESSURE (PSI)	FREE AIR	REAL SURFACE	TIME (MSEC)	PEAK PRESSURE (PSI)
20.0	I	I	3.8	43.0	I	I	5.6	98.0
22.4	I	I			I	I		
25.0	I	I	6.1	37.9	I	I		
30.0	I	I	8.6	32.7	I	I	9.1	55.0
33.5	I	I			I	I		
35.0	I	I	11.2	27.6	I	I	13.7	36.0
40.0	I	I	13.9	22.5	I	I		
44.7	I	I			I	I		
45.0	I	I	16.9	17.3	I	I	18.2	28.0
50.0	I	I	20.1	12.2	I	I	24.8	19.0
55.0	I	I	23.6	7.1	I	I		
60.0	I	I	27.5	1.9	I	I		
67.0	I	I			I	I		

TABLE 3.8

DIPLOLE WEST
EVENT 13 SCALED

TIME-OF-ARRIVAL/PEAK PRESSURE VERSUS DISTANCE
FROM PHOTOGRAPHIC RECORDS

NUMBER OF CHARGES: TWO

CHARGE WEIGHT: 1 SCALED TO 1000#

CHARGE CONFIGURATION: VERTICAL

CHARGE TO SURFACE SEPARATION: 1 SCALED TO 1000# I.E. 25 FT.

CHARGE TO CHARGE SEPARATION: 1 SCALED TO 1000# I.E. 50 FT.

INITIATION TIME DIFFERENTIAL: 0.0 MSEC.

DISTANCE (FT)	ORI PHOTOGRAPHIC VALUES				BRL GAGE VALUES			
	FREL AIR	REAL SURFACE	TIME (MSEC)	PEAK PRESSURE (PSI)	FREL AIR	REAL SURFACE	TIME (MSEC)	PEAK PRESSURE (PSI)
33.3	I	I	7.1	42.2	I	I	9.3	98.0
35.0	I	I			I	I		
37.3	I	I	9.4	39.1	I	I		
40.0	I	I	10.6	74.9	I	I		
45.0	I	I	12.4	65.5	I	I		
50.0	I	I	14.4	62.1	I	I	15.2	55.0
55.0	I	I	16.4	55.6	I	I		
58.8	I	I			I	I		
60.0	I	I	19.5	26.7	I	I		
65.0	I	I	22.3	23.6	I	I		
66.6	I	I			I	I		
70.0	I	I	25.2	20.4	I	I	22.8	36.0
74.5	I	I			I	I		
75.0	I	I	28.2	17.3	I	I		
80.0	I	I	31.3	14.2	I	I		
83.3	I	I			I	I		
85.0	I	I	34.6	11.1	I	I	30.3	28.0
90.0	I	I	38.1	8.0	I	I		
95.0	I	I	41.9	4.9	I	I		
100.0	I	I	45.9	1.8	I	I	41.3	19.0
105.0	I	I	50.3	1.3	I	I		
111.7	I	I			I	I	49.7	6.8

TABLE 3.9

DIPOLE WEST
EVENT 15 FREE AIR

FREE AIR TIME-OF-ARRIVAL/PEAK PRESSURE VERSUS DISTANCE
FROM PHOTOGRAPHIC RECORDS

NUMBER OF CHARGES: TWO
CHARGE HEIGHT: 2108
CHARGE CONFIGURATION: VERTICAL
CHARGE TO SURFACE SEPARATION: 15 (FT)
CHARGE TO CHARGE SEPARATION: 30 (FT)
INITIATION TIME DIFFERENTIAL: 5.0 MSEC.

DISTANCE (FT)	ORI PHOTOGRAPHIC VALUES				BRL GAGE VALUES			
	FREE AIR TIME (MSEC)	PEAK PRESSURE (PSI)	REAL SURFACE TIME (MSEC)	II	FREE AIR TIME (MSEC)	PEAK PRESSURE (PSI)	REAL SURFACE TIME (MSEC)	II
22.4	5.7	41.0		II	5.0	44.0		II
25.0	6.2	34.1		II				II
30.0				II	10.4	23.0		II
33.5	10.0	27.1		II				II
35.0	13.7	20.1		II	16.1	15.0		II
40.0				II				II
44.7	14.9	13.1		II	30.1	6.5		II
50.0	20.6	6.2		II				II
67.0				II				II

TABLE 3.10

DIPLOE WEST
EVENT 16

TIME-OF-ARRIVAL/PEAK PRESSURE VERSUS DISTANCE
GRUM PHOTOGRAPHIC RECORDS

NUMBER OF CHARGES: TWO
CHARGE WEIGHT: 216g
CHARGE CONFIGURATION: VERTICAL
CHARGE TO SURFACE SEPARATION: 15 FT.
CHARGE TO CHARGE SEPARATION: 30 FT.
INITIATION TIME DIFFERENTIAL: 3.0 MSEC.

DISTANCE (FT)	DRT PHOTOGRAPHIC VALUES				BRL GAGE VALUES			
	IDEAL SURFACE	REAL SURFACE	TIME (MSEC)	PEAK PRESSURE (PSI)	IDEAL SURFACE	REAL SURFACE	TIME (MSEC)	PEAK PRESSURE (PSI)
30.0	I	I	12.0	56.1	I	I	12.1	42.8
35.0	I	I	14.2	39.8	I	I	16.4	25.0
40.0	I	I	16.8	23.4	I	I	22.3	16.6
50.0	I	I			I	I		

shockwaves were measured to the actual GZ, part of the difference between the DRI and BRL data for these few events can be attributed to some discrepancy in the assumed gage distance to that of the actual distance from GZ which could have produced a later time-of-arrival at the gages. Another condition which may have caused some divergence between photographic and gage position-time data is the fact that the gages were at different azimuths about GZ, therefore, any asymmetry in the shock envelope could have produced time-of-arrivals which were variant in the direction of the gages. The DRI photographic shockwave position-time data for Events 8 through 16 were determined in a plane through the forty-foot, gun barrel, gage station.

Generally speaking it can be said that the *photographic position-time* data compare well with the actual gage measured values. As was expected, the slope of the curve fit to the shockwave position-time data was greater for the ideal reflective plane than for either the smooth or rough surfaces, except for Event 8 which were about the same. In addition, as was expected, the slope of the curve fit through the shockwave position-time data was greater for the smooth surface than for the rough surface. Except for Event 8, the curve fits to shockwave position-time data along the real surfaces appear to diverge from the curve fits along the ideal plane at later times.

Figures 3.22 and 3.23 present curve fits from Events 8 through 11 for the real and ideal surfaces, respectively. In Figure 3.23 note that the ideal surface curve fits for Events 9 and 10 are about the same; whereas, there is an unsuspected difference between curve fits for

Events 8 and 11. Also note that there is a shifting of curves to the right as expected with an increase in HOB.

In Figure 3.22 for a given HOB the curve fit for the rough surface is to the right of the smooth surface. There is also a decrease in slope which is indicative of a reduced shockwave velocity. In addition both curves (smooth and rough) are shifted to the right with an increase in HOB in a similar manner as for the ideal surface.

The nonsimultaneous detonations, Events 13, 15 and 16, were obtained from 216-pound pentolite charges which were located at an HOB of 15 feet which scaled to 25 feet for a 1,000-pound equivalent charge configuration. Event 12, which also utilized 216-pound charges, was detonated simultaneously so as to determine scaleability to 1,000-pound charges used in Events 8 through 11, i.e., $(w_8/w_{12})^{1/3}$. Event 8 charge configuration and its real surface were closer to Event 12 than any of the other three 1,000-pound events; therefore it was used for comparison purposes. Figures 3.28 and 3.29 show how well the two events scale.

Since no ideal reflective surface exists during nonsimultaneous detonations, only real and FA position-time data were available. No position-time data were obtained along the real reflective surface from Event 15 due to poor ambient lighting which prevented good shock-wave resolution.

3.2 PEAK PRESSURE DATA FROM EVENTS 8 THROUGH 16

DRI Peak pressure values presented in Tables 3.1 through 3.10 were calculated by a velocity method using photographic position-time data. Their values were determined by employing the well known Rankine-Hugoniot equation:

$$P = P_0 (2 \gamma / (\gamma + 1)) [(V/C)^2 - 1]$$

where: P is the peak overpressure above atmospheric (psi)

P₀ is the atmospheric pressure (psi)

γ is the ratio of specific heats of air

V is the shock velocity

C is the calculated sound velocity at detonation

The value of γ varies with the peak pressure and only slightly within the photographed range of shockwave velocities recorded during Events 8 through 16. Even though this variation was small it was taken into account in the peak pressure calculations using data from NAVORD Report 6075 (Ref. 5). Within the range of peak pressures determined herein, γ varied from 1.402 to 1.396.

The sonic velocity (C) at the time of detonation was calculated using the expression:

$$C = 1087.6 + 1.99 t$$

where: C is the sonic velocity (ft/sec)

t is the ambient temperature (degrees centigrade)

The ambient temperatures at the time of detonation varied from + 22.9 to -19.1 °C.

The instantaneous velocities (V's) used in the peak pressure calculations were determined from the slopes along the curve fit to the position-time data at the distances presented in Tables 3.1 through 3.10. Second-order polynomial curve fits were made to the arrival-time data employing the least-squares method.

The DRI photographic values of peak pressure compare well to the BRL gage data. Generally, the best comparisons occur at the mid-gage distances (50 and 60 feet).

3.3 REFLECTION COEFFICIENT FROM EVENTS 8 THROUGH 11

The reflection coefficient (K) is defined as the ratio of weight of a charge in free air to the weight of a charge fired near a reflecting surface so that equal pressures are obtained at equal radial distances (Ref. 6).

Consider: W = weight of charge

R = radial distance

λ = scaled radial distance

By definition:

$$\lambda_f = R_f/W_f^{1/3}$$

These are free air conditions where λ_f is the scaled distance from the center of the charge in free air.

Also,

$$\lambda_m = R_m/W_m^{1/3}$$

These are Mach-region conditions where λ_m is the scaled radial distance from the center of a spherical charge (to the reflecting surface in the Mach-region).

So that for:

$$R_f = R_m$$

then

$$\lambda_f W_f^{1/3} = \lambda_m W_m^{1/3}$$

and for $W_m = 1$ lb.

$$W_f^{1/3} = \lambda_m / \lambda_f$$

or

$$W_f = (\lambda_m / \lambda_f)^3 = K$$

Since the charges in the DIPOLE WEST Series were detonated at an altitude of approximately 2,320 feet above sea level, the peak pressure-distance values were adjusted to sea level by the well known Sachs Scaling law (Ref. 7). These altitude scaling laws, as presented in Ref. 7, assert that in moving a charge of constant weight from one ambient pressure (p_1) to a higher ambient pressure (p_2) the blast wave at any distance R_1 is transformed into another blast wave at a lesser distance R_2 where:

$$R_2 = R_1 (p_1 / p_2)^{1/3}$$

and the peak overpressure is increased in a ratio (p_2 / p_1) or:

$$P_2 = P_1 (p_2 / p_1)$$

For the four events analyzed here the ambient pressure (p_1) varied from 13.49 to 13.68 psi.

The following tabulation presents parameters used in the calculation of the average reflection coefficient for the ideal plane for Event 11 adjusted to sea level and one pound equivalent weight.

Where:

- R radial distance from charge at site
- P calculated peak pressure at site
- R_m radial distance adjusted to sea level
- P_m calculated peak pressure adjusted to sea level
- λ_m R_m scaled to 1-pound
- λ_f free-air distance for 1-pound equivalent weight at sea level for specific values of P_m .

At Site (2320 ft)		Adjusted to Sea Level		Scaled to 1-Pound*		
R (ft)	P (psi)	R _m (ft)	P _m (psi)	λ_m (ft/w ^{1/3})	λ_f (ft/w ^{1/3})	(λ_m/λ_f)
51.4	70.5	49.0	75.7	4.90	3.53	1.388
55.9	62.3	53.3	66.9	5.33	3.70	1.441
60.4	54.2	57.6	58.2	5.76	3.92	1.469
65.0	46.0	62.0	49.4	6.20	4.13	1.501
69.6	37.8	66.3	40.6	6.63	4.49	1.477
74.3	29.6	70.8	31.8	7.08	5.00	1.416
79.1	21.4	75.4	23.0	7.54	5.80	1.300
83.8	13.2	79.9	14.2	7.99	7.25	<u>1.102</u>
*Ref. 6				Average		1.387

The average value of λ_m/λ_f is 1.387. The value of K is $(1.387)^3$ or 2.67, i.e., the 1-pound charge appears to have a weight of 2.67 pounds when its peak pressure output is measured along the ideal reflective surface.

Table 3.11 presents reflection coefficients for various surface material. Note that for both DRI and BRL data the ideal plane reflection coefficients for the different HOB's (15 and 25 feet scaled to 1.5 and 2.5 feet for a 1-pound charge) were, as expected, generally greater than from a concrete surface. Unexpectedly, the smooth hard surface had higher reflection coefficients than the concrete. The rough surface for Events 10 and 11 had reflection coefficients greater than DRI ground (grassy, irregular surface found at 10,800 feet in the Rocky Mountains) and DRI snow (undisturbed snow having a density range from 0.11 to 0.35

grams per cubic centimeter, found at the same 10,800 foot site, Ref. 8) but smaller than for the smooth and concrete surfaces.

TABLE 3.11

Reflection Coefficients for Various Surface Materials

Event	HOB	Surface	DIPOLE WEST DRI	DIPOLE WEST BRL	DIPOLE WEST Average	Concrete* BRL	Ground** DRI	Snow** DRI
8	2.5	Ideal	2.15	2.47	2.31	2.32	1.88	1.50
8	2.5	Smooth	2.49	2.25	2.37	2.32	1.88	1.50
9	1.5	Ideal	2.58	2.48	2.53	2.02	1.65	1.40
9	1.5	Smooth	2.38	2.16	2.27	2.02	1.65	1.40
10	1.5	Ideal	3.15	2.13	2.64	2.02	1.65	1.40
10	1.5	Rough	1.86	1.73	1.80	2.02	1.65	1.40
11	2.5	Ideal	2.67	2.33	2.50	2.32	1.88	1.50
11	2.5	Rough	2.01	1.87	1.94	2.32	1.88	1.50

* Ref. 6

** Ref. 8

3.4 TRIPLE-POINT PATHS EVENTS 8 THROUGH 16

The horizontal and vertical positions of the path of the triple-point (intersection point of the incident, reflected and Mach-region shockwaves) were obtained photographically at the same time as the Mach-region shockwave transit along the reflective surfaces. These data are presented in Figures 3.34 through 3.45. All data were scaled to 1,000-pounds. Figures 3.34 and 3.35 indicate that the triple-point path has a greater slope (also a faster rise with time) from the ideal

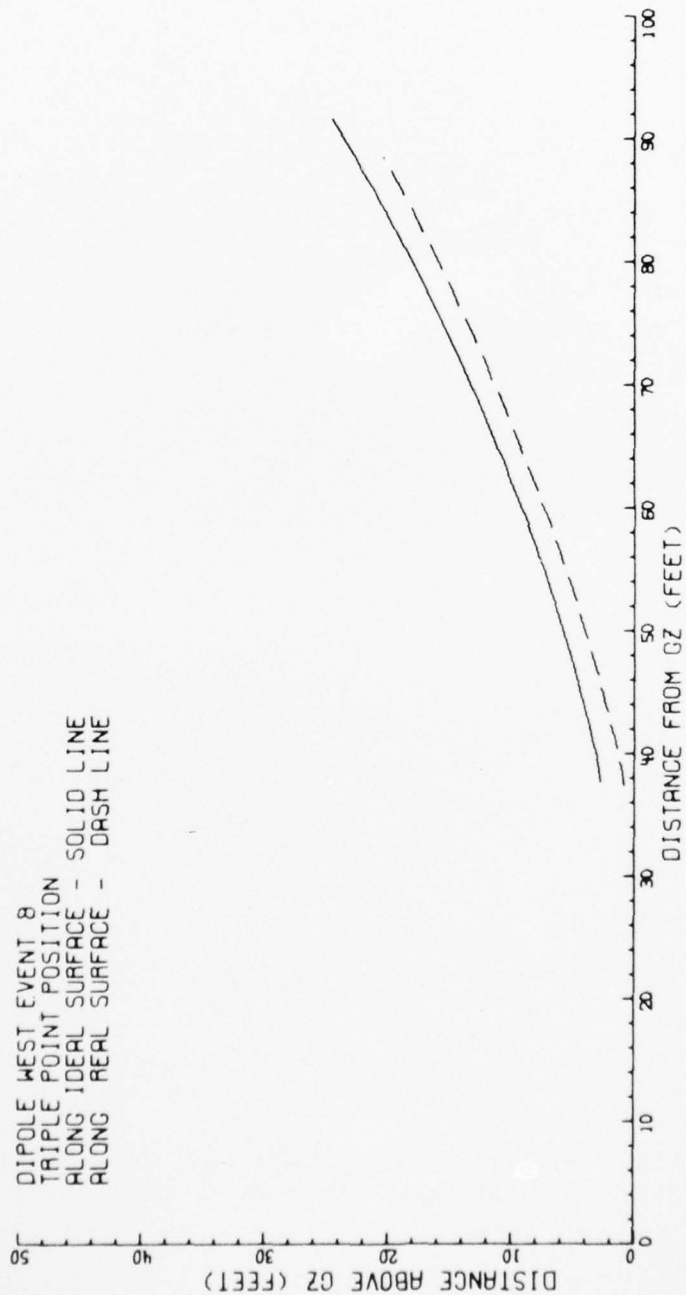


Figure 3.34. Triple-Point Paths From Real and Ideal Surfaces From Event 8,
 HOB \approx 25 Feet.

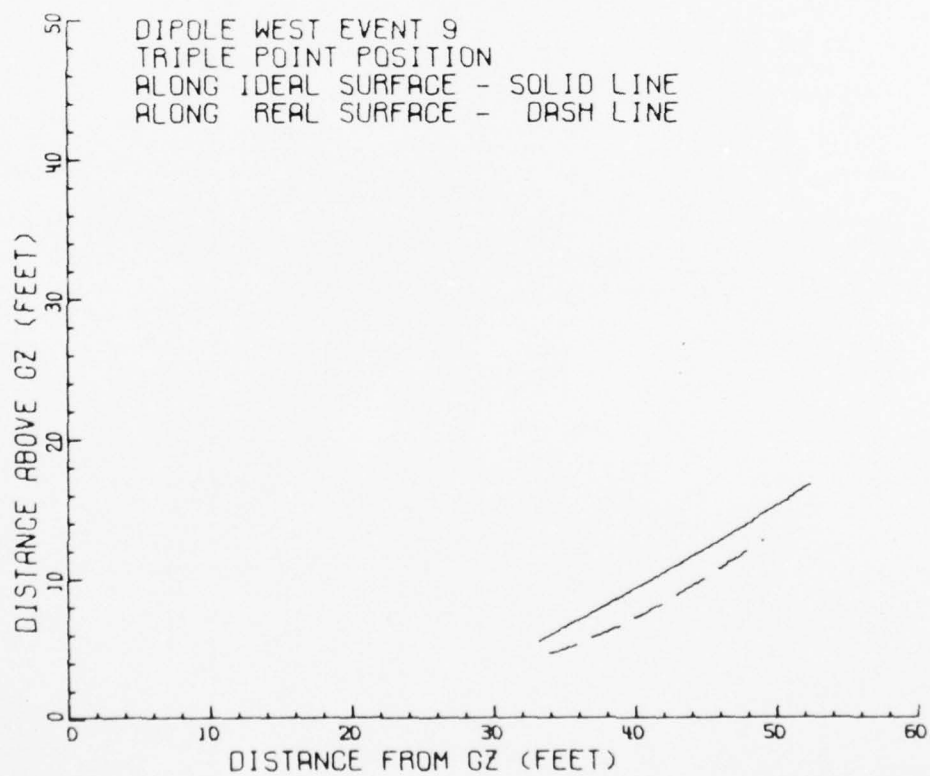


Figure 3.35. Triple-Point Paths From Real and Ideal Surfaces From Event 9, HOB \approx 15 Feet.

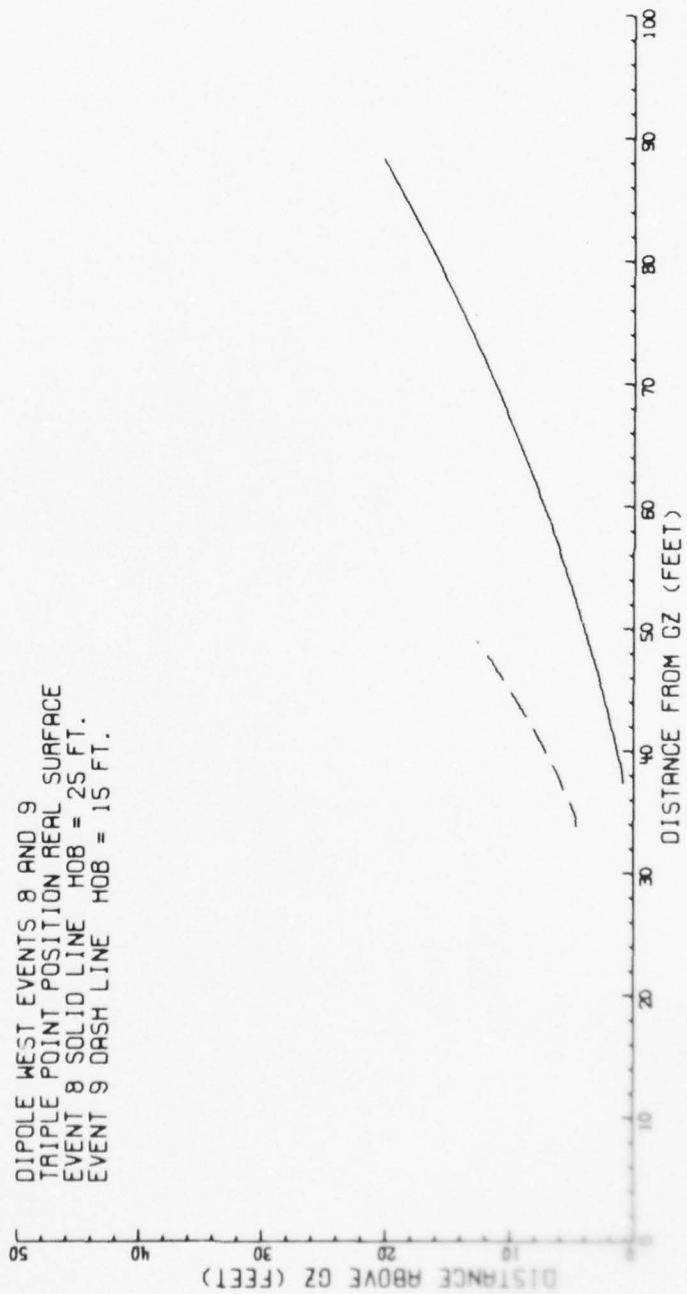


Figure 3.36. Comparison of Triple-Point Paths From Real Surface of Events 8 and 9.

AD-A044 032

DENVER RESEARCH INST COLO
DIPOLE WEST TECHNICAL PHOTOGRAPHY. (U)
FEB 77 J WISOTSKI

F/G 15/6

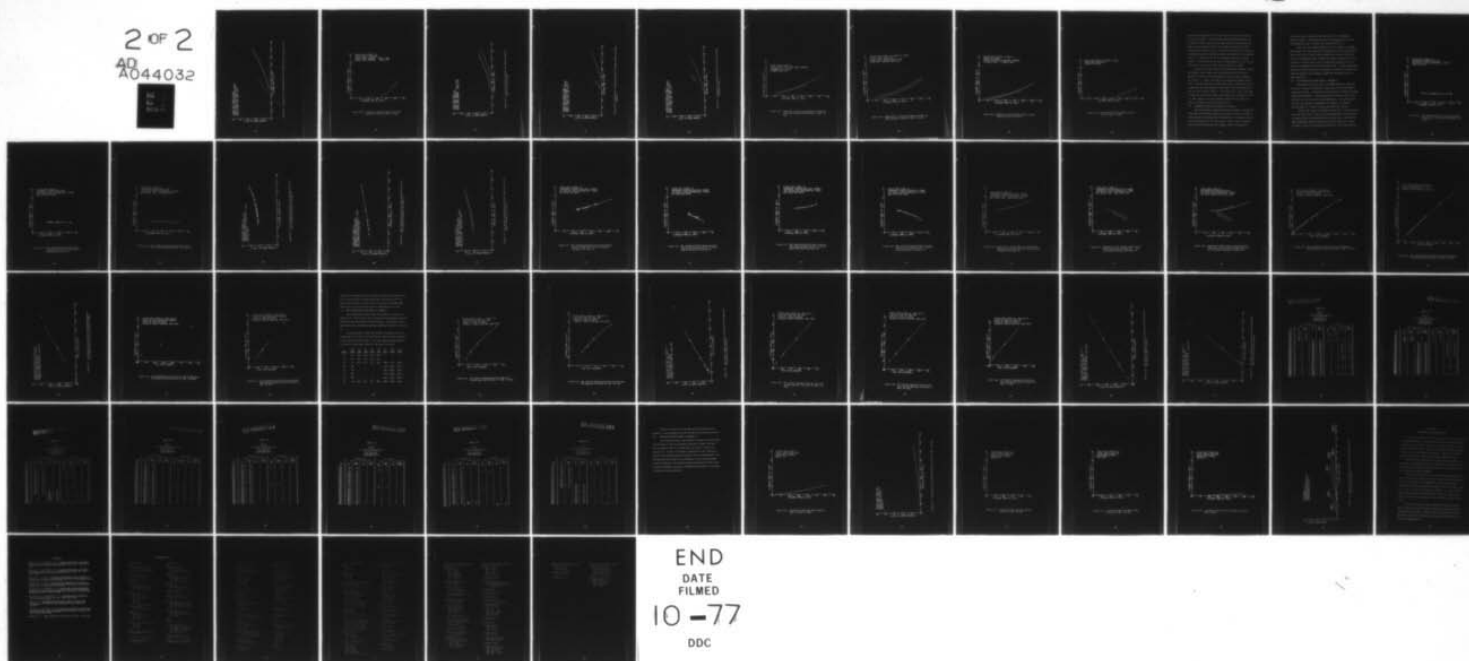
UNCLASSIFIED

DNA-4325F

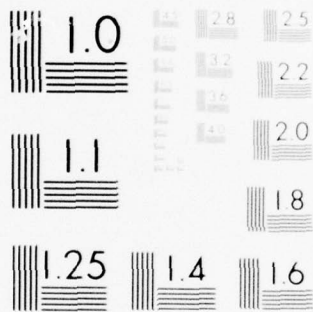
DNA001-73-C-0256
NL

2 OF 2

AD
A044032



END
DATE
FILMED
10 -77
DDC



MICROCOPY RESOLUTION TEST CHART
NATIONAL BUREAU OF STANDARDS-1963-A

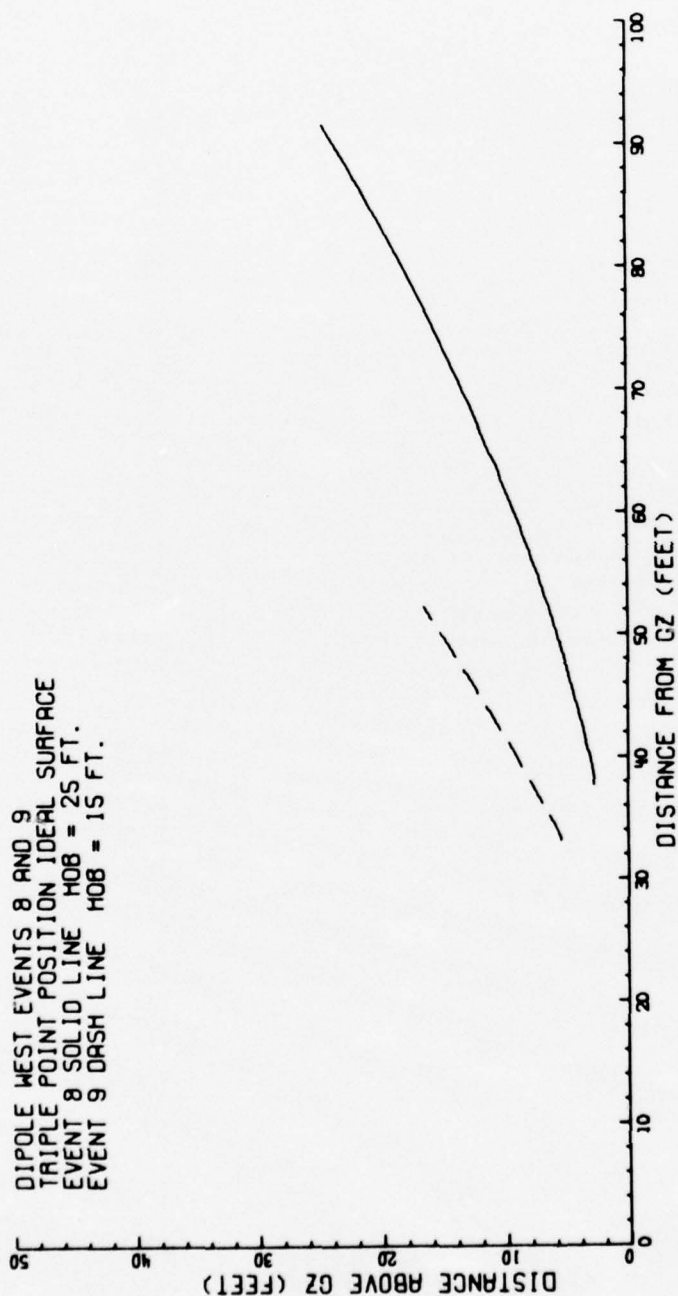


Figure 3.37. Comparison of Triple-Point Paths From Ideal Surface of Events 8 and 9.

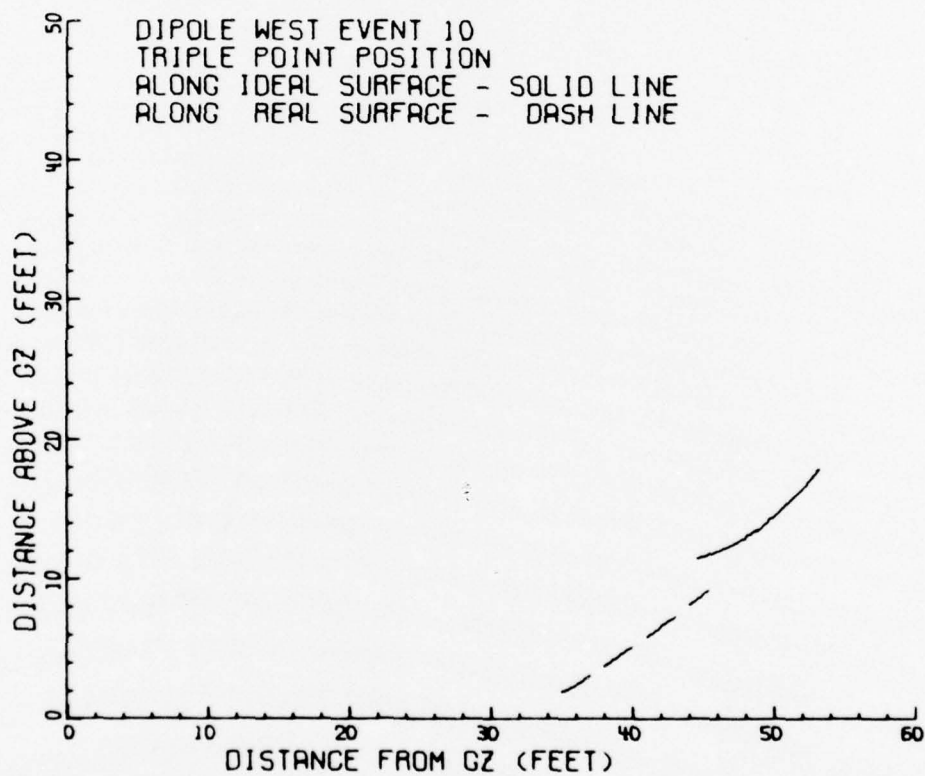


Figure 3.38. Triple-Point Paths From Real and Ideal Surfaces of Event 10, HOB \approx 15 Feet.

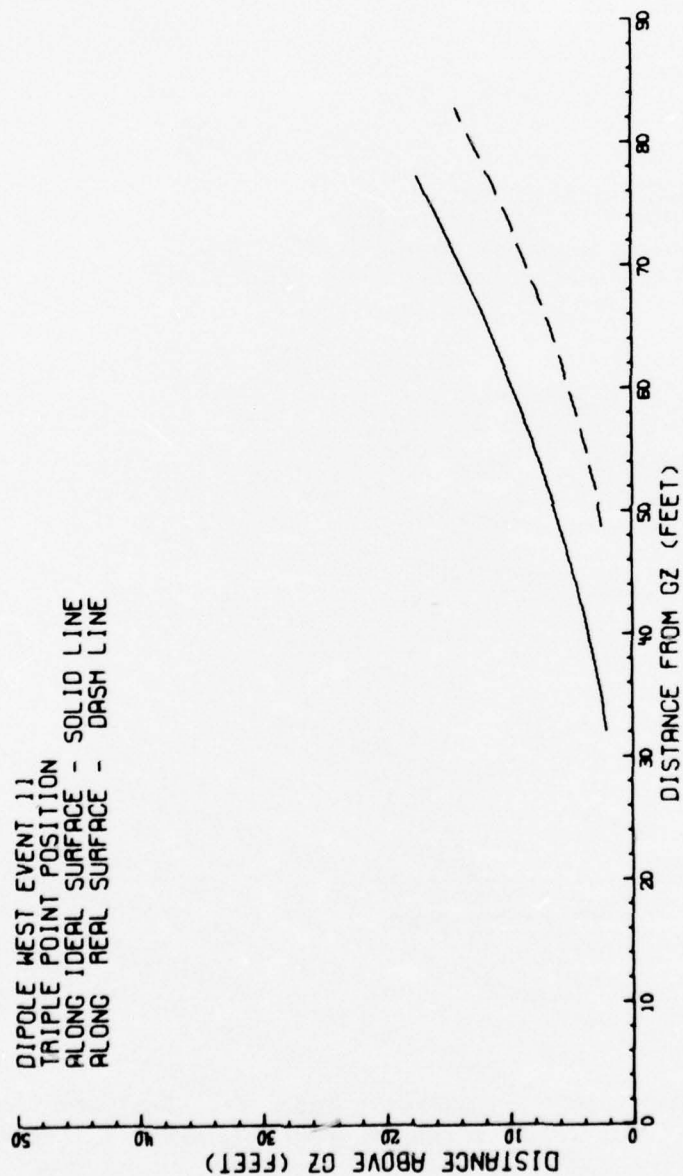


Figure 3.39. Triple-Point Paths From Real and Ideal Surfaces of Event 11, HOB \approx 25 Feet.

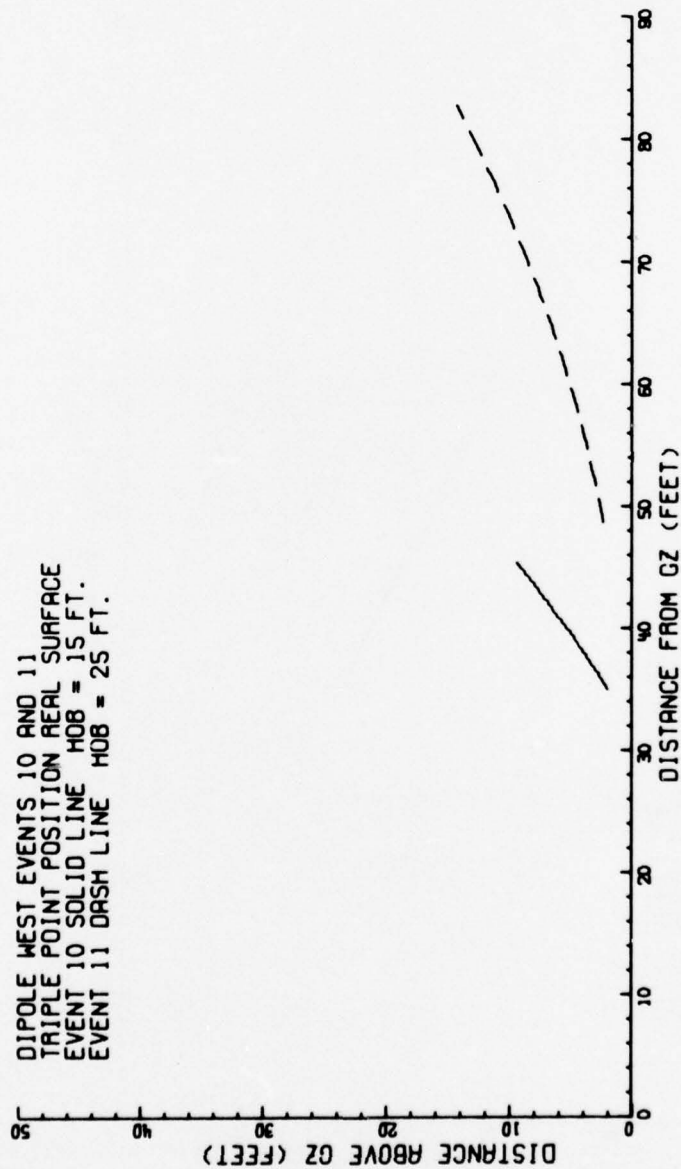


Figure 3.40. Comparison of Triple-Point Paths From Real Surface of Events 10 and 11.

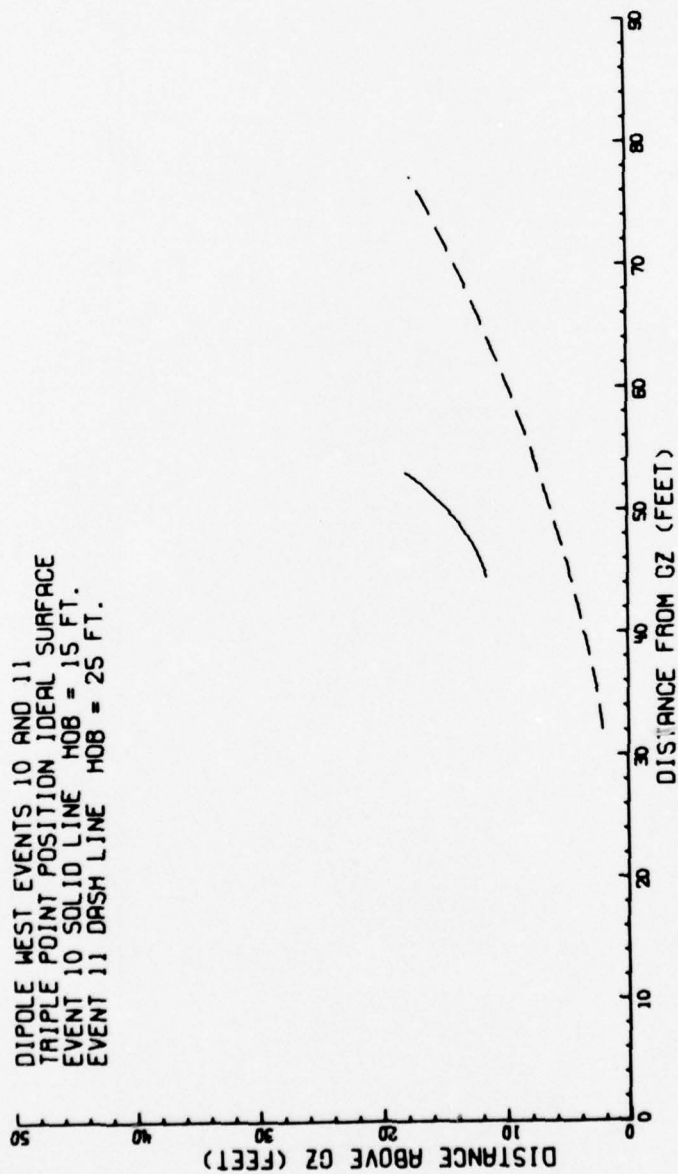


Figure 3.41. Comparison of Triple-Point Paths From Ideal Surface of Events 10 and 11.

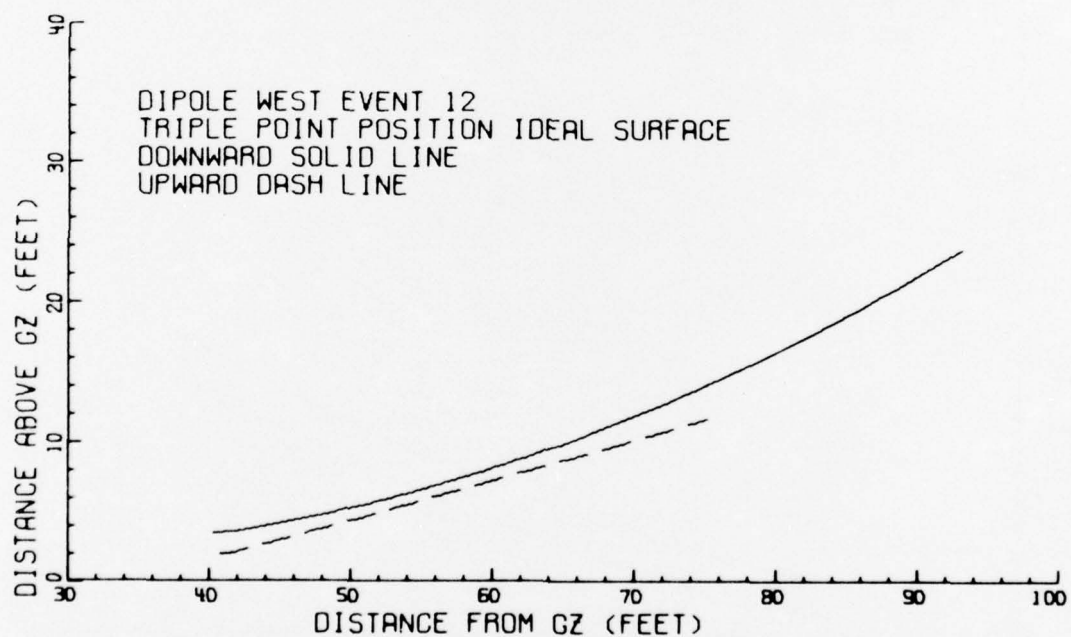


Figure 3.42. Comparison of Upward and Downward Triple-Point Paths From Ideal Surface of Event 12, HOB \approx 15 Feet.

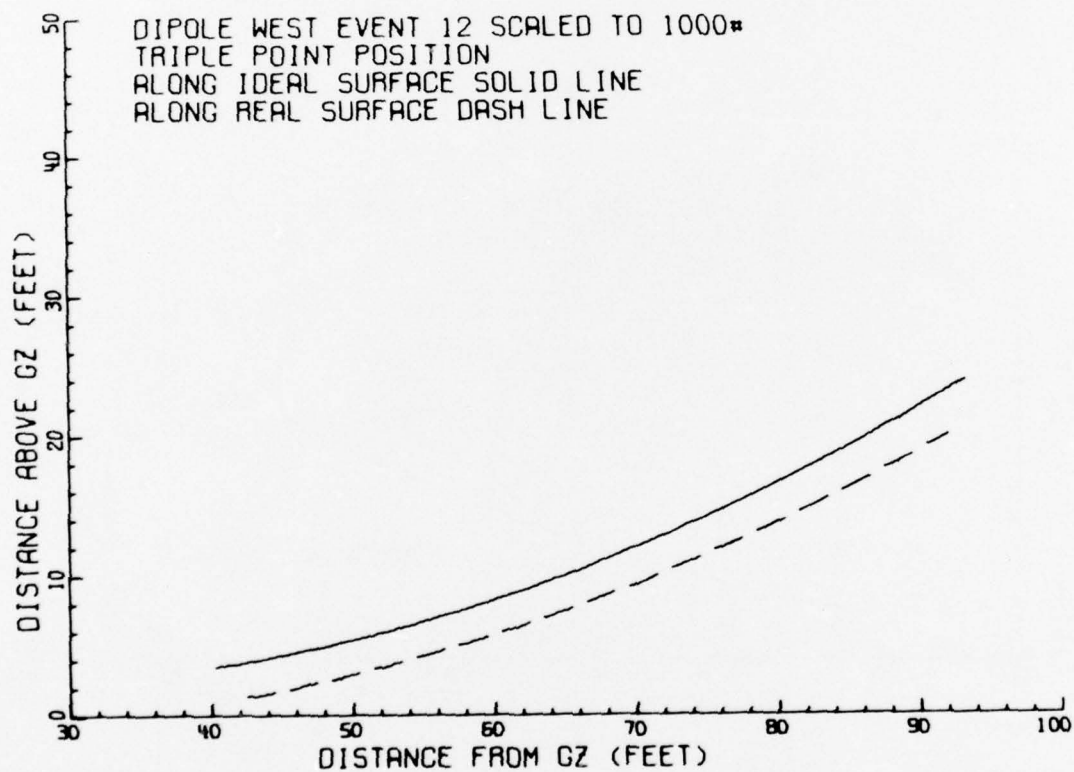


Figure 3.43. Comparison of Triple-Point Paths From Real and Ideal Surfaces of Event 12, HOB \approx 15 Feet.

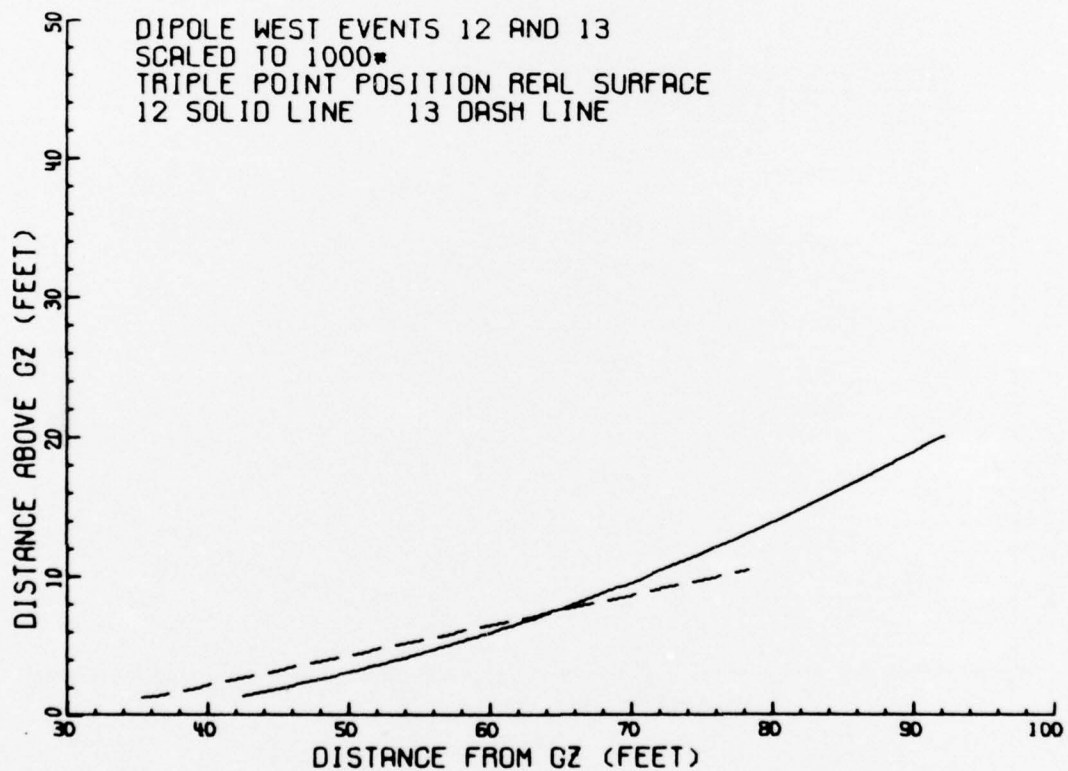


Figure 3.44. Comparison of Triple-Point Paths From Real Surface of Events 12 and 13.

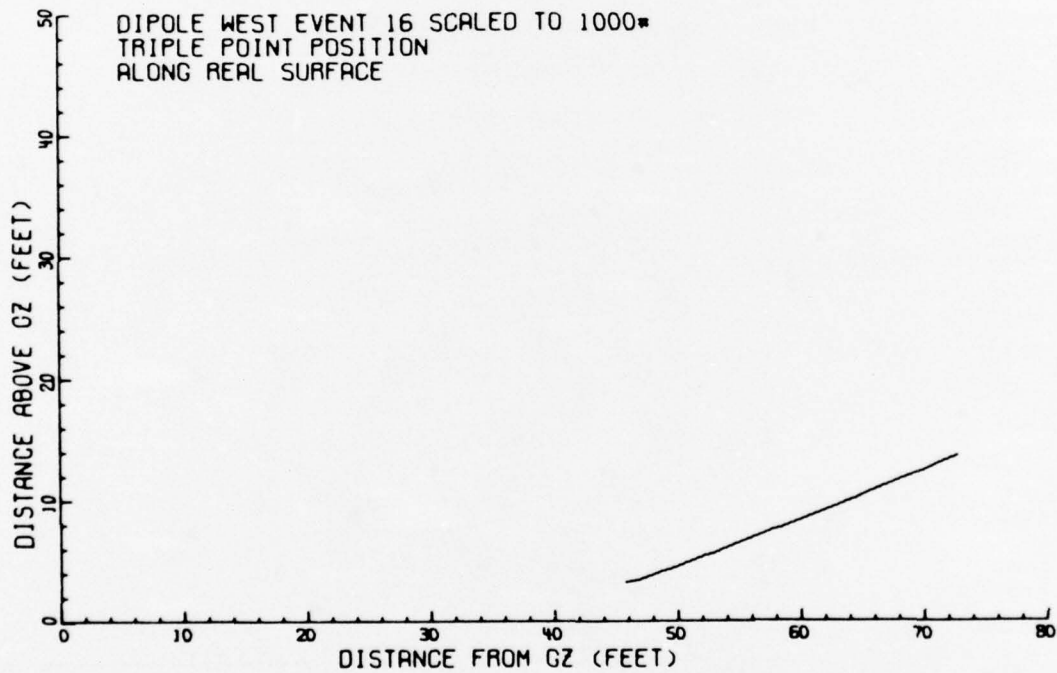


Figure 3.45. Triple-Point Path From Real Surface of Event 16, HOB \approx 15 Feet.

reflective surface than from the real reflective surface for both the 15 and 25 foot HOB's. There are much greater differences between the triple-point paths' slopes from the ideal reflective surface when compared to those obtained from the real rough-soft reflective surface employed during Events 10 and 11. See Figures 3.38 and 3.39. As would be expected the greater the HOB the lesser the slope of the triple-point path, i.e., slower the rise of the triple-point path from a similar surface. This condition can be seen by comparing Events 10 and 11, and 8 and 9 with 12, 13 and 16 along the real reflective surface.

Due to the fact that Event 12 was detonated at an HOB of 15 feet, the backdrop screen allowed the triple point paths from the ideal reflective surface to be viewed upwards as well as normally downward. See Figure 1.1. Figure 3.42 shows close comparisons between the two paths. The ideal reflective surface again shows a steeper slope of the triple-point path when compared to the slope of the triple-point path from the real surface of Event 12. See Figure 3.43. Figure 3.44 shows a comparison of the real-surface triple-point paths from Events 12 and 13. There appears to be good agreement between the two events and Event 16. Compare Figure 3.44 to Figure 3.45.

3.5 INTERSECTION-POINT PATHS EVENTS 13, 15 AND 16

The nonsimultaneous detonations produced shockwaves intersection-point paths which differed between events because of the variations in the separation times between the two detonations. The upper charge was always detonated before the lower charge. Events 13 and 15 produced only one intersection-point path; whereas, Event 16 produced two.

Intersection-point predictions were made by the Air Force Weapons Laboratory (AFWL). The AFWL predictions are presented along with the DRI photographic data in Figures 3.46 through 3.58, Ref. 9.

Event 16, 3 millisecond separation time, was added to the DIPOLE WEST Program after AFWL predictions indicated that two intersection-point paths would exist similar to those obtained from the ideal reflective surface as presented by Event 12 data; and would be generated from some surface of revolution about an axis through both charges which would create two nonsymmetrical intersection-point paths. The DRI photographic data and the AFWL predictions are presented in Figures 3.52 through 3.58. There was generally good agreement between DRI photographic data and AFWL predictions.

3.6 POSITION-TIME DATA FROM EVENTS 17 THROUGH 24

The height-of-burst portion of the DIPOLE WEST Series consisted of Events 17 through 24 whose HOB's ranged from 47 to 144 feet above a smooth-hard surface. The detonations were obtained from center initiated 1,000-pound TNT spheres. The same experimental arena was used for this HOB series as for the multiple charge experiments. The surface camera positions were changed to accommodate the recording of shockwave position-times out to range of approximately 360 feet from GZ.

Figures 3.59 through 3.63 present position-time in the Mach-region along the real surface. Note that the large HOB events did not produce any apparent Mach-region shockwaves which were obvious in the DRI high speed photographs obtained along the real surface except for a small increment of time at late-times during Event 23. The FA position-time

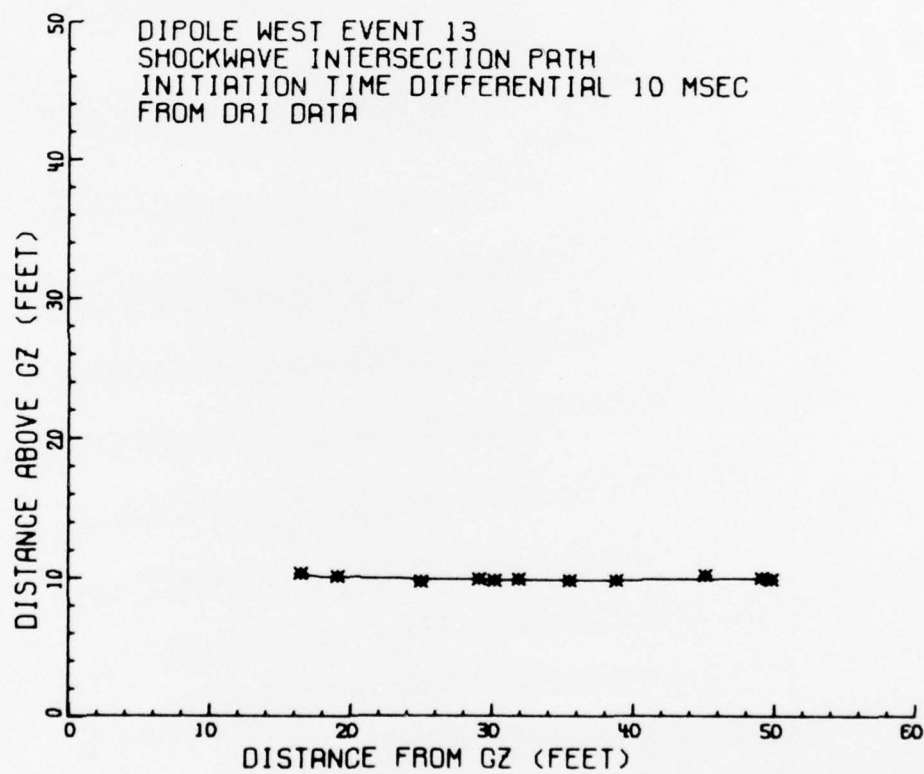


Figure 3.46. DRI Intersection-Point Path Curve and Data Points for a 10 Millisecond Time-Delay From Event 13.

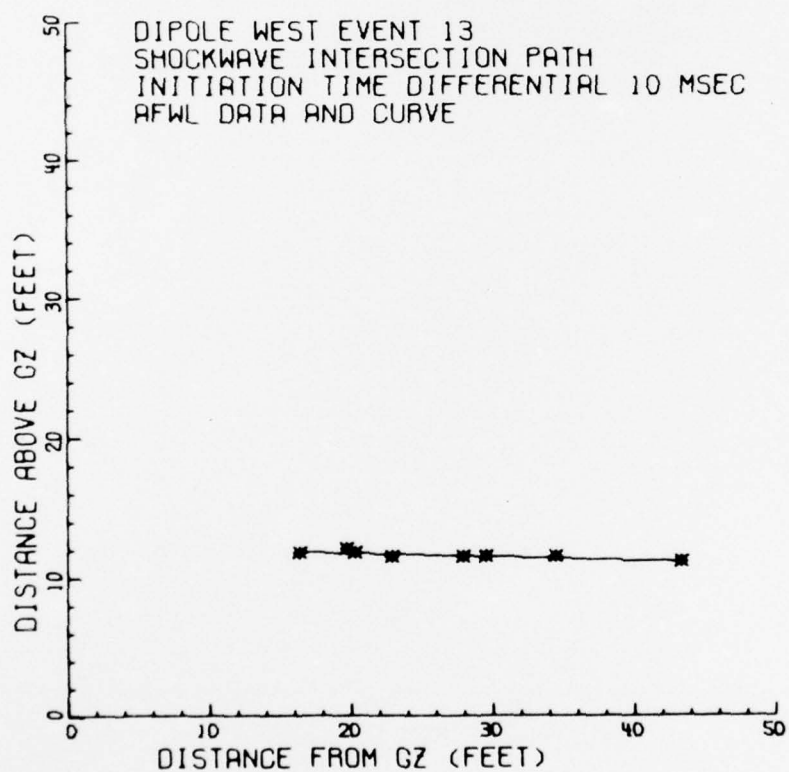


Figure 3.47. AFWL Intersection-Point Path Curve and Data Points for a 10 Millisecond Time-Delay From Event 13.

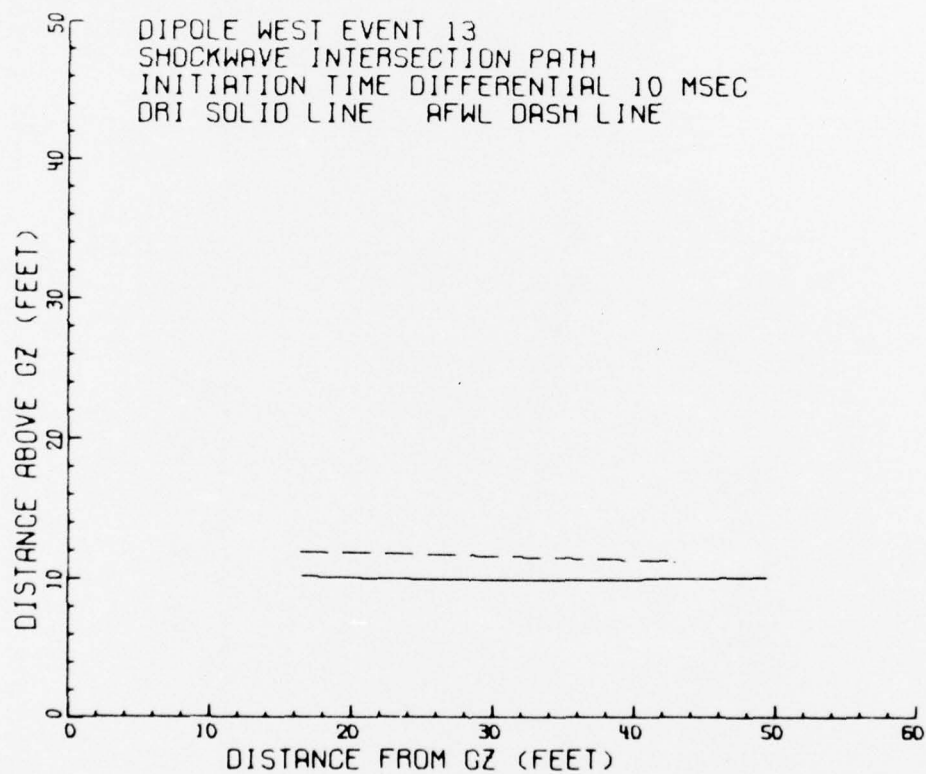


Figure 3.48. DRI and AFWL Intersection-Point Path Curves for a 10 Millisecond Time-Delay From Event 13.

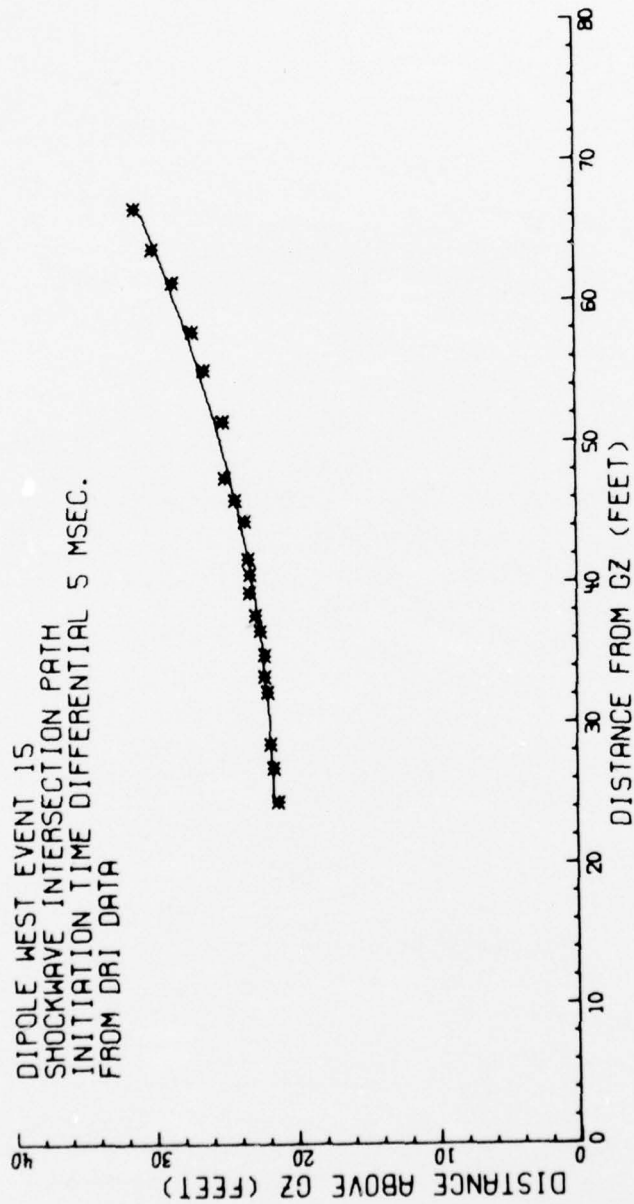


Figure 3.49. DRI Intersection-Point Path Curve and Data Points for a 5 Millisecond Time-Delay From Event 15.

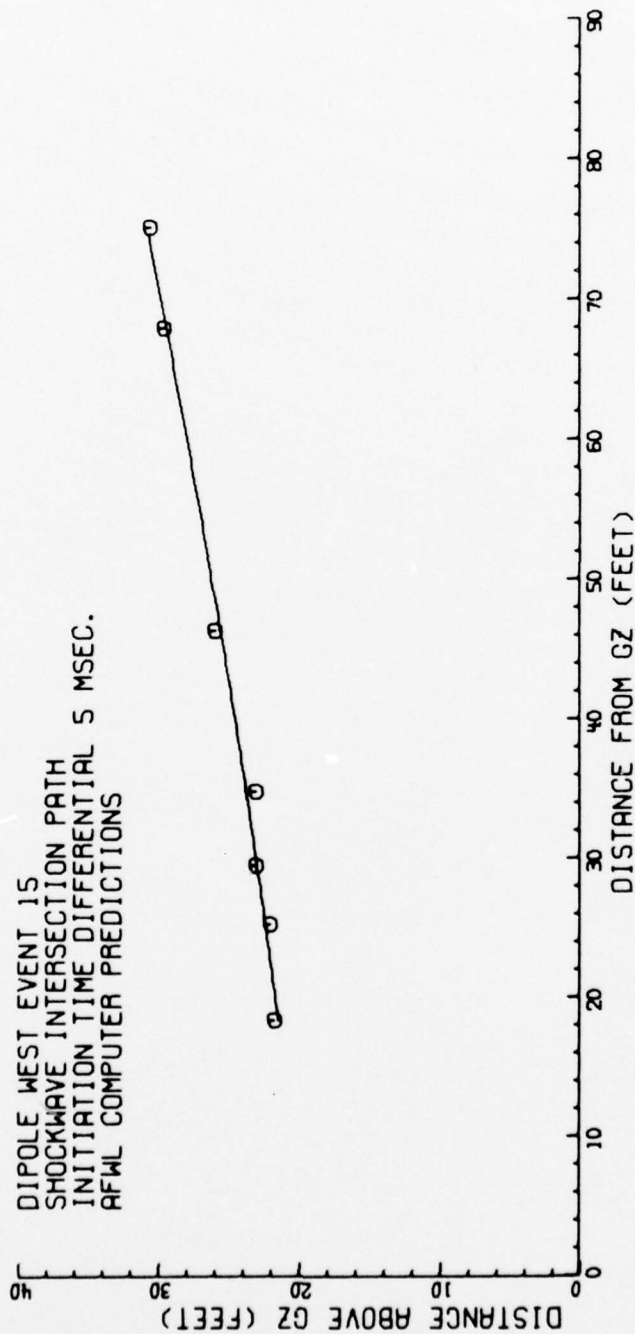


Figure 3.50. AFWL Intersection-Point Path Curve and Data Points for a 5 Millisecond Time-Delay From Event 15.

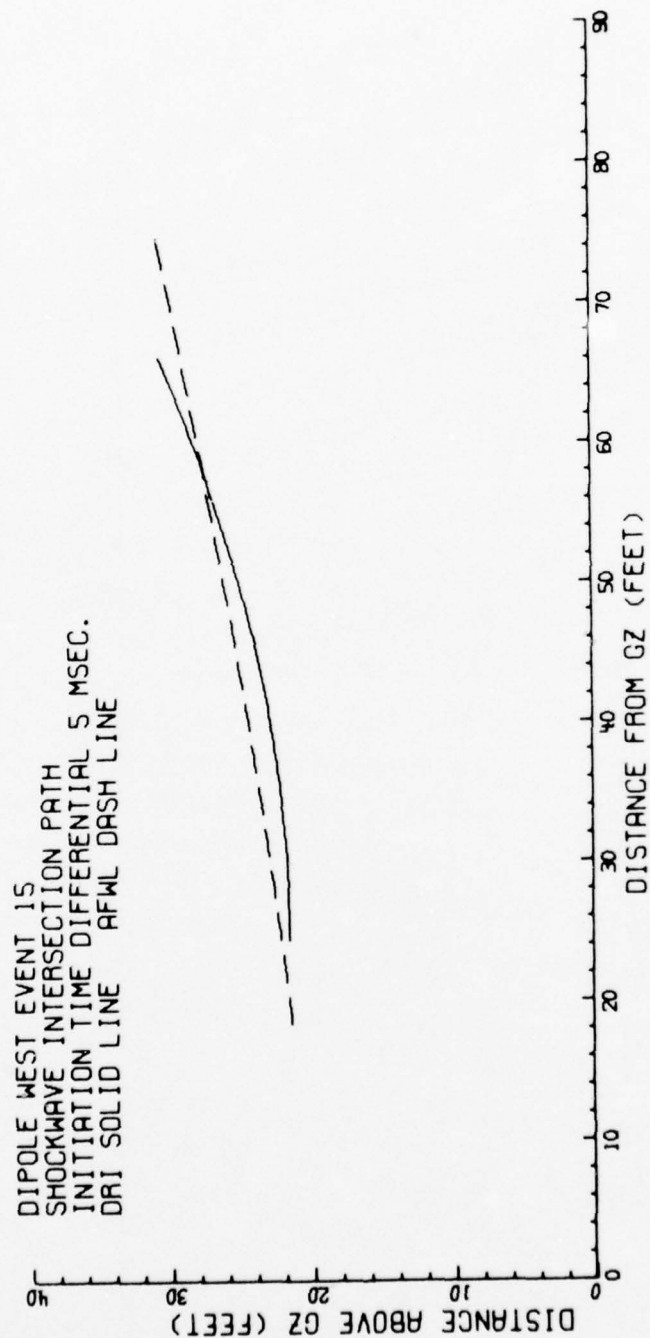


Figure 3.51. DRI and AFWL Intersection-Point Path Curves for a 5 Milli-second Time-Delay From Event 15.

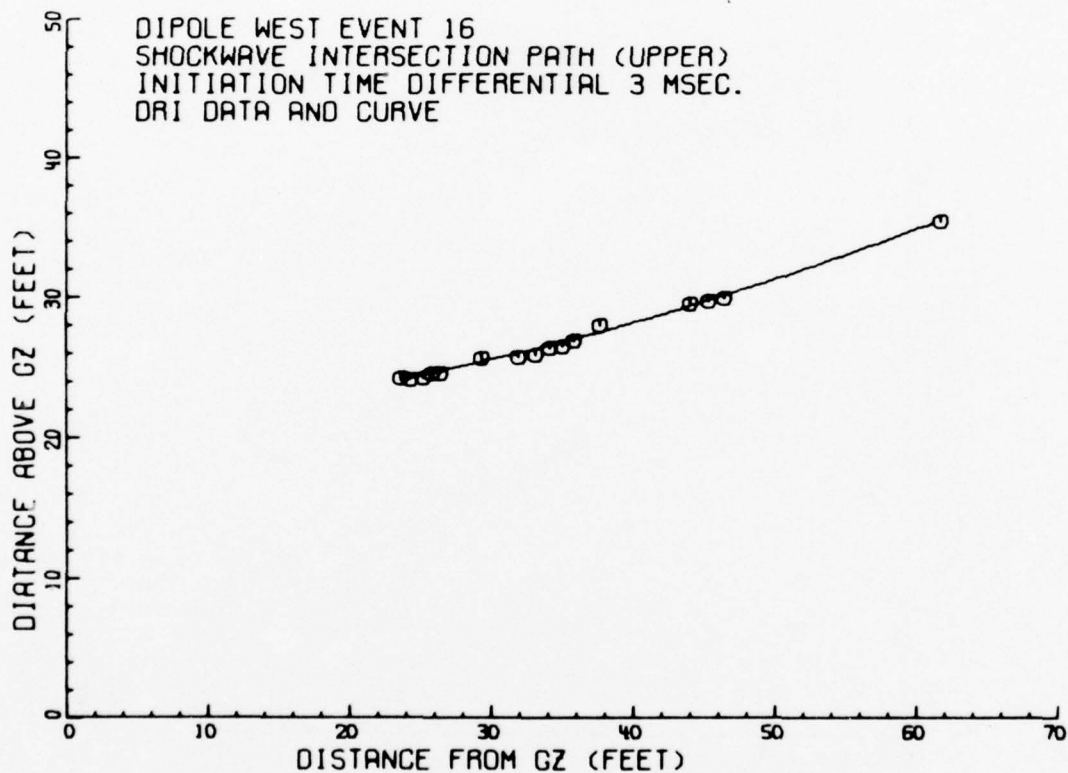


Figure 3.52. DRI Intersection-Point Paths Curve and Data Points of Upper Path for a 3 Millisecond Time-Delay From Event 16.

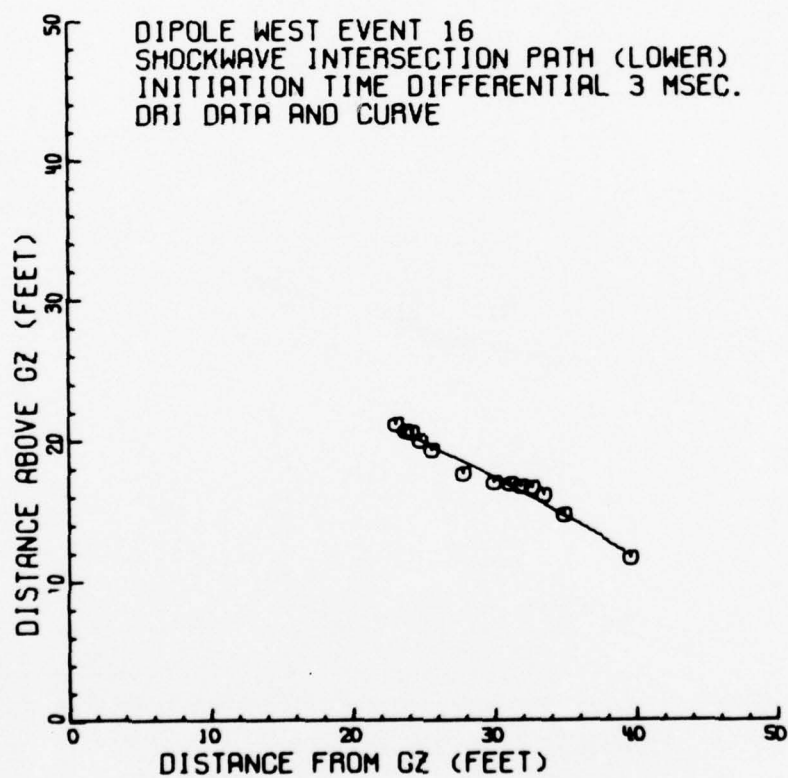


Figure 3.53. DRI Intersection-Point Paths Curve and Data Points of Lower Path for a 3 Milli-second Time-Delay From Event 16.

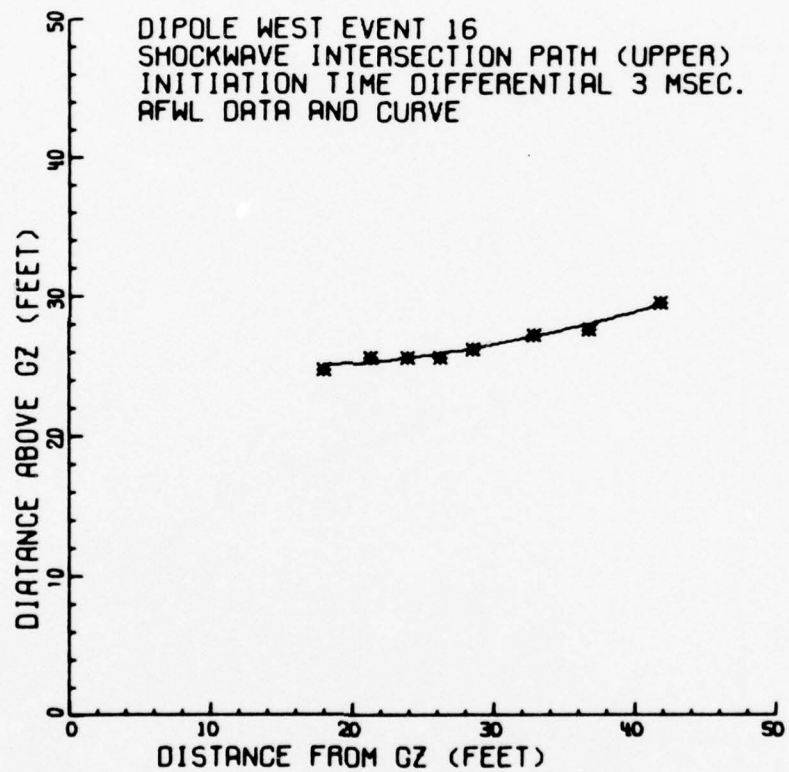


Figure 3.54. AFWL Intersection-Point Paths Curve and Data Points of Upper Path for a 3 Millisecond Time-Delay From Event 16.

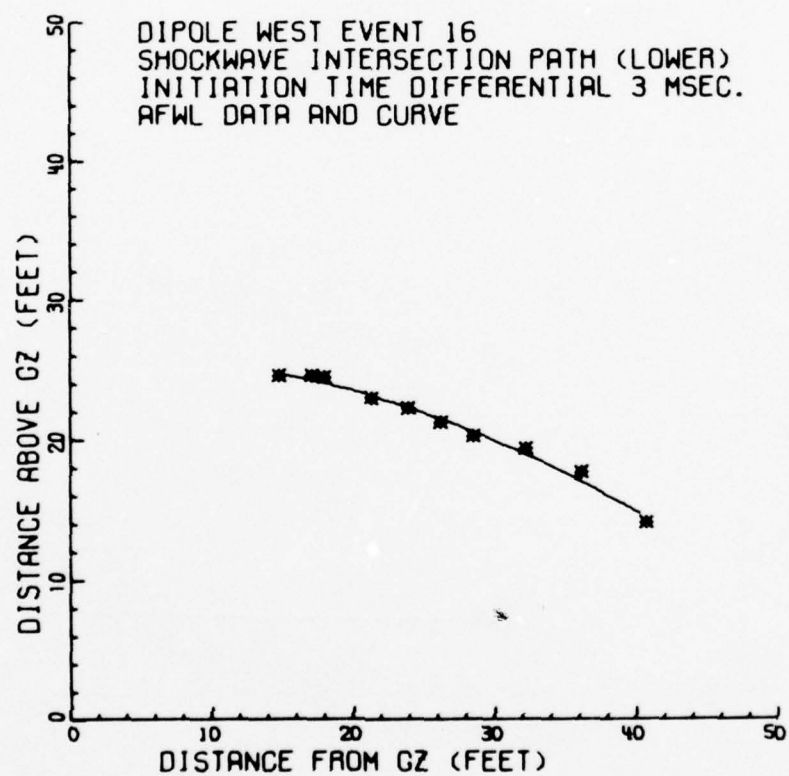


Figure 3.55. AFWL Intersection-Point Paths Curve and Data Points of Lower Path for a 3 Milli-second Time-Delay From Event 16.

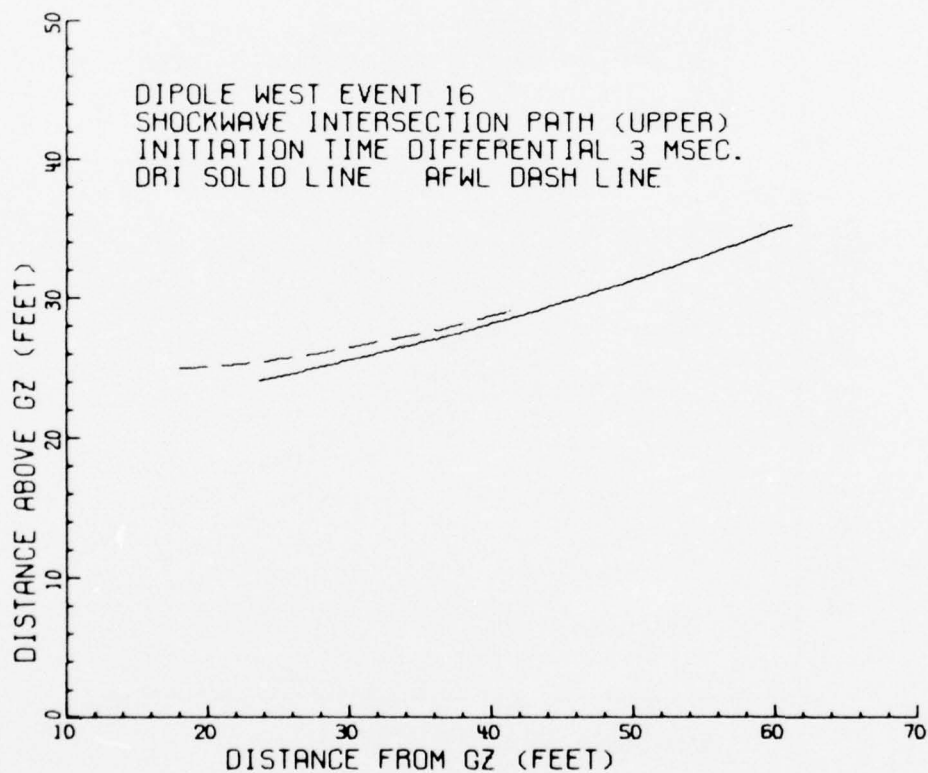


Figure 3.56. Comparison of DRI and AFWL Intersection-Point Paths Curves of Upper Path for a 3 Millisecond Time-Delay From Event 16.

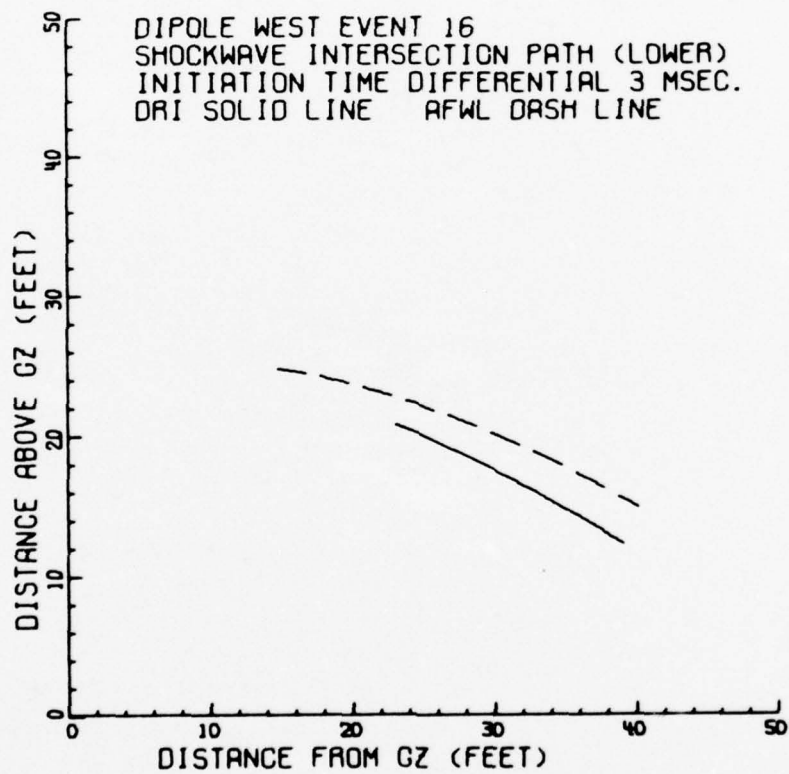


Figure 3.57. Comparison of DRI and AFWL Intersection-Point Path Curves of Lower Path for a 3 Millisecond Time-Delay From Event 16.

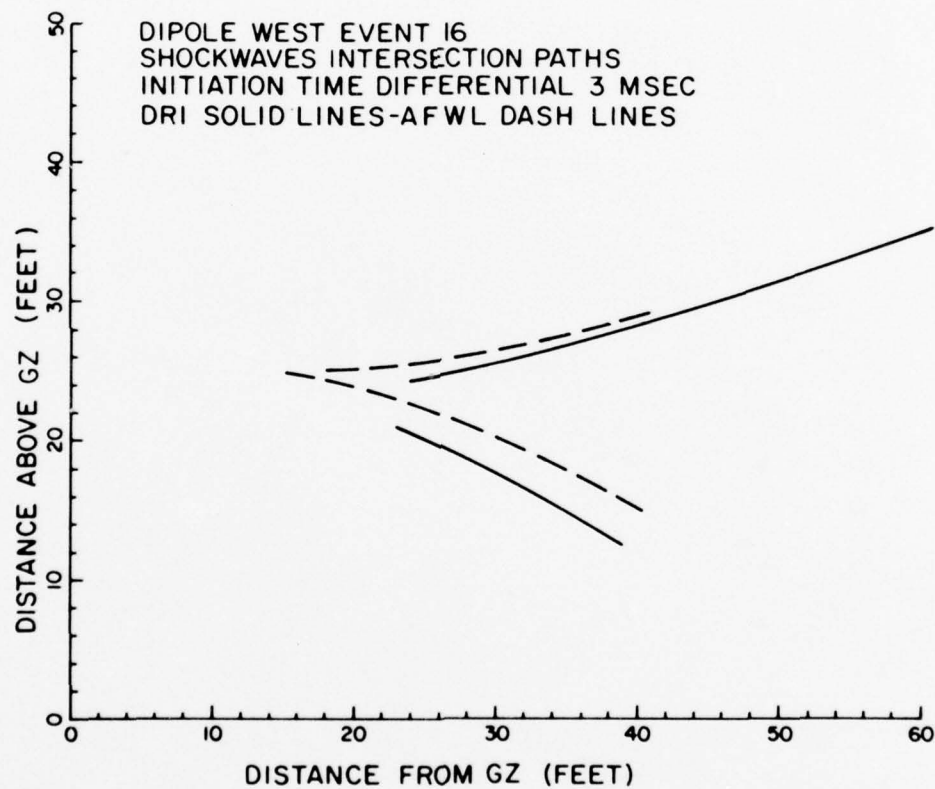


Figure 3.58. Comparison of DRI and AFWL Intersection-Point Path Curves of Both Lower and Upper Paths for a 3 Millisecond Time-Delay From Event 16.

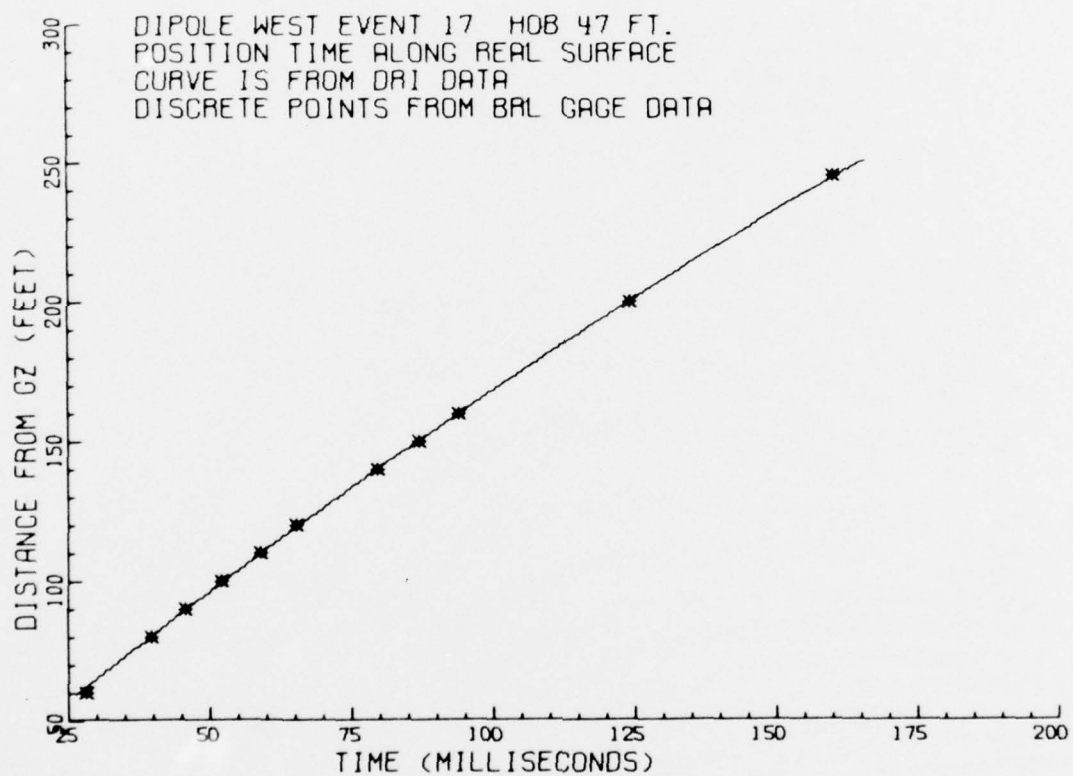


Figure 3.59. DRI Shockwave Position-Time Curve and BRL Gage Data Along Real Surface From Event 17, HOB \approx 47 Feet.

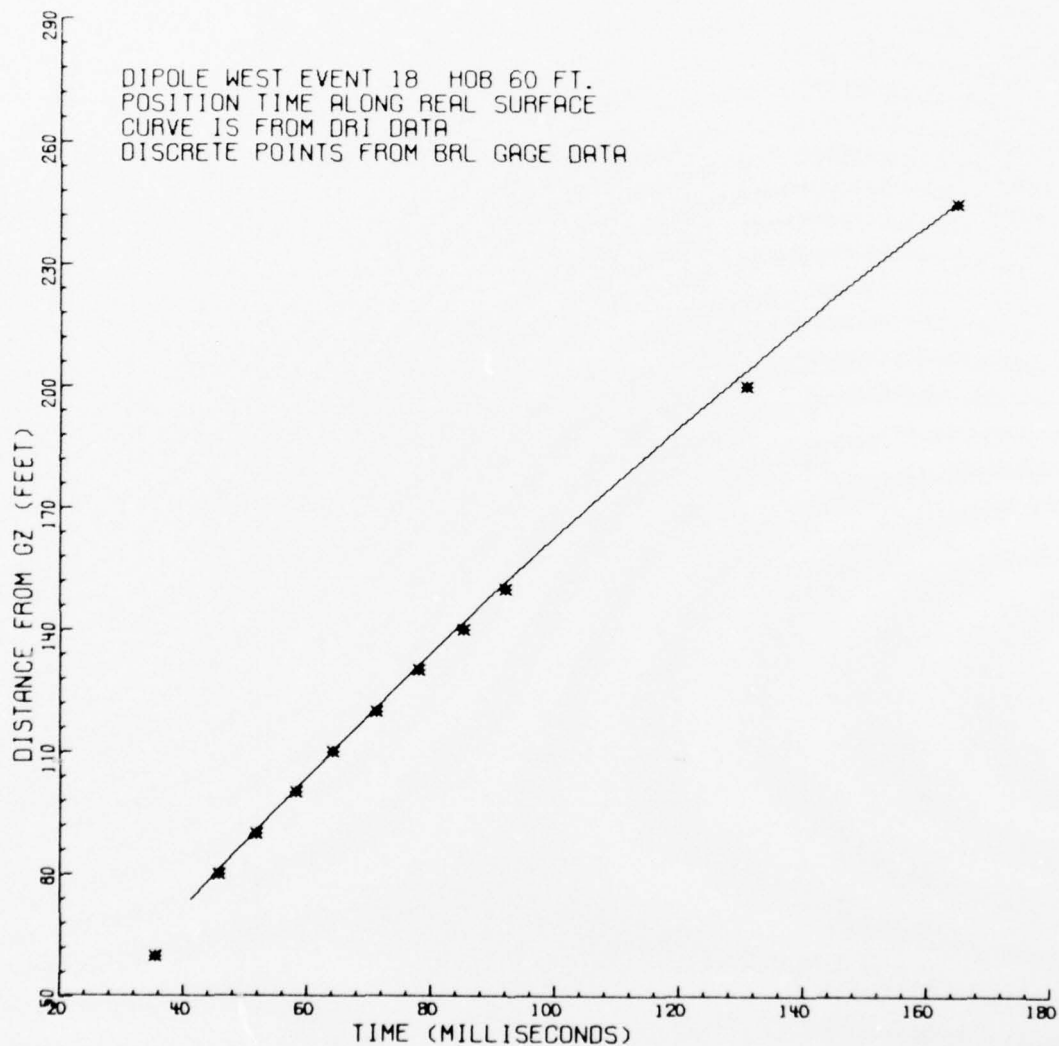


Figure 3.60. DRI Shockwave Position-Time Curve and BRL Gage Data Along Real Surface From Event 18, HOB \approx 60 Feet.

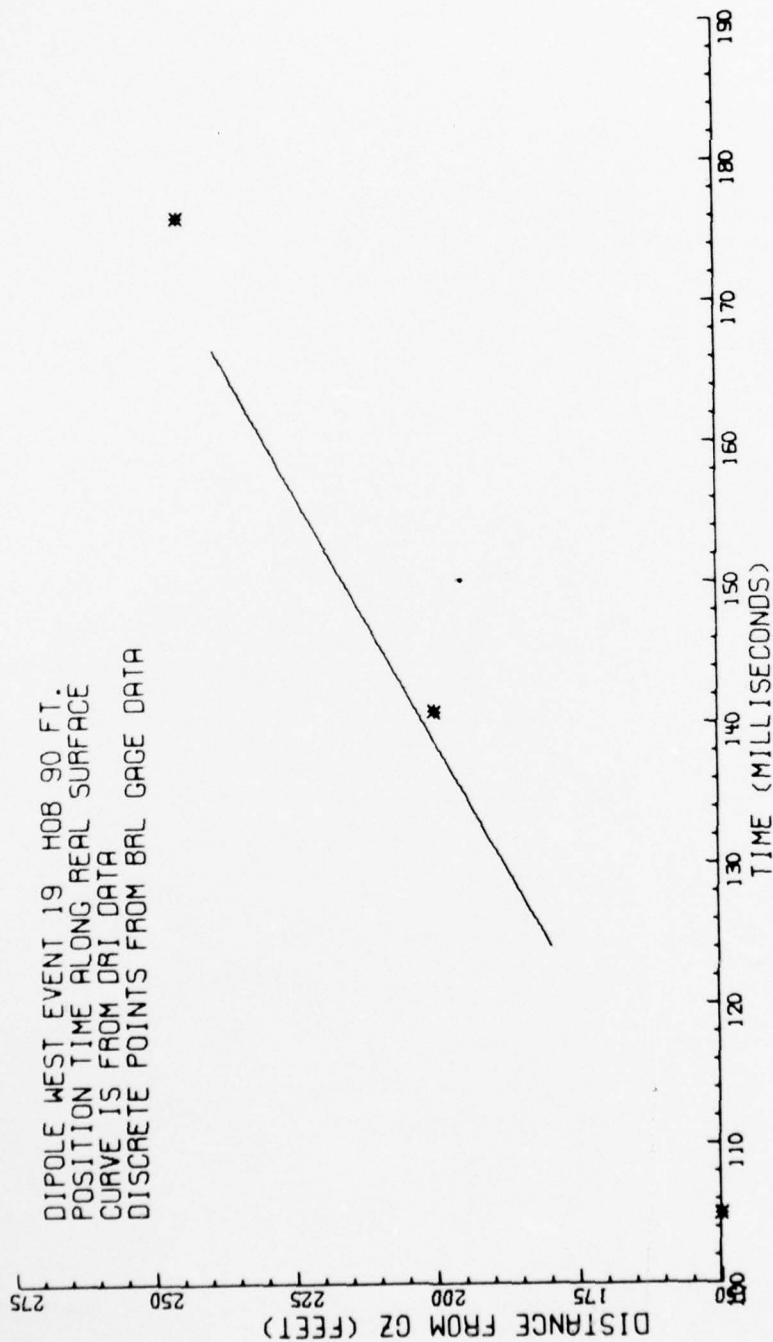


Figure 3.61. DRI Shockwave Position-Time Curve and BRL Gage Data Along Real Surface From Event 19, HOB \approx 90 Feet.

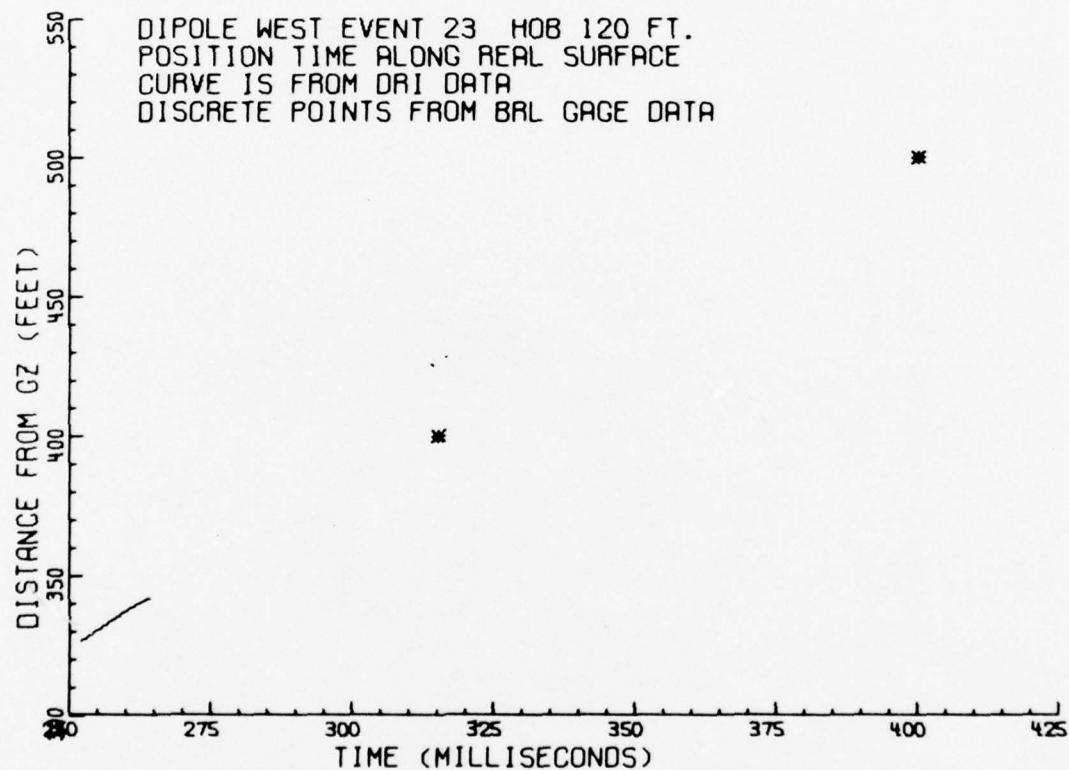


Figure 3.62. DRI Shockwave Position-Time Curve and BRL Gage Data Along Real Surface From Event 23, HOB \approx 120 Feet.

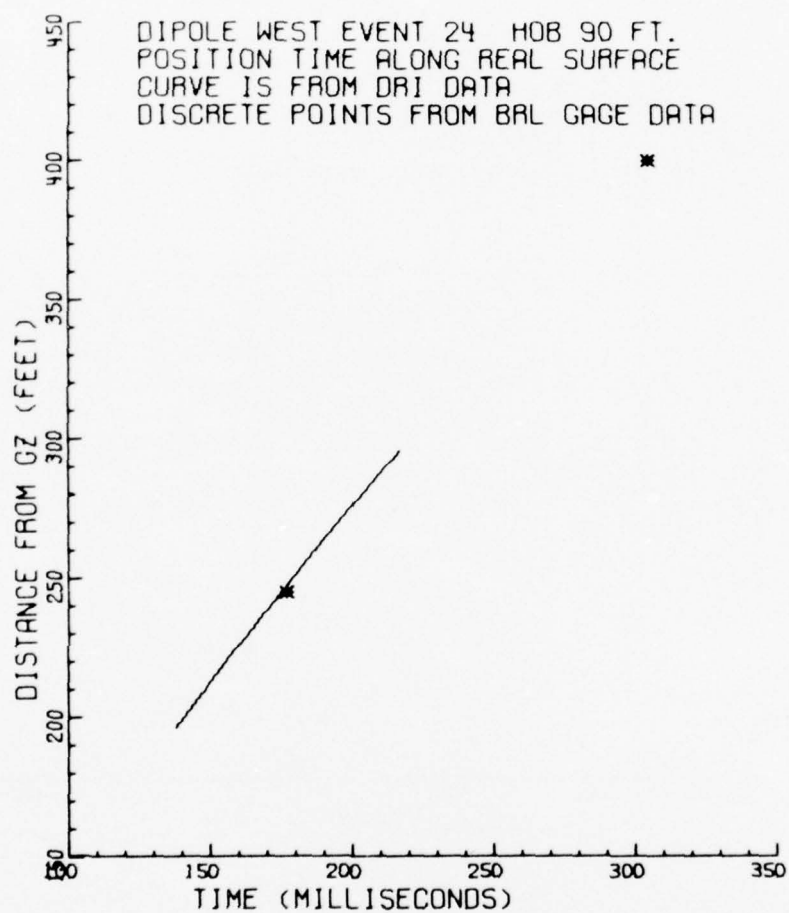


Figure 3.63. DRI Shockwave Position-Time Curve and BRL Gage Data Along Real Surface From Event 24, HOB \approx 90 Feet.

data from all the HOB events are presented in Figures 3.64 through 3.71. The FA position-times at the BRL gages were determined by using the slant ranges measured from the center of the charge to the BRL gages mounted above the ground surface and the shockwave arrival times.

3.7 PEAK PRESSURE DATA FROM EVENTS 17 THROUGH 24

DRI and BRL peak pressure values are presented in Tables 3.12 through 3.19. The DRI values were calculated using shockwave velocities determined from photographic position-time data. The equations used in the peak pressure calculations have been mentioned previously in Section 3.2.

The presented BRL FA data were obtained from gages which were situated 20, 30, 40, 60, 90, 150 and 245 feet from GZ and at a height of 30 feet above the ground surface. The slant ranges from the center of the charge to these gages varied for the events as follows:

<u>Event</u>	<u>HOB (ft)</u>	<u>20 (ft)</u>	<u>30 (ft)</u>	<u>40 (ft)</u>	<u>60 (ft)</u>	<u>90 (ft)</u>	<u>150 (ft)</u>	<u>245 (ft)</u>
17	47	26.2	34.4	43.5	62.4	-	-	-
18	60	36.1	42.4	50.0	67.1	-	-	-
19	90	63.2	67.1	72.1	84.9	108.2	161.6	252.2
20	120	-	-	-	-	127.3	174.9	261.0
21	144	-	-	-	-	145.2	188.4	270.2
22	144	-	-	-	-	145.2	188.4	270.2
23	120	-	-	-	-	127.3	174.9	261.0
24	90	63.2	67.1	72.1	84.9	108.2	161.6	252.2

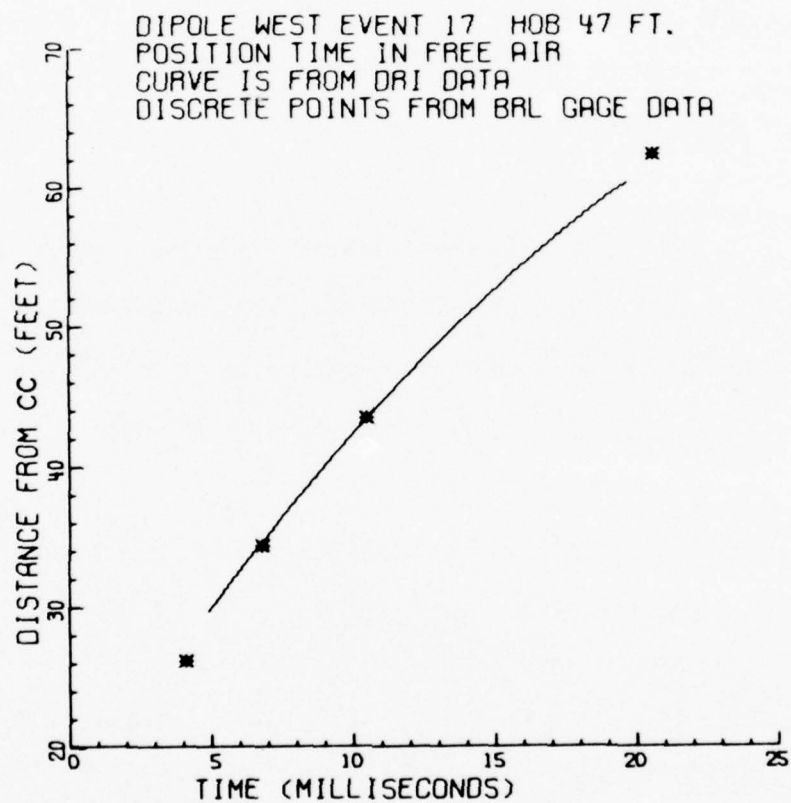


Figure 3.64. DRI Free-Air Shockwave Position-Time Curve
and BRL Gage Data From Event 17, HOB \approx 47 Feet.

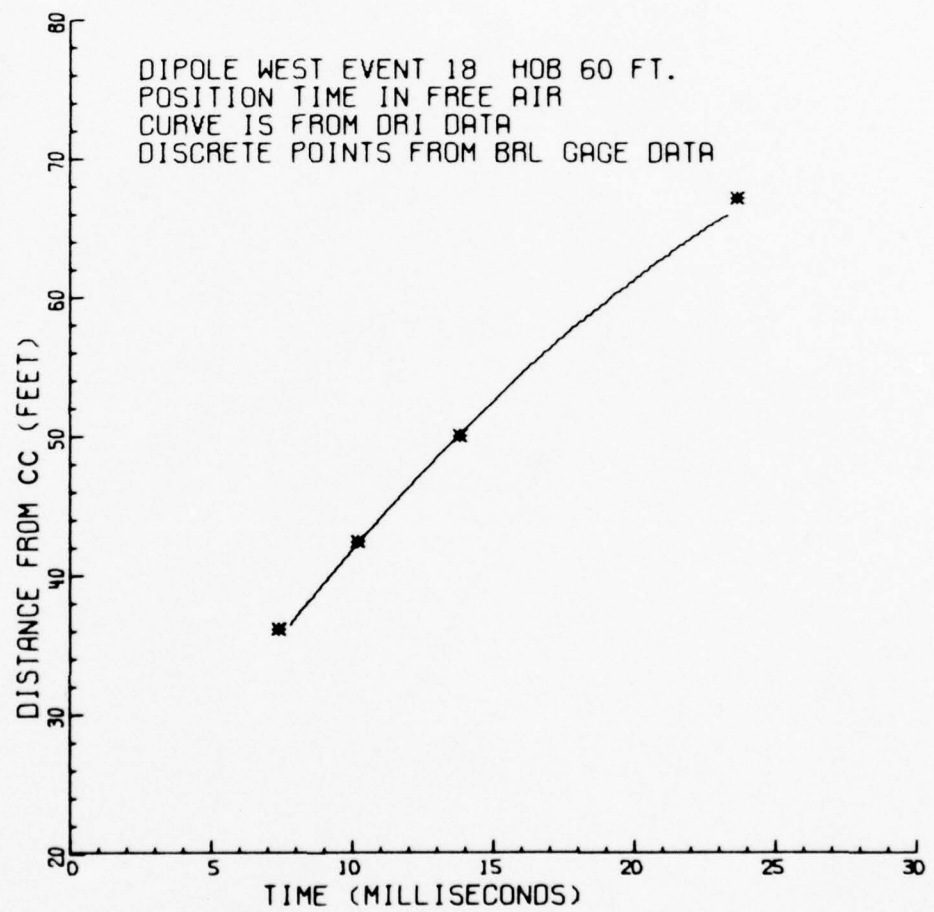


Figure 3.65. DRI Free-Air Shockwave Position-Time Curve and BRL Gage Data From Event 18, HOB \approx 60 Feet.

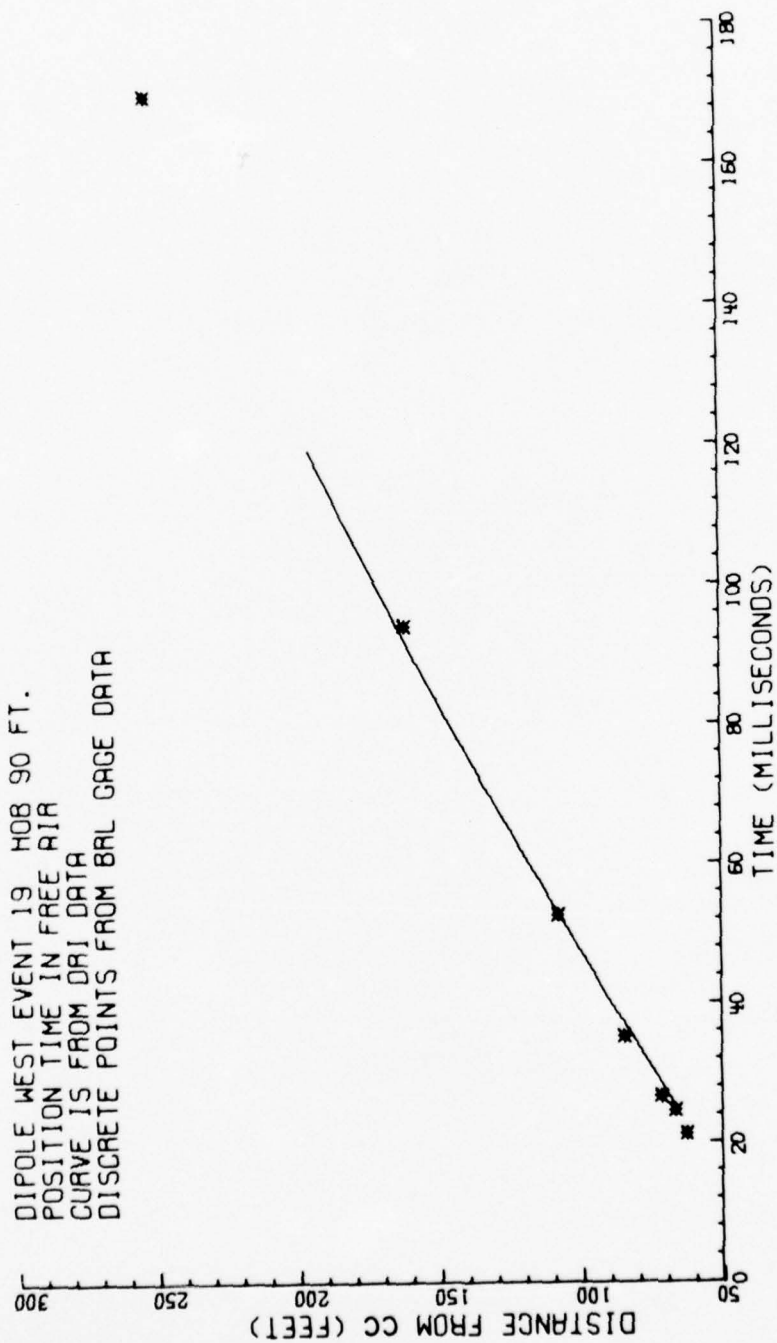


Figure 3.66. DRI Free-Air Shockwave Position-Time Curve and BRL Gage Data
 From Event 19, HOB \approx 90 Feet.

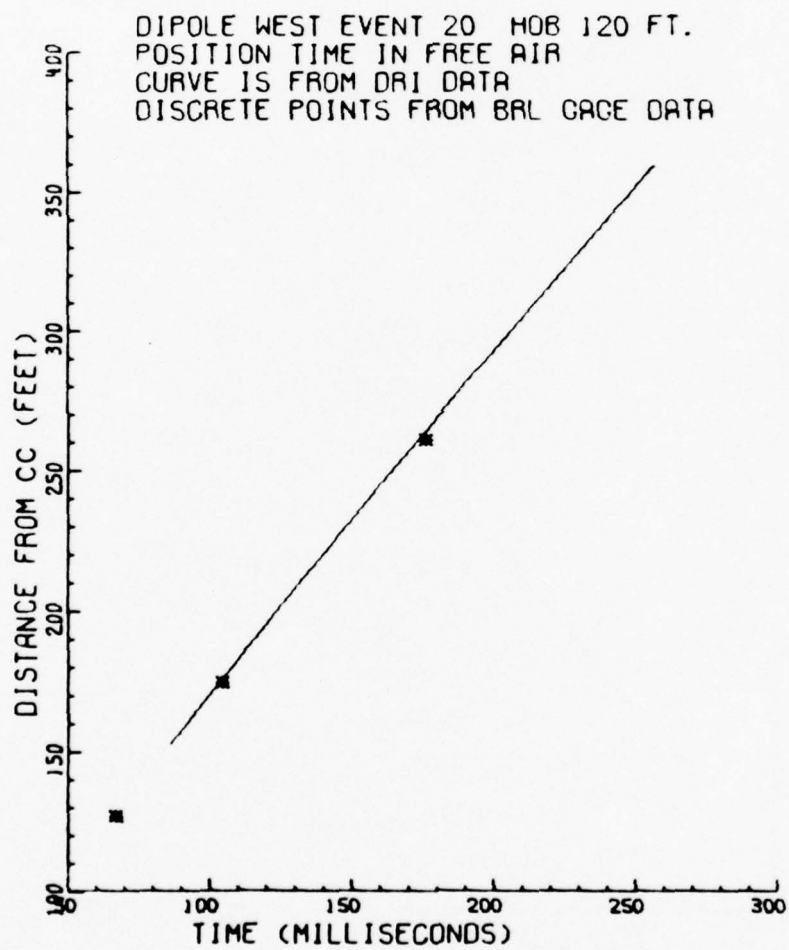


Figure 3.67. DRI Free-Air Shockwave Position-Time Curve and BRL Gage Data From Event 20, HOB \approx 120 Feet.

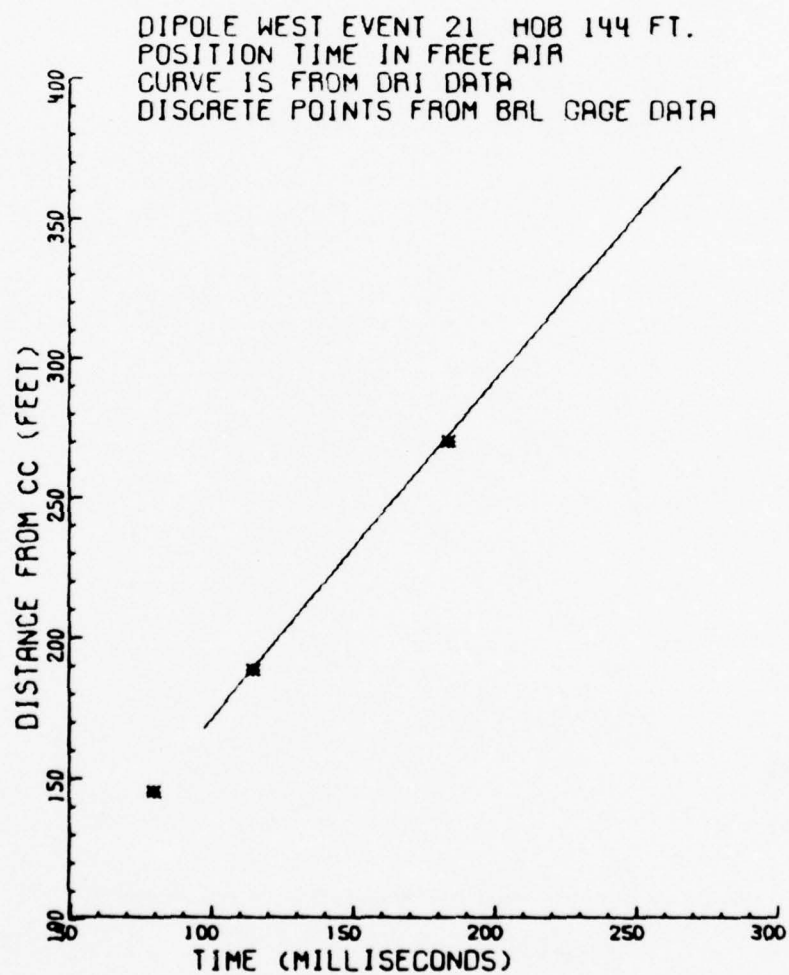


Figure 3.68. DRI Free-Air Shockwave Position-Time Curve and BRL Gage Data From Event 21, HOB \approx 144 Feet.

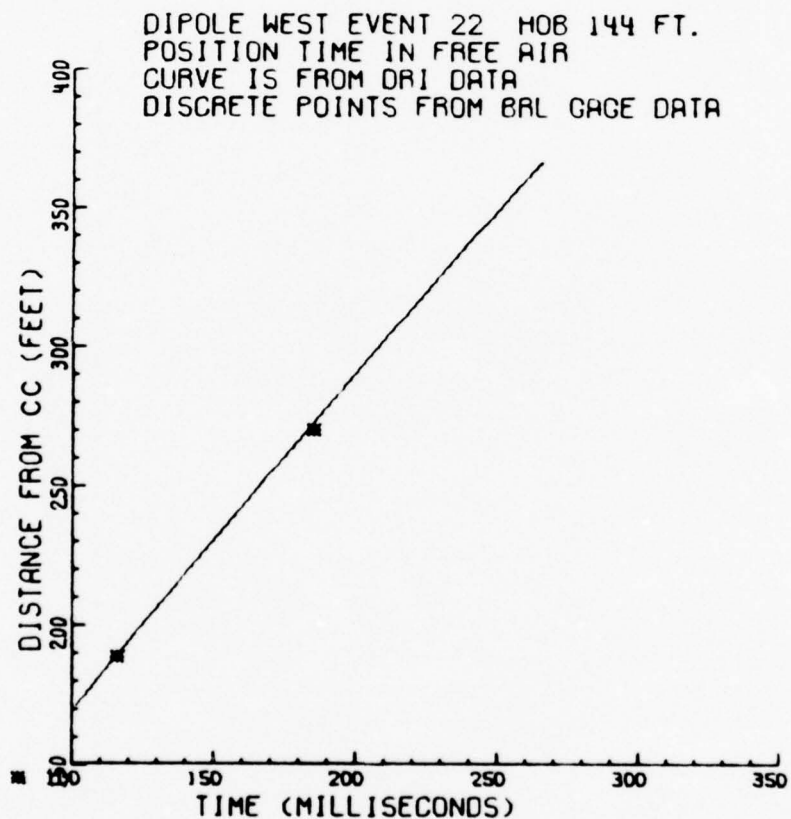


Figure 3.69. DRI Free-Air Shockwave Position-Time Curve and BRL Gage Data From Event 22, HOB \approx 144 Feet.

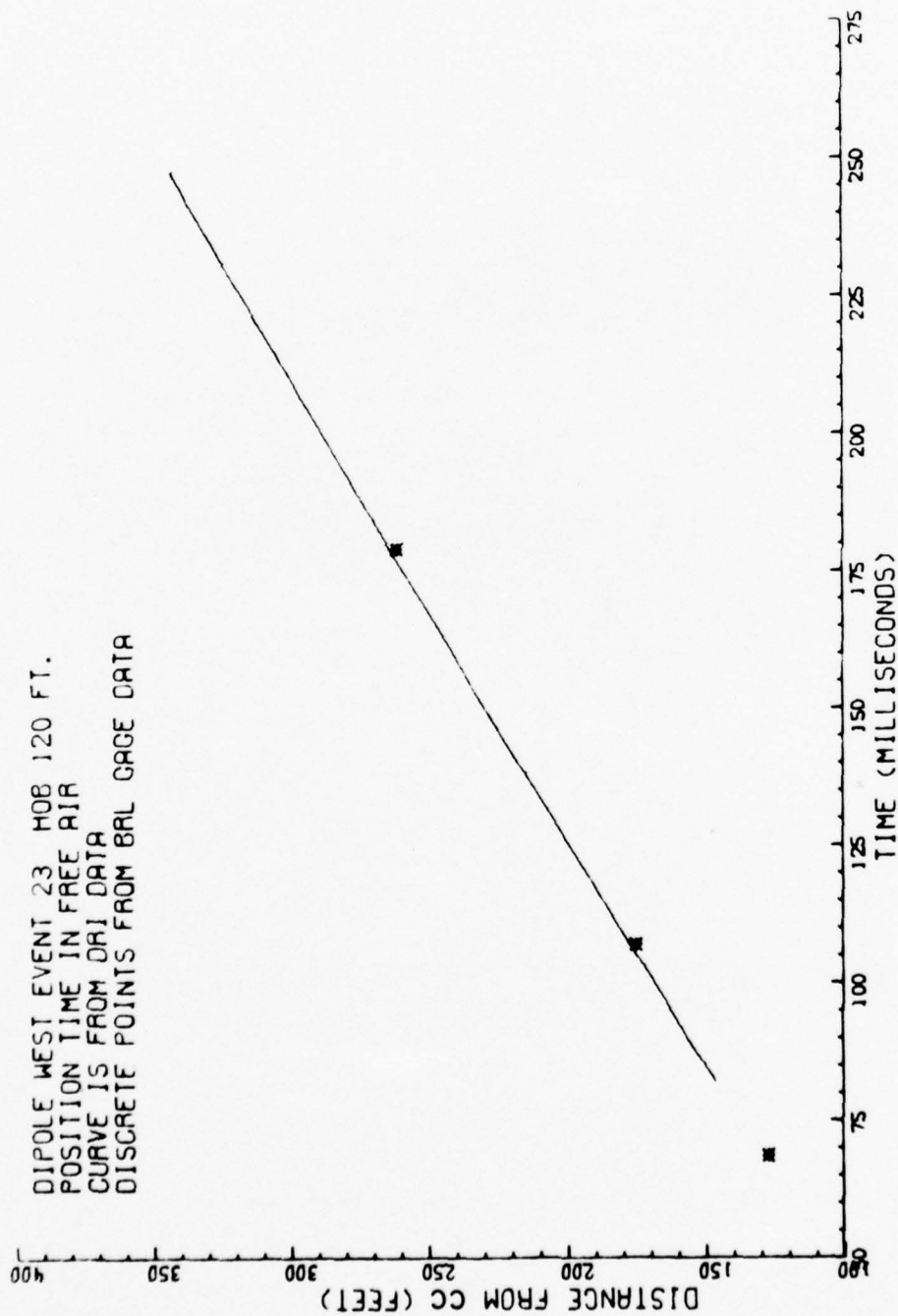


Figure 3.70. DRI Free-Air Shockwave Position-Time Curve and BRL Gage Data
 From Event 23, HOB \approx 120 Feet.

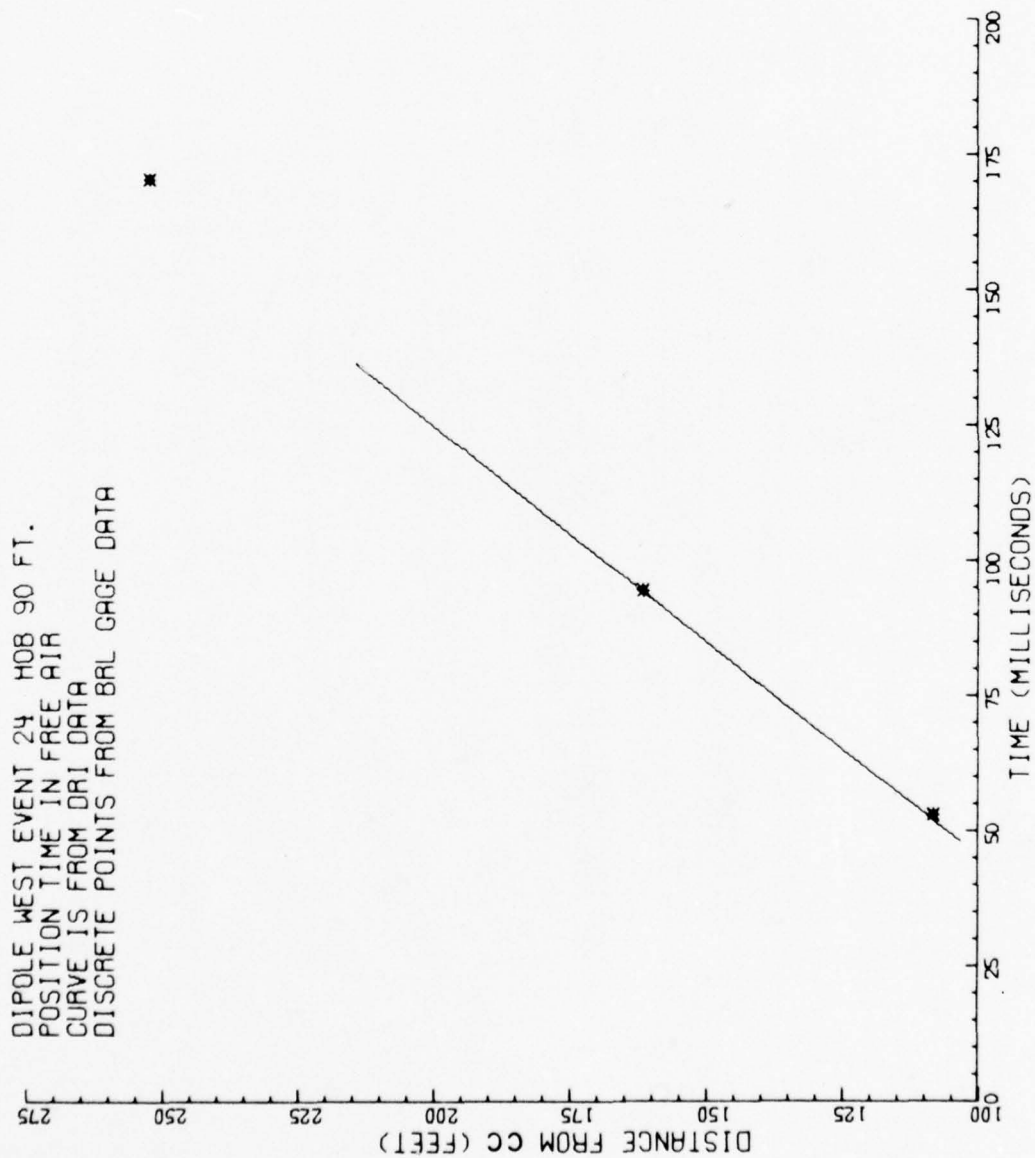


Figure 3.71. DRI Free-Air Shockwave Position-Time Curve and BRL Gage Data From Event 24, HOB \approx 90 Feet.

BEST AVAILABLE COPY

TABLE 3.12

DIPLOE WEST
EVENT 17

TIME-OF-ARRIVAL/PEAK PRESSURE VERSUS DISTANCE
FROM PHOTOGRAPHIC RECORDS

NUMBER OF CHARGES: ONE
CHARGE WEIGHT: 1000#
CHARGE CONFIGURATION: VERTICAL
HEIGHT OF BURST: 47 FT.

DRI PHOTOGRAPHIC VALUES						BRL GAGE VALUES					
FREE AIR			REFLECTIVE SURFACE			FREE AIR			REFLECTIVE SURFACE		
DISTANCE (FT)	TIME (MSEC)	PEAK PRESSURE (PSI)	TIME (MSEC)	PEAK PRESSURE (PSI)		TIME (MSEC)	PEAK PRESSURE (PSI)	TIME (MSEC)	PEAK PRESSURE (PSI)		
20.2						4.1	112.0				
30.0	9.1	71.0									
34.4						6.8	65.6				
35.0	7.0	61.0									
40.0	9.0	51.1									
43.5						10.5	42.4				
45.0	11.2	41.1									
50.0	13.7	31.1									
55.0	16.3	21.1									
60.0	19.4	11.0	27.2	15.2		20.6	16.5	28.2	28.5		
62.0											
65.0			30.3	14.9							
70.0			33.5	14.5							
75.0			36.7	14.1							
80.0			39.9	13.7				39.7	16.0		
85.0			43.1	13.3							
90.0			46.3	12.9				45.8	17.0		
95.0			49.6	12.5							
100.0			52.8	12.1				52.1	12.7		
105.0			56.2	11.7							
110.0			59.5	11.3				58.9	9.3		
115.0			62.8	10.9							
120.0			66.2	10.5				65.3	8.0		
125.0			69.6	10.1							
130.0			73.0	9.7							
135.0			76.5	9.3							
140.0			80.0	9.0				79.8	8.5		
145.0			83.5	8.6							
150.0			87.0	8.2				87.1	6.7		
155.0			90.6	7.8							
160.0			94.2	7.4				94.0	5.4		
165.0			97.8	7.0							
170.0			101.5	6.6							
175.0			105.2	6.2							
180.0			108.9	5.8							
185.0			112.7	5.4							
190.0			116.4	5.0							
195.0			120.1	4.6							
200.0			123.8	4.2				124.0	4.5		
205.0			127.5	3.8							
210.0			131.2	3.4							
215.0			135.0	3.1							
220.0			140.0	2.7							
225.0			144.1	2.3							
230.0			148.2	1.9							
235.0			152.4	1.5							
240.0			156.6	1.1							
245.0			160.8	0.7				160.0	2.9		
250.0			165.1	0.3							

BEST AVAILABLE COPY

TABLE 3.13

DIPLOE WEST
EVENT 18
TIME-OF-ARRIVAL/PEAK PRESSURE VERSUS DISTANCE
FROM PHOTOGRAPHIC RECORDS
NUMBER OF CHARGES: ONE
CHARGE HEIGHT: 1000F
CHARGE CONFIGURATION: VERTICAL
HEIGHT OF BURST: 60 FT.

DRI PHOTOGRAPHIC VALUES					BRL GAGE VALUES				
FREE AIR					REFLECTIVE SURFACE				
DISTANCE (FT)	TIME (MSEC)	PEAK PRESSURE (PSI)	TIME (MSEC)	PEAK PRESSURE (PSI)	DISTANCE (FT)	TIME (MSEC)	PEAK PRESSURE (PSI)	TIME (MSEC)	PEAK PRESSURE (PSI)
30.1					30.1	7.4	57.0		
40.0	9.3	54.0			40.0	10.2	39.4		
42.4					42.4	13.8	29.2		
45.0	11.4	44.0			45.0			35.4	24.5
50.0	13.8	35.2			50.0				
55.0	14.3	25.5			55.0				
60.0	19.2	15.8			60.0				
65.0	22.6	9.1			65.0	23.6	15.4		
67.1					67.1				
75.0					75.0				
80.0					80.0			45.8	19.0
85.0					85.0				
90.0					90.0			51.8	18.4
96.0					96.0				
100.0					100.0			58.1	13.4
105.0					105.0				
110.0					110.0			64.2	11.3
115.0					115.0				
120.0					120.0			71.2	7.5
125.0					125.0				
130.0					130.0			78.0	6.8
135.0					135.0				
140.0					140.0			85.2	6.0
145.0					145.0				
150.0					150.0			92.1	7.9
155.0					155.0				
160.0					160.0				
165.0					165.0				
170.0					170.0				
175.0					175.0				
180.0					180.0				
185.0					185.0				
190.0					190.0				
195.0					195.0				
200.0					200.0			130.5	4.8
205.0					205.0				
210.0					210.0				
215.0					215.0				
220.0					220.0				
225.0					225.0				
230.0					230.0				
235.0					235.0				
240.0					240.0				
245.0					245.0			104.5	3.6

BEST AVAILABLE COPY

TABLE 3.14

DIPLOE WEST
EVENT 19

TIME-OF-ARRIVAL/PEAK PRESSURE VERSUS DISTANCE
FROM PHOTOGRAPHIC RECORDS

NUMBER OF CHARGES: ONE
CHARGE HEIGHT: 1000"
CHARGE CONFIGURATION: VERTICAL
HEIGHT OF BURST: 90 FT.

DRI PHOTOGRAPHIC VALUES					BRL GAGE VALUES				
DISTANCE (FT)	FREE AIR		REFLECTIVE SURFACE		FREE AIR		REFLECTIVE SURFACE		
	TIME (MSEC)	PEAK PRESSURE (PSI)	TIME (MSEC)	PEAK PRESSURE (PSI)	TIME (MSEC)	PEAK PRESSURE (PSI)	TIME (MSEC)	PEAK PRESSURE (PSI)	
63.2					21.2	17.0			
67.1					24.5	15.0			
70.0	27.7	15.6							
72.1					26.6	15.0			
75.0	30.9	13.1							
80.0	34.2	12.6							
84.9					35.2	9.8			
85.0	37.5	12.1							
90.0	40.8	11.6							
95.0	44.2	11.1							
100.0	47.6	10.6							
105.0	51.0	10.1							
108.2					52.5	5.5			
110.0	54.5	9.6							
115.0	58.0	9.1							
120.0	61.5	8.6							
125.0	65.1	8.1							
130.0	68.7	7.6							
135.0	72.3	7.1							
140.0	76.0	6.6							
145.0	79.7	6.1							
150.0	83.5	5.6					105.0	7.9	
155.0	87.3	5.1							
160.0	91.1	4.6							
161.6					94.1	2.6			
165.0	95.0	4.1							
170.0	99.0	3.6							
175.0	103.0	3.1							
180.0	107.0	2.6	124.5	8.2					
185.0	111.1	2.1	128.1	8.2					
190.0	115.3	1.6	131.6	8.2					
195.0	119.5	1.1	135.2	8.1					
200.0			138.8	8.1			140.8	4.8	
205.0			142.4	8.1					
210.0			146.0	8.1					
215.0			149.6	8.0					
220.0			153.2	8.0					
225.0			156.7	8.0					
230.0			160.3	8.0					
235.0			163.9	7.9					
240.0							174.0	4.5	
252.2					169.8	2.0			

BEST AVAILABLE COPY

TABLE 3.15

DIPLOE WEST
EVENT 20
TIME-OF-ARRIVAL/PEAK PRESSURE VERSUS DISTANCE
FROM PHOTOGRAPHIC RECORDS

NUMBER OF CHARGES ONE
CHARGE WEIGHT 1000#
CHARGE CONFIGURATION VERTICAL
HEIGHT OF BURST 120 FT.

DIPLOE PHOTOGRAPHIC VALUES					DIPLOE GAGE VALUES				
DISTANCE (FT)	FREE AIR		REFLECTIVE SURFACE		DISTANCE (FT)	FREE AIR		REFLECTIVE SURFACE	
	TIME (MSEC)	PEAK PRESSURE (PSI)	TIME (MSEC)	PEAK PRESSURE (PSI)		TIME (MSEC)	PEAK PRESSURE (PSI)	TIME (MSEC)	PEAK PRESSURE (PSI)
127.1					127.1				
159.0	88.5	3.9			159.0	67.2	4.0		
160.0	92.5	3.8			160.0				
169.0	96.5	3.7			169.0				
170.0	100.4	3.7			170.0				
174.8					174.8	104.3	2.4		
179.0	104.4	3.6			179.0				
180.0	108.4	3.5			180.0				
189.0	112.4	3.4			189.0				
190.0	116.4	3.4			190.0				
199.0	120.4	3.3			199.0				
200.0	124.4	3.2			200.0				
209.0	128.4	3.1			209.0				
210.0	132.5	3.1			210.0				
219.0	136.5	3.0			219.0				
220.0	140.6	2.9			220.0				
229.0	144.6	2.8			229.0				
230.0	148.7	2.8			230.0				
239.0	152.7	2.7			239.0				
240.0	156.8	2.6			240.0				
249.0	160.9	2.5			249.0				
250.0	165.0	2.5			250.0				
259.0	169.1	2.4			259.0				
260.0	173.2	2.3			260.0				
261.0					261.0	176.0	2.0		
269.0	177.4	2.2			269.0				
270.0	181.5	2.2			270.0				
279.0	185.6	2.1			279.0				
280.0	189.8	2.0			280.0				
289.0	193.9	1.9			289.0				
290.0	198.1	1.9			290.0				
299.0	202.3	1.8			299.0				
300.0	206.4	1.7			300.0				
309.0	210.6	1.7			309.0				
310.0	214.8	1.6			310.0				
319.0	219.1	1.5			319.0				
320.0	223.3	1.4			320.0				
329.0	227.5	1.4			329.0				
330.0	231.7	1.3			330.0				
339.0	236.0	1.2			339.0				
340.0	240.2	1.1			340.0				
349.0	244.5	1.1			349.0				
350.0	248.8	1.0			350.0				
359.0	253.1	0.9			359.0				
360.0	257.3	0.8			360.0				

BEST AVAILABLE COPY

TABLE 3.16

UTPULF TEST
EVENT 21

TIME-OF-ARRIVAL/PEAK PRESSURE VERSUS DISTANCE
FROM PHOTOGRAPHIC RECORDS

NUMBER OF CHARGES: ONE
CHARGE WEIGHT: 10000
CHARGE CONFIGURATION: VERTICAL
HEIGHT OF BURST: 144 FT.

DISTANCE (FT)	DRI PHOTOGRAPHIC VALUES				BRL GAGE VALUES			
	FREE AIR		REFLECTIVE SURFACE		FREE AIR		REFLECTIVE SURFACE	
	TIME (MSEC)	PEAK PRESSURE (PSI)	TIME (MSEC)	PEAK PRESSURE (PSI)	TIME (MSEC)	PEAK PRESSURE (PSI)	TIME (MSEC)	PEAK PRESSURE (PSI)
144.1					80.0	3.5		
170.0	100.1	2.9						
175.0	104.2	2.8						
180.0	109.2	2.8						
185.0	112.3	2.8						
189.4					115.0	2.3		
190.0	116.4	2.7						
195.0	120.4	2.7						
200.0	124.5	2.6						
204.0	128.6	2.6						
210.0	133.7	2.5						
215.0	137.8	2.5						
220.0	141.9	2.4						
225.0	146.0	2.4						
230.0	149.1	2.3						
235.0	153.2	2.3						
240.0	157.3	2.2						
245.0	161.5	2.2						
250.0	165.6	2.1						
254.0	169.7	2.1						
260.0	173.8	2.0						
265.0	177.0	2.0						
270.0	180.2	2.0						
270.2					183.7	1.8		
275.0	184.3	1.9						
280.0	188.5	1.9						
285.0	192.7	1.8						
290.0	196.8	1.8						
295.0	203.0	1.7						
300.0	207.2	1.7						
304.0	211.4	1.6						
310.0	215.6	1.6						
315.0	219.8	1.5						
320.0	224.0	1.5						
325.0	228.2	1.4						
330.0	232.4	1.4						
335.0	236.7	1.3						
340.0	240.9	1.3						
345.0	245.1	1.3						
350.0	249.4	1.2						
355.0	253.6	1.2						
360.0	257.8	1.1						
365.0	262.2	1.1						
370.0	266.4	1.0						

BEST AVAILABLE COPY

TABLE 3.17

DIPOLE TEST
EVENT 22

TIME-OF-ARRIVAL/PEAK PRESSURE VERSUS DISTANCE
FROM PHOTOGRAPHIC RECORDS

NUMBER OF CHARGES: ONE
CHARGE WEIGHT: 1000#
CHARGE CONFIGURATION: VERTICAL
HEIGHT OF BURST: 144 FT.

ORT PHOTOGRAPHIC VALUES					BRL GAGE VALUES				

BEST AVAILABLE COPY

TABLE 3.18

DIPLOE WEST
EVENT 23

TIME OF ARRIVAL/PEAK PRESSURE VERSUS DISTANCE
FROM PHOTOGRAPHIC RECORDS

NUMBER OF CHARGES: ONE
CHARGE HEIGHT: 10000
CHARGE CONFIGURATION: VERTICAL
HEIGHT OF BURST: 120 FT.

DIPLOE PHOTOGRAPHIC VALUES					DIPLOE GAGE VALUES				
FREE AIR					REFLECTIVE SURFACE				
DISTANCE (FT)	TIME (MSEC)	PEAK PRESSURE (PSI)	TIME (MSEC)	PEAK PRESSURE (PSI)	DISTANCE (FT)	TIME (MSEC)	PEAK PRESSURE (PSI)	TIME (MSEC)	PEAK PRESSURE (PSI)
127.3					127.3	68.4	4.1		
150.0	84.3	3.1			150.0				
155.0	89.3	3.0			155.0				
160.0	93.4	3.0			160.0				
165.0	97.5	2.9			165.0				
170.0	101.6	2.8			170.0				
174.9					174.9	106.9	2.7		
175.0	105.7	2.8			175.0				
180.0	109.8	2.7			180.0				
185.0	113.9	2.6			185.0				
190.0	118.0	2.6			190.0				
195.0	122.1	2.5			195.0				
200.0	126.2	2.4			200.0				
205.0	130.4	2.3			205.0				
210.0	134.6	2.3			210.0				
215.0	138.7	2.2			215.0				
220.0	142.9	2.1			220.0				
225.0	147.1	2.1			225.0				
230.0	151.2	2.0			230.0				
235.0	155.4	1.9			235.0				
240.0	159.6	1.9			240.0				
245.0	163.8	1.8			245.0				
250.0	168.0	1.7			250.0				
255.0	172.3	1.6			255.0				
260.0	176.5	1.6			260.0	179.1	1.6		
265.0					265.0				
270.0	180.7	1.5			270.0				
275.0	185.0	1.4			275.0				
280.0	189.2	1.4			280.0				
285.0	193.5	1.3			285.0				
290.0	197.8	1.2			290.0				
295.0	202.1	1.2			295.0				
300.0	206.3	1.1			300.0				
305.0	210.6	1.0			305.0				
310.0	215.0	0.9			310.0				
315.0	219.3	0.8			315.0				
320.0	223.6	0.7			320.0				
325.0	227.9	0.7			325.0				
330.0	232.3	0.6			330.0				
335.0	236.6	0.6	254.8	10.6	335.0				
340.0	241.0	0.5	258.5	4.8	340.0				
345.0	245.4	0.5	262.7	0.4	345.0				
350.0					350.0				
400.0					400.0			315.2	2.3
500.0					500.0			400.0	1.5

BEST AVAILABLE COPY

TABLE 3.19

DIPLOLE WEST
EVENT 26

TIME-OF-ARRIVAL/PEAK PRESSURE VERSUS DISTANCE
FROM PHOTOGRAPHIC RECORDS

NUMBER OF CHARGES: ONE
CHARGE HEIGHT: 1000'
CHARGE CONFIGURATION: VERTICAL
HEIGHT OF BURST: 90 FT.

DISTANCE (FT)	DNT PHOTOGRAPHIC VALUES				BRL GAGE VALUES			
	FREE AIR		REFLECTIVE SURFACE		FREE AIR		REFLECTIVE SURFACE	
	TIME (MSEC)	PEAK PRESSURE (PSI)	TIME (MSEC)	PEAK PRESSURE (PSI)	TIME (MSEC)	PEAK PRESSURE (PSI)	TIME (MSEC)	PEAK PRESSURE (PSI)
105.0	49.5	4.0						
108.2					53.0	5.5		
110.0	53.4	4.0						
115.0	57.4	4.0						
120.0	61.4	3.9						
125.0	65.4	3.9						
130.0	69.4	3.9						
135.0	73.3	3.9						
140.0	77.3	3.9						
145.0	81.3	3.9						
150.0	85.3	3.9						
155.0	89.3	3.9						
160.0	93.3	3.8			94.5	3.0		
161.8								
165.0	97.3	3.8						
170.0	101.2	3.8						
175.0	105.2	3.8						
180.0	109.2	3.8						
185.0	113.2	3.8						
190.0	117.2	3.8						
195.0	121.2	3.8						
200.0	125.2	3.7	140.8	6.4				
205.0	129.2	3.7	144.8	6.1				
210.0	133.2	3.7	148.8	5.9				
215.0	137.2	3.7	152.2	5.7				
220.0			156.0	5.4				
225.0			159.9	5.2				
230.0			163.7	5.0				
235.0			167.6	4.7				
240.0			171.5	4.5				
245.0			175.5	4.3			177.0	4.1
250.0			179.4	4.0				
252.2					170.5	1.8		
255.0			183.4	3.8				
260.0			187.4	3.5				
265.0			191.4	3.3				
270.0			195.5	3.1				
275.0			199.6	2.8				
280.0			203.7	2.6				
285.0			207.8	2.4				
290.0			212.0	2.1				
295.0			216.2	1.9				
400.0							304.0	2.1

The DRI time-of-arrivals and peak pressure calculations are generally in good agreement with both the BRL FA and surface gage data.

3.8 TRIPLE-POINT PATHS EVENTS 17 THROUGH 24

The triple-point paths were generally limited to the lower HOB's. A small amount of data were obtained from Event 23 (HOB = 120 feet). The triple-point paths for the HOB series are given in Figure 3.72 through 3.76. Figure 3.77 presents a compilation of the triple-point data from the multiple detonation events as well as the HOB series. No considerations were made for the difference in the surface geologies and the difference in the explosive output of pentolite to that of TNT. As would be expected, the greater the HOB the more shallow is the slope of the path of the triple-point.

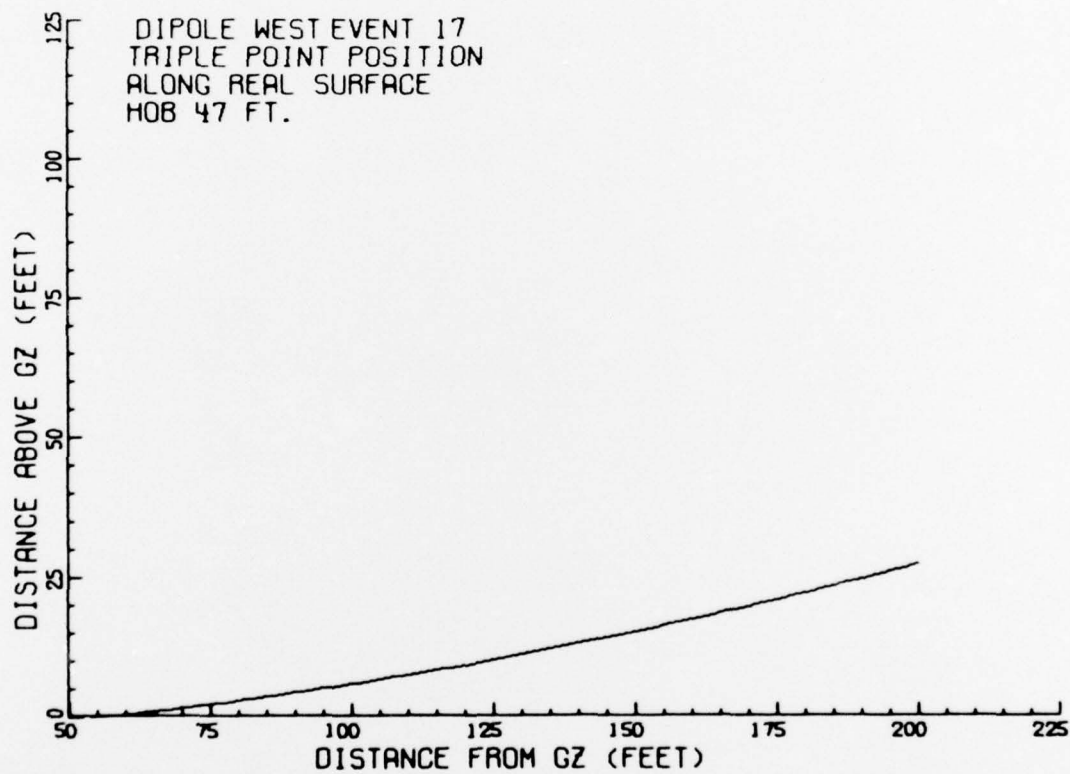


Figure 3.72. Triple-Point Path From Real Surface of Event 17, HOB \approx 47 Feet.

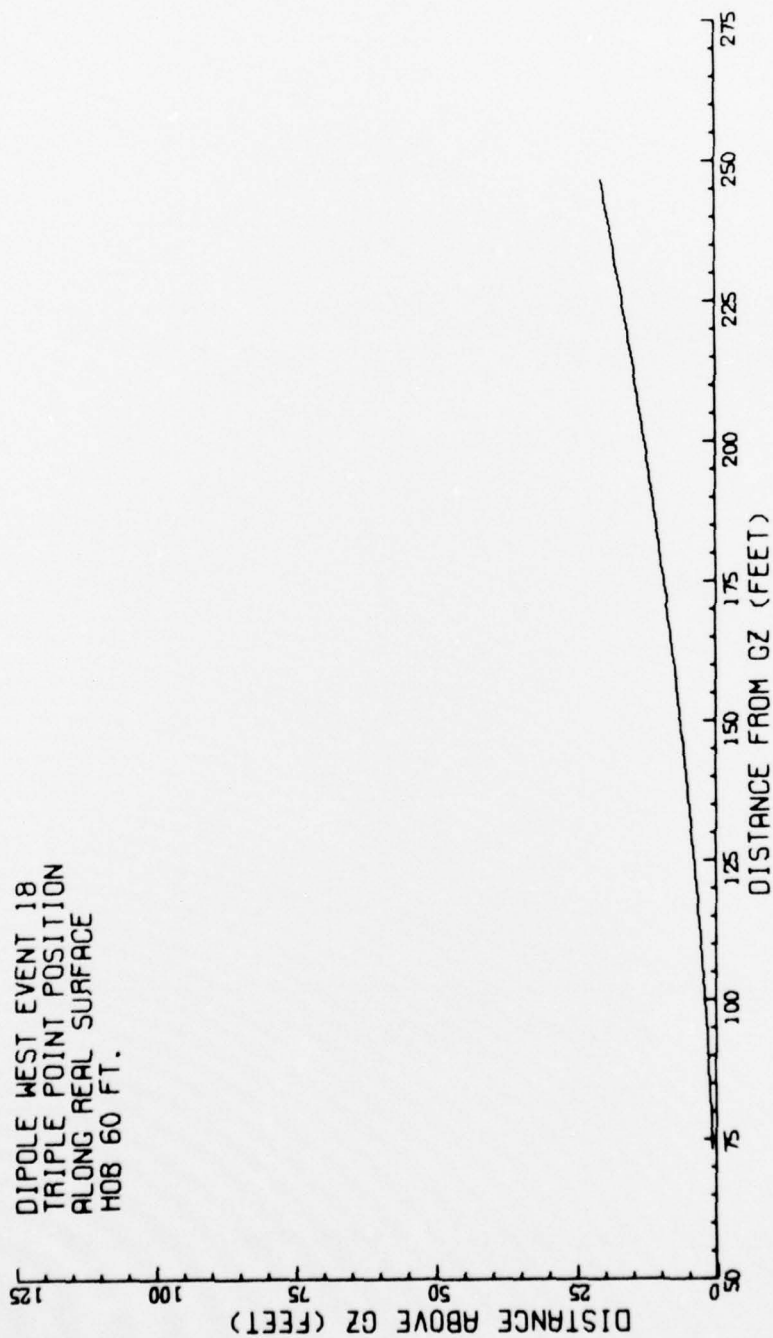


Figure 3.73. Triple-Point Path From Real Surface of Event 18, HOB \approx 60 Feet.

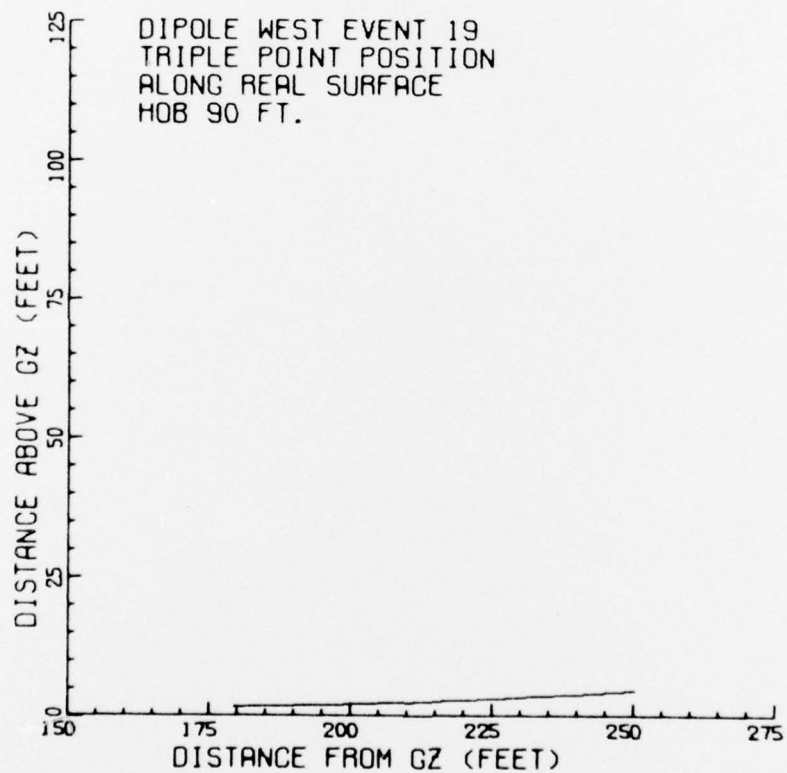


Figure 3.74. Triple-Point Path From Real Surface of Event 19, HOB \approx 90 Feet.

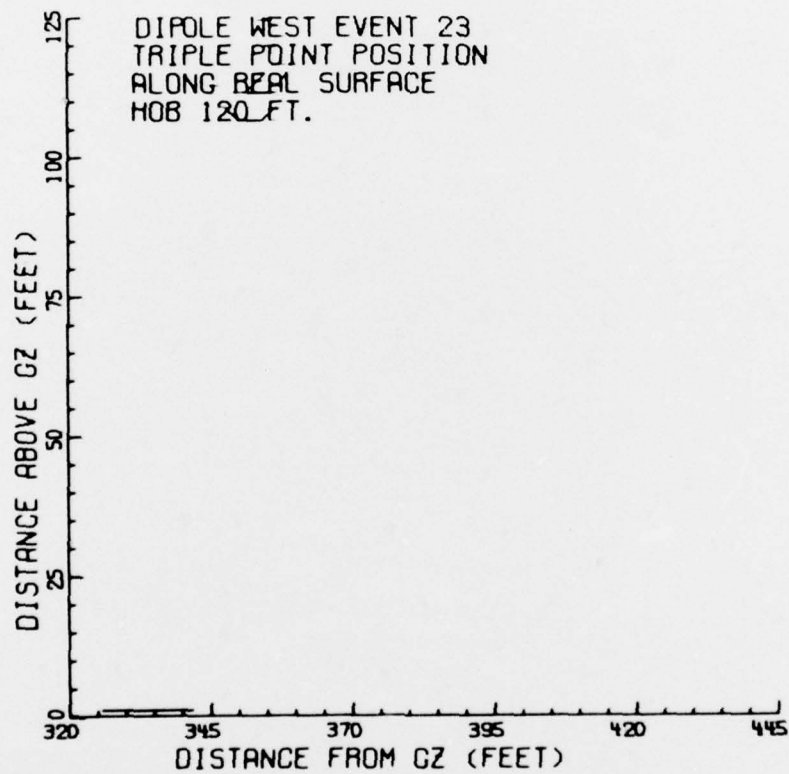


Figure 3.75. Triple-Point Path From Real Surface
of Event 23, HOB \approx 120 Feet.

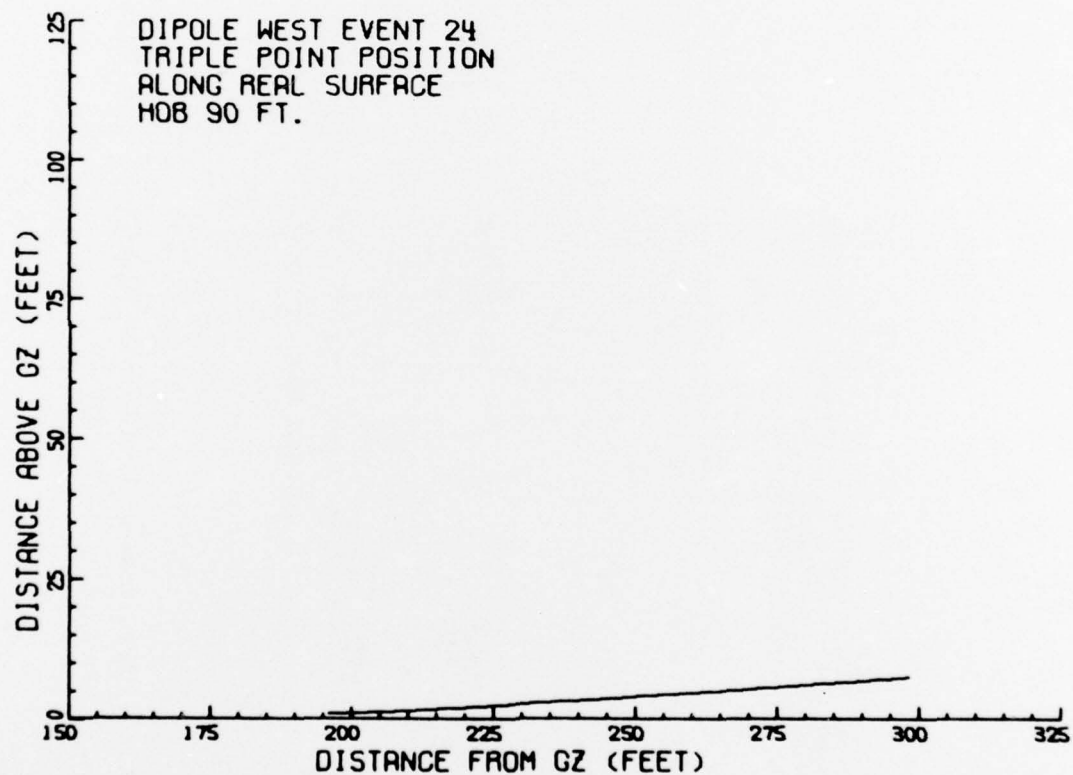


Figure 3.76. Triple-Point Path From Real Surface of Event 24,
HOB \approx 90 Feet.

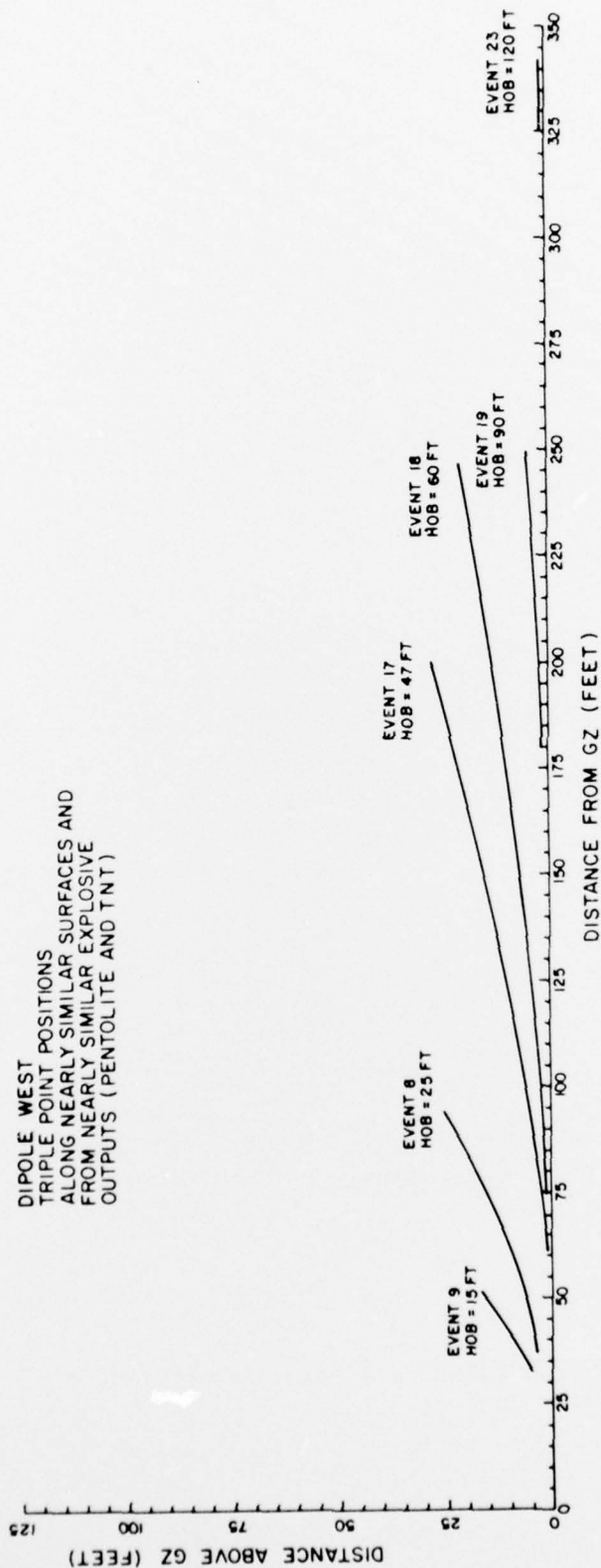


Figure 3.77. Comparison of Triple-Point Paths From Real Surface of Events 8, 9, 17, 18, 19, and 23.

SECTION 4

CONCLUSIONS AND RECOMMENDATIONS

The results presented in this report show merit in the utilization of photographic records as an experimental tool in the determination of shockwave position-time (time-of-arrival) and the calculation of peak pressure along their paths. Though the photographic method's accuracy is not as good as direct gage measurements, it does allow a means of checking the relative values obtained through electronic means.

Because of the limited number of gages which may be used in a gage-array, the photographic method of determining position-time of the triple-point and shockwaves intersection-point is more accurate than those obtained by gage measurements.

Some of the inaccuracies found in photographic measurements are due to the distortion caused in the shockfront by obstructions and variations in the contrast of the backdrops. These conditions may be improved by reducing some obstructions (tower structure, markers, poles, etc.) which exist near the surfaces of interest. It is also believed that smaller separations in the backdrops contrasting images would improve shockwave front resolution in the high pressure region (100 to 10 psi).

The DRI time-of-arrival data compared very well with the BRL data; whereas, there were differences between the calculated and measured peak pressure values. Longer periods of view before and past a gage array would allow more accurate calculations of peak pressures at the extreme gage positions.

REFERENCES

1. Keefer, J. H. and Reisler, R. E., Project DIPOLE WEST - Multiburst Environment (Simultaneous Detonations), BRL Report No. 1766, March 1975.
2. Reisler, R. E. and Pettit B. A., Project DIPOLE WEST - Multiburst Environment (Non-Simultaneous Detonations), BRL Report No. 1921, Sept. 1976.
3. Reisler, R. E., et al., Air Blast from Height-of-Burst Studies in Canada, Vol. I, HOB 5.4 to 71.9 Feet, BRL Report 1950, December 1976.
4. Reisler, R. E., et al., Air Blast from Height-of-Burst Studies in Canada, Vol. II, HOB 45.4 to 144.5 Feet, BRL Report in Publication.
5. Willell, J. E., and Lehto, D. L., Normal Shock (Rankine-Hugoniot) Relationships for Various Altitudes from Sea Level to 300,000 Feet, NAVORD Report 6075, 14 April 1958.
6. Eberhard, R. A. and Kingery, C. H., A Coefficient of Reflection Over a Concrete Surface, BRL Report 860, April 1953.
7. Sachs, R. G., The Dependence of Blast on Ambient Pressure and Temperature, BRL Report No. 466, Aberdeen Proving Ground, MD, May 1944.
8. Wisotski, J. and Snyder, W. H., A Study of the Effects of Snow Cover on High Explosive Blast Parameters, Denver Research Institute, DRI Report 2303, March 1966.
9. Needham, C. E., AFWL DIPOLE WEST Calculations, Letter, 14 May 1976.

DISTRIBUTION LIST

DEPARTMENT OF DEFENSE

Director
 Defense Advanced Rsch. Proj. Agency
 ATTN: Strategic Tech. Office

Defense Communication Engineer Center
 ATTN: Code 720, John Worthington

Director
 Defense Communications Agency
 ATTN: NMCSSC, Code 510

Defense Documentation Center
 Cameron Station
 12 cy ATTN: TC

Director
 Defense Intelligence Agency
 ATTN: DT-2, Wpns. & Sys. Div.
 ATTN: (DIA-DT-2), Tony Dorr
 ATTN: DT-1C, Nuc. Eng. Branch
 ATTN: DI-7D

Director
 Defense Nuclear Agency
 ATTN: DDST
 ATTN: TISI, Archives
 3 cy ATTN: TITL, Tech. Library
 ATTN: STSP
 ATTN: SPAS
 ATTN: SPSS
 ATTN: SPTD

Dir. of Defense Rsch. & Engineering
 Department of Defense
 ATTN: S&SS (OS)
 ATTN: DD/S&SS, John B. Walsh

Commander
 Field Command
 Defense Nuclear Agency
 ATTN: FCPR
 ATTN: FCTMOT/LCDR Strode
 ATTN: FCTMOF
 ATTN: FCTMD

Director
 Joint Strat. Target Planning Staff, JCS
 ATTN: JPTP
 ATTN: JLTW-2
 ATTN: JPTM
 ATTN: JPST

Chief
 Livermore Division, Field Command, DNA
 Lawrence Livermore Laboratory
 ATTN: FCPRL

OJCS/J-5
 ATTN: J-5, Plans & Policy Nuc. Div.

Studies Analysis & Gaming Agency
 Joint Chiefs of Staff
 ATTN: SDEB

DEPARTMENT OF THE ARMY

Director
 BMD Advanced Tech. Center
 Huntsville Office
 ATTN: Marcus Whitfield
 ATTN: ATC-T, Melvin T. Capps
 ATTN: CRDABH-S, William C. Loomis

Program Manager
 BMD Program Office
 ATTN: DACS-BMZ-D, Julian Davidson
 ATTN: DACS-BMT, John Shea
 ATTN: DACS-BMZ
 ATTN: Technology Division
 ATTN: DACS-BMT, Clifford E. McLain

Commander
 BMD System Command
 ATTN: BDMSSC-TEB, R. Simpson
 ATTN: BDMSC-TEN, Noah J. Hurst

Dep. Chief of Staff for Rsch. Dev. & Acq.
 Department of the Army
 ATTN: NCB Division

Deputy Chief of Staff for Ops. & Plans
 Department of the Army
 ATTN: Dir. of Nuc. Plans & Policy

Commander
 Harry Diamond Laboratories
 ATTN: DRXDO-NP, Francis N. Wimenitz
 ATTN: DRXDO-RC, Robert B. Oswald, Jr.
 ATTN: DRXDO-NP, Louis J. Belliveau
 ATTN: DRXDO-RBH, James H. Gwalney

Commander
 Picatinny Arsenal
 ATTN: SARPA-FR-E, Louis Avrami
 ATTN: SMUPA-MD, Henry Opat
 ATTN: SARPA-ND-C-T, Donald Miller
 ATTN: F. Cotton
 ATTN: Al Loeb

Director
 TRASANA
 ATTN: R. E. DeKinder, Jr.

Director
 US Army Ballistic Research Labs.
 ATTN: DRXRD-BVL, William J. Schuman, Jr.
 ATTN: DRXBR-TB, J. T. Frasier
 ATTN: DRXBR-X, Julius J. Meszaros
 ATTN: DRDAR-BLE, J. H. Keefer
 ATTN: Robert E. Eichelberger
 ATTN: Richard Vitali

Commander
 US Army Mat. & Mechanics Rsch. Center
 ATTN: DRXMR-HH, John F. Dignam

Commander
 US Army Materiel Dev. & Readiness Command
 ATTN: DRCDE-D, Lawrence Flynn

DEPARTMENT OF THE ARMY (Continued)

Commander
US Army Missile Command
ATTN: DRS-RKP, W. B. Thomas
ATTN: Troy Smith
ATTN: DRSMI-RRR, Bud Gibson
ATTN: DRSMI-XS, Chief Scientist
ATTN: DRCPM-PE-EA, Wallace O. Wagner

Commander
US Army Nuclear Agency
ATTN: COL Deverill
ATTN: MAJ J. Vecke
ATTN: ATCA-NAW
ATTN: MONA-SA
ATTN: MONA-WE
ATTN: CDC-NVA

Chief
US Army Research Office
ATTN: Technical Library

DEPARTMENT OF THE NAVY

Chief of Naval Material
Navy Department
ATTN: MAT 0323, Irving Jaffe

Chief of Naval Operations
Navy Department
ATTN: Robert A. Blaise
ATTN: Code 604C3, Robert Piacesi
ATTN: OP 62
2 cy ATTN: OP 981

Chief of Naval Research
Navy Department
ATTN: Code 464, Thomas P. Quinn

Director
Naval Research Laboratory
ATTN: Code 5180, Mario A. Persechino
ATTN: Code 2600, Tech. Lib.
ATTN: Code 7770, Gerald Cooperstein

Commander
Naval Sea Systems Command
Navy Department
ATTN: Code 0351
ATTN: 0333A, Marlin A. Kinna
ATTN: ORD-0333A

Officer in Charge
Naval Surface Weapons Center
ATTN: Code 2302, Leo F. Gowen
ATTN: Code WA501, Navy Nuc. Prgms. Off.
ATTN: Code 241, Joseph Petes
ATTN: Code 322, Victor C. Dawson
ATTN: Code 323, W. Carson Lyons

Commanding Officer
Naval Weapons Evaluation Facility
ATTN: Peter Hughes
ATTN: Lawrence R. Oliver

Director
Strategic Systems Project Office
Navy Department
ATTN: NSP-272
ATTN: NSP-273

DEPARTMENT OF THE AIR FORCE

Commandant
AF Flight Dynamics Laboratory, AFSC
ATTN: FXG

AF Geophysics Laboratory, AFSC
ATTN: Chan Touart

AF Materials Laboratory, AFSC
ATTN: LPH, Gordon Griffith
ATTN: MBC, Donald L. Schmidt
ATTN: MBE, George F. Schmitt
ATTN: Bill Kessler
ATTN: MAS
ATTN: T. Nicholas
ATTN: LTM

AF Rocket Propulsion Laboratory, AFSC
ATTN: RTSN, G. A. Beale

AF Weapons Laboratory, AFSC
ATTN: Dr. Minge
ATTN: DYS, Lt E. J. Burns
ATTN: Al Sharp
ATTN: SAB
ATTN: DYT
ATTN: DYV
ATTN: ALO, Maj Lawrence T. James
ATTN: SUL
2 cy ATTN: NTO
ATTN: Tech. Review

AFTAC
ATTN: Col Earnest F. Dukes, Jr.

Headquarters
Air Force Systems Command
ATTN: SOSS
ATTN: XRTO

Commander
Arnold Engineering Development Center
ATTN: XOA

Commander
ASD
ATTN: EWFS, D. Ward

Commander
Foreign Technology Division, AFSC
ATTN: PDBG
ATTN: TDFBD, J. D. Pumphrey
ATTN: TDPTN

Hq. USAF/RD
ATTN: RD
ATTN: David S. Hyman
ATTN: RDQ
ATTN: RDQSM
ATTN: RDPM

Hq. USAF/XO
ATTN: XOSS

SAMSO/DY
ATTN: DYS

SAMSO/MN
ATTN: MNNR

DEPARTMENT OF THE AIR FORCE (Continued)

SAMSO/RS

ATTN: RSSE
ATTN: RST
ATTN: RSS

Commander in Chief
Strategic Air Command

ATTN: XPFS
ATTN: DOXT
ATTN: NRI
ATTN: XPQM
ATTN: XOBM

ENERGY RESEARCH & DEVELOPMENT ADMINISTRATION

Division of Military Application
US Energy Rsch. & Dev. Admin.
ATTN: Doc. Con. for Res. & Dev. Branch

University of California
Lawrence Livermore Laboratory

ATTN: Larry W. Woodruff, L-96
ATTN: C. Joseph Taylor, L-92
ATTN: Joseph B. Knox, L-216
ATTN: Joseph E. Keller, Jr., L-125
ATTN: G. Staihle, L-24

Los Alamos Scientific Laboratory

ATTN: Doc. Con. for T. Talley
ATTN: Doc. Con. for Richard A. Gentry
ATTN: Doc. Con. for John McQueen
ATTN: Doc. Con. for Donald Kerr
ATTN: Doc. Con. for R. S. Thurston
ATTN: Doc. Con. for J. W. Taylor

Sandia Laboratories

Livermore Laboratory
ATTN: Raymond Ng
ATTN: Doc. Con. for C. S. Hoyle
ATTN: Doc. Con. for T. Gold
ATTN: Doc. Con. for 8131, H. F. Norris, Jr.

Sandia Laboratories

ATTN: Doc. Con. for A. W. Synder
ATTN: Doc. Con. for M. L. Merritt
ATTN: Doc. Con. for Walter Herrmann
ATTN: Doc. Con. for Albert Chabai
ATTN: Doc. Con. for B. Caskey
ATTN: Doc. Con. for R. R. Boade
ATTN: Doc. Con. for Thomas B. Cook
ATTN: Doc. Con. for D. McCloskey

DEPARTMENT OF DEFENSE CONTRACTORS

Acurex Corporation

ATTN: J. Courtney
ATTN: C. Nardo
ATTN: J. Huntington
ATTN: Robert M. Kendall

Aeronautical Rsch. Assoc. of Princeton, Inc.
ATTN: Coleman Donaldson

Aerospace Corporation

ATTN: R. Mortensen
ATTN: W. Mann
ATTN: W. Barry
ATTN: R. Allen
ATTN: R. Strickler
ATTN: J. McClelland
ATTN: Richard Crolius, A2-Rm. 1027

DEPARTMENT OF DEFENSE CONTRACTORS (Continued)

Analytic Services, Inc.

ATTN: Jack Selig

ARO, Incorporated

ATTN: John C. Adams

Avco Research & Systems Group

ATTN: John E. Stevens, J100
ATTN: Doc. Con.
ATTN: S. Skemp, J200
ATTN: George J. Davis
ATTN: J. Patrick
ATTN: William C. Reinecke, K100
ATTN: George Weber, J230
ATTN: John Gilmore, J400

Battelle Memorial Institute

ATTN: Merwyn R. Vanderlind
ATTN: F. Unger
ATTN: Richard Castle
ATTN: W. Pfeifer

The Boeing Company

ATTN: Robert Dyrdaahl
ATTN: William Crist
ATTN: Brian Lempriere
ATTN: Ed York
ATTN: Robert Holmes

Boeing Wichita Company

ATTN: T. Swaney

Brown Engineering Company, Inc.

ATTN: Ronald Patrick

California Research & Technology, Inc.

ATTN: Ken Kreyenhagen

Calspan Corporation

ATTN: M. S. Holden
ATTN: Romeo A. DeLiberis
ATTN: M. G. Dunn

University of Dayton

Industrial Security Super KL-505
ATTN: Hallock F. Swift
ATTN: D. Gerdiman

University of Denver

ATTN: John Wisotski

Effects Technology, Inc.

ATTN: Richard Parise
ATTN: Robert Wengler

Ford Aerospace & Communications Operations

ATTN: P. Spangler

Gard, Incorporated

ATTN: Marion J. Balcerzak
ATTN: W. F. Byrne

General Dynamics Corp.

Fort Worth Division
ATTN: R. Shemensky

ION Physics Corporation

ATTN: Robert D. Evans

DEPARTMENT OF DEFENSE CONTRACTORS (Continued)

General Electric Company
Space Division
Valley Forge Space Center

ATTN: C. Kyriss
ATTN: A. Martellucci
ATTN: B. M. Maguire
ATTN: Phillip Cline
ATTN: Carl Anderson
ATTN: Daniel Edelman
ATTN: G. Harrison

General Electric Company
TEMPO-Center for Advanced Studies
ATTN: B. Gambill
ATTN: DASIAC

General Research Corporation
ATTN: John Ise, Jr.
ATTN: T. Stathacopoulos
ATTN: Robert E. Rosenthal

Institute for Defense Analyses
ATTN: IDA Librarian, Ruth S. Smith
ATTN: Joel Bengston

Kaman Avidyne
Division of Kaman Sciences Corp.
ATTN: Norman P. Hobbs
ATTN: E. S. Criscione
ATTN: Ray Reutnick

Kaman Sciences Corporation
ATTN: John R. Hoffman
ATTN: Frank H. Shelton
ATTN: Donald C. Sachs
ATTN: John Keith
ATTN: Thomas Meagher
ATTN: R. Keefe

LFE Corp., Environmental Anal. Lab. Div.
ATTN: Marcel Nathans

Lockheed Missiles & Space Company, Inc.
ATTN: Art Thomas, Dept. 85-85
ATTN: Arthur Collins, Dept. 81-14
ATTN: L. D. Hull
ATTN: Charles M. Lee
ATTN: Gerald T. Chrusciel

Lockheed Missiles & Space Company
ATTN: T. R. Fortune

Lockheed Missiles & Space Company, Inc.
ATTN: E. G. Borgardt
ATTN: Raymond R. Capiaux

Martin Marietta Aerospace
Orlando Division
ATTN: Joyce Legare, MR-328
ATTN: William A. Gray, MP-61
ATTN: Gene Aiello
ATTN: H. Rosenthal
ATTN: G. Fotieo
ATTN: James M. Potts, MP-61
ATTN: Laird Kinnaird

DEPARTMENT OF DEFENSE CONTRACTORS (Continued)

McDonnell Douglas Corporation
ATTN: R. J. Reck
ATTN: H. Hurwicz
ATTN: Ken Kratch
ATTN: J. F. Garibotti
ATTN: L. Cohen
ATTN: J. Kirby
ATTN: Robert W. Halprin

McDonnell Douglas Corporation
ATTN: Jean McGrew

National Academy of Sciences
ATTN: National Materials Advisory Board
for Donald G. Groves
ATTN: National Materials Advisory Board
for Edward R. Dyer

Northrop Corporation
ATTN: Don Hicks

Pacific-Sierra Research Corp.
ATTN: Gary Lang

Physical Sciences, Inc.
ATTN: M. S. Finson

Physics International Company
ATTN: Doc. Con. for James Shea

Prototype Development Associates, Inc.
ATTN: John McDonald
ATTN: John Slaughter

R & D Associates
ATTN: Albert L. Latter
ATTN: Cyrus P. Knowles
ATTN: Harold L. Brode
ATTN: Jerry Carpenter
ATTN: F. A. Field

The Rand Corporation
ATTN: R. Robert Rapp

Raytheon Company
ATTN: Library

Science Applications, Inc.
ATTN: Dwane Hove
ATTN: R. Fisher
ATTN: G. Ray
ATTN: John Warner

Science Applications, Inc.
ATTN: Lyle Dunbar
ATTN: Carl Swain

Science Applications, Incorporated
ATTN: William R. Seebaugh
ATTN: William M. Layson

Southern Research Institute
ATTN: C. D. Pears

Stanford Research Institute
ATTN: George R. Abrahamson
ATTN: D. L. Huestis
ATTN: Donald Curran
ATTN: Philip J. Dolan
ATTN: Herbert E. Lindberg
ATTN: OAI

DEPARTMENT OF DEFENSE CONTRACTORS (Continued)

Stanford Research Institute

ATTN: Harold Carey

ATTN: W. B. Reuland

Systems, Science & Software, Inc.

ATTN: G. A. Gurtman

ATTN: Russell E. Duff

Terra Tek, Inc.

ATTN: Sidney Green

DEPARTMENT OF DEFENSE CONTRACTORS (Continued)

TRW Defense & Space Sys. Group

ATTN: Peter Brandt, E1-2006

ATTN: Thomas G. Williams

ATTN: D. H. Baer, R1-2136

ATTN: Peter K. Dai, R1/2170

ATTN: W. W. Wood

ATTN: R. K. Plebuch, R1-2078

2 cy ATTN: I. E. Alber, R1-1008

TRW Defense & Space Sys. Group

San Bernardino Operations

ATTN: Earl W. Allen, 520/141

ATTN: V. Blankenship

ATTN: E. Y. Wong, 527/712

ATTN: William Polich

ATTN: L. Berger